博士学位請求論文

論文題目　Oxygen removal efficiency from microalgal culture by gas-permeating photobioreactor

専 攻 名　環境共生工学専攻

学籍番号　15D5701

氏　　名　岸　正敏

指導教員　戸田　龍樹

創 価 大 学 大 学 院
工 学 研 究 科

DISSERTATION

OXYGEN REMOVAL EFFICIENCY FROM MICROALGAL CULTURE BY GAS-PERMEATING PHOTOBIOREACTOR

February 19, 2018

SOKA UNIVERSITY
GRADUATE SCHOOL OF ENGINEERING

MASATOSHI KISHI

OXYGEN REMOVAL EFFICIENCY FROM MICROALGAL CULTURE BY GAS-PERMEATING PHOTOBIOREACTOR

February, 2018

MASATOSHI KISHI

page

CONTENTS

ACKNOWLEDGEMENTS

Foremost, I would like to express my utmost gratitude to my advisor, Professor Tatsuki Toda, for his guidance and support. I am very thankful that he trusted me and did not give up on me even at difficult moments. He granted me to take part in various projects (Lake Biwa, COSMOS, and Branding projects), which have given me the opportunities not only to deepen the experience and knowledge but also to contribute to the society through research. I expand my appreciation to the co-supervisors, Professor Ken Furuya and Professor Junichi Ida for putting great efforts into my dissertation and for their insightful comments and suggestions throughout my research.

I am indebted to Professor Tatsushi Matsuyama for his sincere guidance, especially with physical and mathematical problems. I am grateful to Professor Satoru Taguchi for providing me the initiative to study microalgae, and Professor Victor Kuwahara for help me expand the interest. My sincere thanks go to Dr. Kenji Tsuchiya and Dr. Shinichi Akizuki, who always trusted my potential and encouraged me. I would also like to appreciate Dr. Tomoyo Katayama for her kind advice at difficult moments. I would like to thank Dr. Minako Kawai and Dr. Erjin Eio for giving me necessary guidance towards the pursuit of Ph.D.

I would like to appreciate Dr. Mitsuhiko Koyama and Mrs. Yukiko Koyama for their friendship and being a close role model for a researcher and a good couple. I thank my fellow algae team members, without whom my research was not complete: especially to Ms. Mako Tagawa, Mr. Kenji Tanaka, Mr. Kenta Nagatsuka, Ms. Midori Goto, and Ms. Hidemi Onouchi. Special thanks go to Ms. Yumi Hosokawa and Ms. Maki Kobayashi who helped my experiments.

Great appreciation to “Environment Research and Technology Development Fund” from the Ministry of the Environment, Japan (4-1406), Japan Science and Technology Agency (JST)/Japan International Cooperation Agency (JICA), Science and Technology Research Partnership for Sustainable Development (SATREPS) and Sasagawa Research Fund for supporting the completion of the research.

I would like to thank my parents Mr. Toshio Kishi and Mrs. Kumiko Kishi for giving me such opportunity to go to Soka University of America and pursue Ph.D. afterwards. I also thank my siblings and relatives for the tremendous encouragements.

Finally, I would like to express my appreciation to the founder of Soka University, Dr. Daisaku Ikeda, for the continuous encouragements and the dream that he entrusts on us.

ABSTRACT

Microalgae is widely applied to commercial production of neutraceuticals, cosmeceuticals, feed and other products. To improve the productivity and cost-effectiveness, high-density microalgae culture is desirable. Moreover, closed culture system is preferred for clean algal biomass production for neutraceuticals and food market. However, owing to the oxygen accumulation during high-density culture especially in closed reactors, the productivity is often limited. The current measures to remove dissolved oxygen is aeration, but its extensive energy consumption raises the total maintenance cost. In this context, a low-cost oxygen removal is desired. Gas-liquid separation modules based on gas-permeating films have been applied in beverage and fuel industries, but have only recently been proposed in the algae industry. While the previous studies focused on hollow-fiber modules for increased surface, it is hardly practical for a large-scale operation because of potential clogging and partial accumulation of dissolved oxygen far from the module. Hence, the current study proposed a bag photobioreactor whose one side is composed of gas-permeating microporous film, enabling low-energy dissolved oxygen removal from the whole reactor. The major aim of this Ph.D. thesis is to develop a novel gas-permeating bag photobioreactor, to construct its effective operation model, and to evaluate its performance and cost-effectiveness.

Firstly, in Chapter II, oxygen permeabilities were evaluated for different types of plastic films and membranes. While silicone and fluororesin exhibited a high oxygen permeability compared with polyethylene film, the microporous film had approximately 3,000 times higher permeability than these common gas-permeable materials. Based on the obtained permeability, a flat-panel bag reactor with its one side composed of the microporous film was designed and constructed, so that it has a high specific surface and light utilization. The developed gas-permeating reactor had approximately 20 times higher oxygen mass transfer coefficient than common bag reactors without aeration. The obtained oxygen removal performance was comparatively evaluated with aeration and algal co-culture system. While mass transfer coefficient of gas-permeable photobioreactor was roughly 3.5-

fold smaller than aeration, the energy consumption was calculated to be close to 20-fold less. While algal co-culture also exhibited a low energy consumption, the gas-permeating reactor was found to be superior in terms applicability especially in a productive culture with high oxygen production.

Secondly, in Chapter III, a suitable CO_2 supply system for the gas-permeating reactor was suggested and evaluated. Since gas-permeating reactor allows algal culture without aeration inside the reactor for oxygen removal, it is desirable to reduce the aeration for CO_2 supply as well. The current study developed a model for two-phase CO_2 supply system, in which a CO_2 absorption column effectively absorb CO_2 gas and convert it to bicarbonate, which is then transferred to the gas-permeating reactor as an inorganic carbon source. Based on the experimental data obtained in a semi-continuous two-phase CO_2 supply system, the model was demonstrated to predict the CO_2 absorption behavior. The productivity of *Arthrospira platensis* in the gas-permeating reactor was then evaluated under differing photon flux density 100-800 μmol m^{-2} s^{-1}. The maximum productivity 1.98 g-dry-weight (DW) L^{-1} d^{-1} was obtained with 325 μmol m^{-2} s^{-1} which was 1.5-times higher than that of conventional polypropylene bag reactor 1.31 gDW L^{-1} d^{-1}. Based on this figure, two-phase CO_2 supply was applied to the gas-permeating reactor, achieving a stable CO_2 absorption and growth with reduced aeration into the bag reactor.

Finally, the current study evaluated the energy and cost balance of the developed gas-permeating photobioreactor in comparison to the conventional bag reactor. It was demonstrated that the energy consumption could be reduced by 4-fold at maximum owing to the less requirement for aeration and circulation. On the other hand, the reactor maintenance cost becomes large owing to the relatively high cost of the microporous film under the current basis. However, if the cost of gas-permeating films become cheaper, the overall cost was demonstrated to be less expensive than the conventional bag reactors. This study demonstrated that the newly developed gas-permeating reactor is cost and energy efficient in the high-density microalgae/cyanobacteria culture.

CHAPTER I

General Introduction

1.1. Application of microalgae and cyanobacteria in the world

Microalgae and cyanobacteria are defined as microscopic photosynthetic eukaryotic and prokaryotic organisms, respectively. Owing to their long history on the earth, microalgae and cyanobacteria have diversified into wide taxonomic groups. Human has only identified less than 40% out of an estimated total number of 73 thousand species (Guiry, 2012; De Clerck et al., 2013). Out of identified species, only a few thousand strains are kept in collections, and a few hundred are investigated for chemical content (Olaizola, 2003; Spolaore et al., 2006). The applicability of microalgae and cyanobacteria is, therefore, yet to be fully discovered.

The history of algal utilization is long. The first record of microalgal utilization dates back 2,000 years to the Chinese, who collected *Nostoc* from lakes during the famine to survive (Spolaore et al., 2006). The cultivation of microalgae, however, is rather recent; the investigation of algal cultivation for human use had begun in 1940s when the rapid population growth alarmed severe food shortage (Ferreira et al., 2012). Back then, for example, outdoor cultivation of *Chlorella* species and its usage as a human protein source was intensely studied (Ben-Amotz et al., 2009). In 1970s, the concept of recycling wastewater nutrients for the cultivation of algal biomass as a protein source was published by Oswald and his co-workers (Oswald, 1977), which eventually opened a way for mass algae cultivation in open ponds. The application of algal products has now widened to (1) natural pigments such as β-carotene from *Dunaliella* spp. (Fig. I-1-a) and phycocyanin from cyanobacteria such as *Arthrospira platensis* (Fig. I-1-b) (e.g., García-González et al., 2005; Belay, 2013; Hu et al., 2017), (2) essential fatty acids such as docosahexaenoic acid (DHA) from *Crypthecodinium cohnii* and *Schizochytrium* spp. (e.g., Borowitzka, 1999; Olaizola, 2003; Wen and Chen, 2003; Pyle, 2008), (3) health supplements derived from *Haematococcus lacustris* (Fig. I-1-c) and *Chlorella* spp. (e.g., Borowitzka, 1992; Lorenz and Cysewski, 2000; Orosa et al., 2001; Ip

and Chen, 2005; Wang and Chen, 2008), (4) wastewater reclamation and biogas purification (González et al., 2008; Wang et al., 2010; e.g., González-Fernández et al., 2011; Rawat et al., 2011; Chiu et al., 2015; Kishi et al., 2015, in press; Posadas et al., 2015; Toledo-Cervantes et al., 2016), (5) biofuel production (e.g., Kumar et al., 2010a; Park et al., 2011; Pittman et al., 2011; Richardson et al., 2014), and so on. There are also emerging microalgal strains potential to be used for commercial production, such as *Chromochloris zofingiensis* (Fig. I-1-d) for astaxanthin production (Imaizumi et al., 2014, 2016; Liu et al., 2014), *Botryococcus braunii* and *Aurantiochytrium* spp. for hydrocarbon that can be used both for cosmetics and fuel. The global market for algae industries has now developed to US$ 1.25×10^9 per year (Spolaore et al., 2006).

Although the number of commercially applied algal species has been increasing slowly, still an only limited number of species listed above are mass-cultured. The most produced algal genera are *Arthrospira,* and *Chlorella* comes next (Spolaore et al., 2006). One of the reasons for the limited application is the cost-effectiveness of the algal products over the cultivation cost. Expensive closed photobioreactors have been only successful for the production of valuable products, such as astaxanthin from *Haematococcus lacustris* or radio-labeled organic compounds from various microalgae (Borowitzka, 1999). Heterotrophic fermenters could be cost-effective when the growth of algae is substantially higher with substrate addition, and the product price is relatively high, such as DHA from *Cryptecodinium cohnii* and *Schizochytrium* spp. The cheapest and predominant method of cultivation, open pond system, is only commercially successful either with extremophiles (e.g., alkalihalophilic *Arthrospira* and halophilic *Dunaliella*), fast-growing species (such as *Chlorella* with maximum specific growth rate of over 6 d^{-1}), or applications that do not require pure unialgal culture such as feed and wastewater treatment (Borowitzka, 1999). Other species need to be cultured in a closed bioreactor. Therefore, a cheap and productive culture method with closed reactors is required to meet the high demand for microalgae and to widen its application. Improvements in algal productivity, cost-effectiveness, and energy-effectiveness are

awaited.

1.2. Types of photobioreactors: pros and cons

In the search for higher productivity and cost-effectiveness, various reactor designs have been attempted. As mentioned above, the most widespread reactor is an open-air system, which includes tank reactor, circular pond, and raceway pond (Fig. I-2-a). It is commonly accepted that open-pond system is the most cost-effective; nevertheless, species control and predator control have been difficult issues (Richardson et al., 2012; Montemezzani et al., 2015). To meet the demand for high purity and high productivity, various types of closed photobioreactors have been designed. Column reactors (Fig. I-2-b) allow high productivity due to effective bubble mixing, although scale up is somewhat difficult. Flat panel reactors (Fig. I-2-c,d) offer very high productivity owing to the short optical path length (OPL) combined with vigorous mixing with aeration (Hu et al., 1996, 1998b; Qiang and Richmond, 1996). Scaling up of flat panel reactors is easier than that with column reactors. A recent configuration of flat panel airlift reactor (Subitec, Germany; Fig. I-2-d) allows further mixing efficiency by placing airflow baffles.

One attempt to decrease the cost of a reactor is to increase the lifetime with glass tubes rather than plastics. While the initial cost is higher, reactor maintenance and renewal can be reduced. Moreover, scaling up of the reactor is one of the easiest among closed bioreactors, because the simple connection between tubes is enough for making the system larger (Borowitzka, 1999). However, since the mixing is implemented by pumping, the flow is rather closer to laminar than turbulent, making the photosynthetic efficiency lower than flat panel reactors unless the pumping speed is maintained at a high level (Molina et al., 2001).

The opposite way to reduce the cost of reactors is the utilization of plastic film as reactor material. While the lifetime of plastic bag reactors may become shorter ($\leq$ 1 year), the initial and renewal costs are low (Norsker et al., 2011). The reactor shape can be formed into virtually any

shape similar to the conventional photobioreactors such as tubular bag (Fig. I-2-e) and flat panel bag (Fig. I-2-f) reactors. While earlier studies on economic assessment concluded the cost superiority of open ponds (Richardson et al., 2012), recent improvements in reactor cost and productivity have led to higher cost-effectiveness with closed photobioreactors than open ponds (Norsker et al., 2011; Richardson et al., 2014). These improvements have opened up the way for further commercial applications of microalgae and cyanobacteria.

However, the "best" reactor is yet to be decided (Carvalho and Meireles, 2006; Posten, 2009; Chen et al., 2011). Although extremely high productivities were achieved with flat panel reactors (Hu et al., 1996, 1998a,b; Qiang and Richmond, 1996; Qiang et al., 1998), the required aeration rate was as high as 4.2 L L^{-1} min^{-1} for optimum growth. In an economic assessment, the energy requirement with flat panel reactors for less vigorous aeration (1 L L^{-1} min^{-1}) would occupy over 40% of the total production cost (Norsker et al., 2011), making the flat panel most expensive option. It was therefore implied that a reactor such that allows reduction in aeration energy consumption, while maintaining a high productivity, could support the cost-effectiveness of algal cultivation.

1.3. Benefit of high-density culture and problem of oxygen accumulation

For commercial microalgae production, high-density culture is demanded because of the high productivity and cost-effectiveness. Firstly, it has been known that high cell density culture in a short OPL of less than 5 cm enables higher areal productivity than that with a longer OPL (Richmond, 2013). Since a short OPL enables a rapid cell movement between the illuminated photic zone and dark zone, algae cells experience light-dark cycles in a range of milliseconds (Hu et al., 1998b). Since the photosystem unit turnover rate is 1 to 15 ms, the high-frequency light-dark cycle increases the photosynthetic efficiency (Dubinsky, 1992). The highest areal production would be achieved when the cell density is at the optimal cell density, at which only 5 to 10% of the

reactor depth is photic zone so that the light/dark duration is in less than 1 to 10 ratio (Richmond, 2013). If the algae are under strong light intensity continuously, on the other hand, the cells cannot utilize the light efficiently and may be subject to photoinhibition (Burlew, 1953).

Secondly, the dense culture reduces the total culture volume necessary to produce a certain amount of biomass compared to that with low-density open ponds (Christenson and Sims, 2011). The reduction in culture volume would reduce the water usage and labor for handling. Furthermore, dense biomass diminishes the cost and energy to harvest and concentrate or dry the biomass.

Despite the various advantages of high-density culture, it is vulnerable to oxygen (O_2) accumulation. In cultures of microalgae optimally supplied with CO_2, the dissolved O_2 (DO) concentration reaches over 400% in an open pond and over 600% in a closed reactor (Vonshak, 1997; Torzillo et al., 1998; Richmond, 2013). The time for the O_2 buildup to an inhibitory level is as short as 6 minutes in an *Arthrospira platensis* culture in an outdoor closed reactor (Vonshak et al., 1996). Oxygen buildup is problematic because higher O_2/CO_2 ratio stimulates the oxygenase activity of ribulose bisphosphate carboxylase oxygenase (RubisCO) which could eliminate the CO_2 fixation ability (Shelp and Canvin, 1980). Oxygen accumulation would also limit the rate of photolysis of water into oxygen, proton, and electron, because of the higher concentration of the end product (Carvalho et al., 2006). Moreover, oxygen accumulation may increase the photooxidative damage of the cells. Upon radiation with appropriate energy, oxygen radicals may develop during the respiratory gas exchange and cause toxic effects on cells due to membrane damage. The DO inhibition could lead to up to 30-60% decrease of *A. platensis* production (Marquez et al., 1995; Vonshak et al., 1996; Torzillo et al., 1998; Clausen and Junge, 2005). Many algal strains cannot survive in the significantly O_2-oversaturated environment longer than 2–3 h (Pulz, 2001). Therefore, it is necessary to consider efficient O_2 removal in high-density algal culture.

1.4. Current dissolved oxygen removal methods

Most classic and powerful dissolved oxygen (DO) removal method is aeration. Aeration

is commonly performed by bubbling through perforated glass or other gas diffusers placed at the bottom of a bioreactor or of a separate gas-exchanger unit. The oxygen mass transfer of aeration is relatively high. If directly supplied to the bioreactor, aeration also has an important role in mixing the culture. The disadvantage of aeration is the high energy consumption. In order to achieve the most effective O_2 removal in high-density culture, the air flow rate of over 3 L L^{-1} min^{-1} is desired (Hu et al., 1996). As described above (cf. section 1.2), the energy for aeration could exceed 40% of total production cost (Norsker et al., 2011). A less energy-intensive oxygen-removal method is desired.

Another recent O_2 removal technology is the use of fluorochemicals as an O_2 carrier (Lee et al., 2013). This method utilizes different types of liquid fluorochemicals that are not miscible with water and have a high O_2 dissolution. Since the chemicals have higher oxygen dissolution, when they are mixed with algal culture, they take up and retain DO. The liquid is eventually replenished with the recycled fluorochemical after N_2 gas sparging to remove DO. Although this method was effective in removing DO at lab-scale, the large-scale operation is difficult with the need for special apparatus to treat fluorochemicals.

One of potential O_2 removal methods is co-culture with other oxygen-consuming heterotrophic microorganisms such as bacteria, fungi, yeast, and heterotrophic microalgae. In such symbiosis, the heterotrophic organisms can consume photosynthetic oxygen for metabolizing organic compounds in the medium while producing CO_2, providing an optimum condition for microalgal growth (Fig. I-3). This system mimics the natural symbiotic relationship for the enhancement of microorganisms (Kazamia et al., 2012; Fuentes et al., 2016). Although this system has long been applied especially in wastewater treatment (Borde et al., 2003; Muñoz et al., 2003, 2006), few studies have focused on DO removal by the symbiotic microorganisms during high-density algal culture.

As a less energy-intensive alternative, gas-permeable membranes has been proposed to be

used for oxygen removal in a few papers and patents (Takizawa, 1993; Posten, 2009; Willson et al., 2009). Surprisingly, it was found that CO_2 mass transfer coefficient was higher with diffusion through hydrophobic microporous membrane than the direct contact of gas and water (Balgobin, 2012). Gas-permeable membranes, therefore, could allow gas exchange with a less interfacial area than bubbling.

Previous studies on the application of the gas-permeating films on microorganism culture focused on CO_2 supplementation. One of the major forms of CO_2 supplementation is using hollow fiber gas-permeable tubes (Carvalho and Malcata, 2001; Kumar et al., 2010b; Mortezaeikia et al., 2016). To date, little is known for the effectiveness of the oxygen removal efficiencies of gas-permeating films from microalgae culture. One patent suggests the use of a small-unit constructed with gas-permeable films incorporated with optical fiber to achieve attached growth of microalgae on the surface of the gas-permeable membrane (Takizawa, 1993). This method is effective in supplying CO_2 and removing DO. However, it can be expected that although the module was successful in a laboratory scale reactor, the complex structure may not be suitable for a large-scale operation. The possible application of hollow fiber modules may also suffer from difficulty in scaling up. Since the oxygen during outdoor culture could accumulate to an inhibitory level within 6 mins, the oxygen removal apparatus need to be set up quite frequently (Vonshak et al., 1996). Another study suggests insertion of a single tube made of gas-permeable film throughout a bag reactor (Willson et al., 2009). However, the interfacial area may not be large enough to remove the oxygen produced by a dense algal culture, and furthermore, the reactor would still need the mixture with aeration to efficiently create turbulence alongside the gas-permeating film. If a gas-permeating bag photobioreactor with enough interfacial area for photosynthetic oxygen removal can be developed, non-aerated microalgal culture may be possible, reducing the high cost for aeration. Therefore, the oxygen-removal efficiencies of various gas-permeating materials need to be evaluated for the development of a novel gas-permeating photobioreactor suitable for microalgae

culture.

1.5. Objectives

This Ph.D. thesis aims to improve the oxygen removal technology in high-density microalgae culture by achieving the following objectives:

1) To develop a novel gas-permeating bag photobioreactor through comparison of different film materials (Chapter II)
2) To critically compare the performance of the developed gas-permeating reactor with other existing oxygen removal techniques, especially algal-bacterial symbiosis (Chapter II), and
3) To construct an optimized operational model for non-aerated photobioreactor, combined with two-phase CO_2 supply system, and critically evaluate the performance of the process (Chapter III).

Thereafter, based on the obtained results Chapter II through Chapter III, the feasibility of the gas-permeating photobioreactor was evaluated in terms of electricity and cost-effectiveness as part of the general discussion (Chapter IV).

Figures

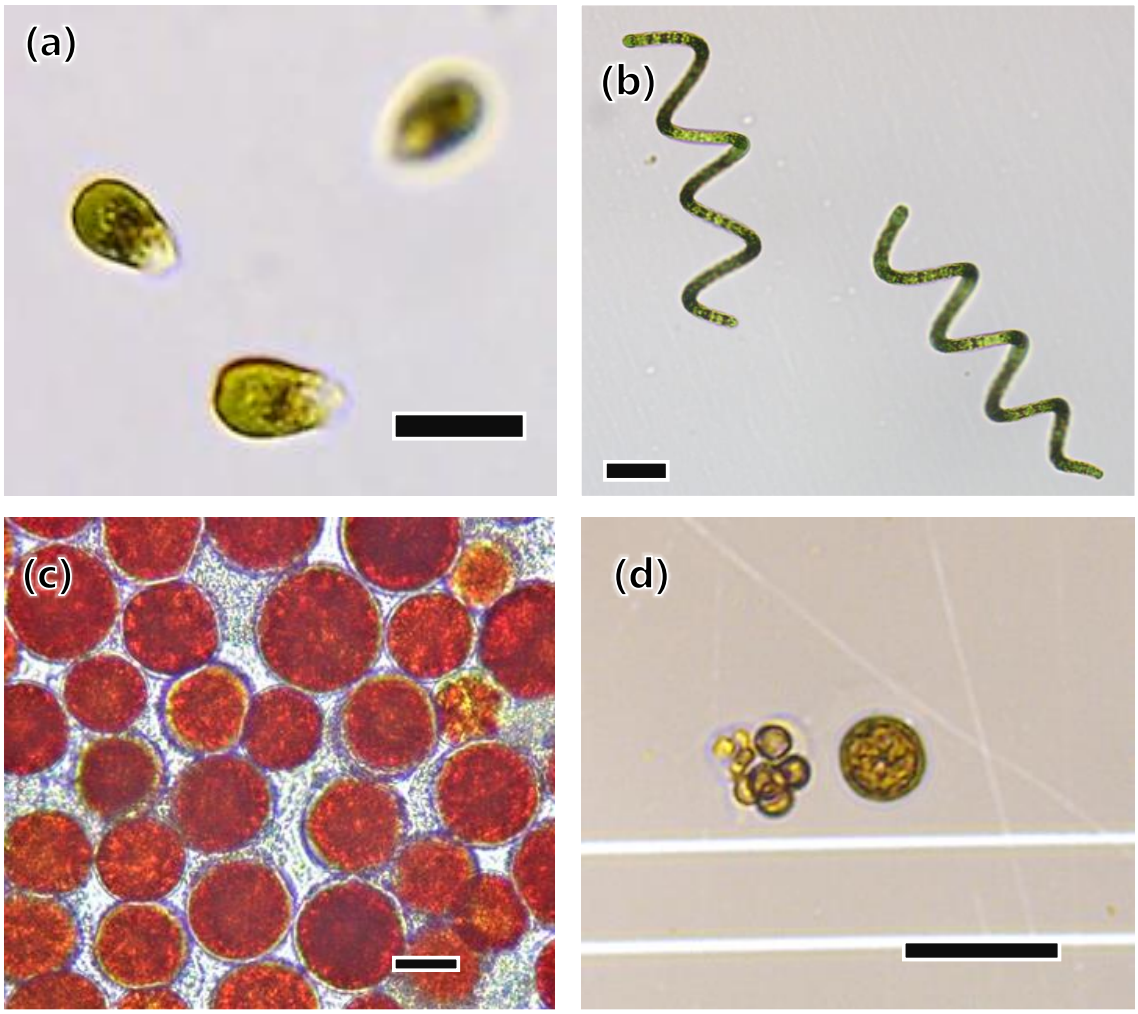

Fig. I-1. Major and potential commercial microalgal species (a) *Dunaliella salina* NIES-2257, (b) *Arthrospira* (Spirulina) *platensis* NIES-39, (c) *Haematococcus lacustris* (*pluvialis*) NIES-144, (d) *Chromochloris zofingiensis* ATCC-30412. All scale bars indicate 20 μm.

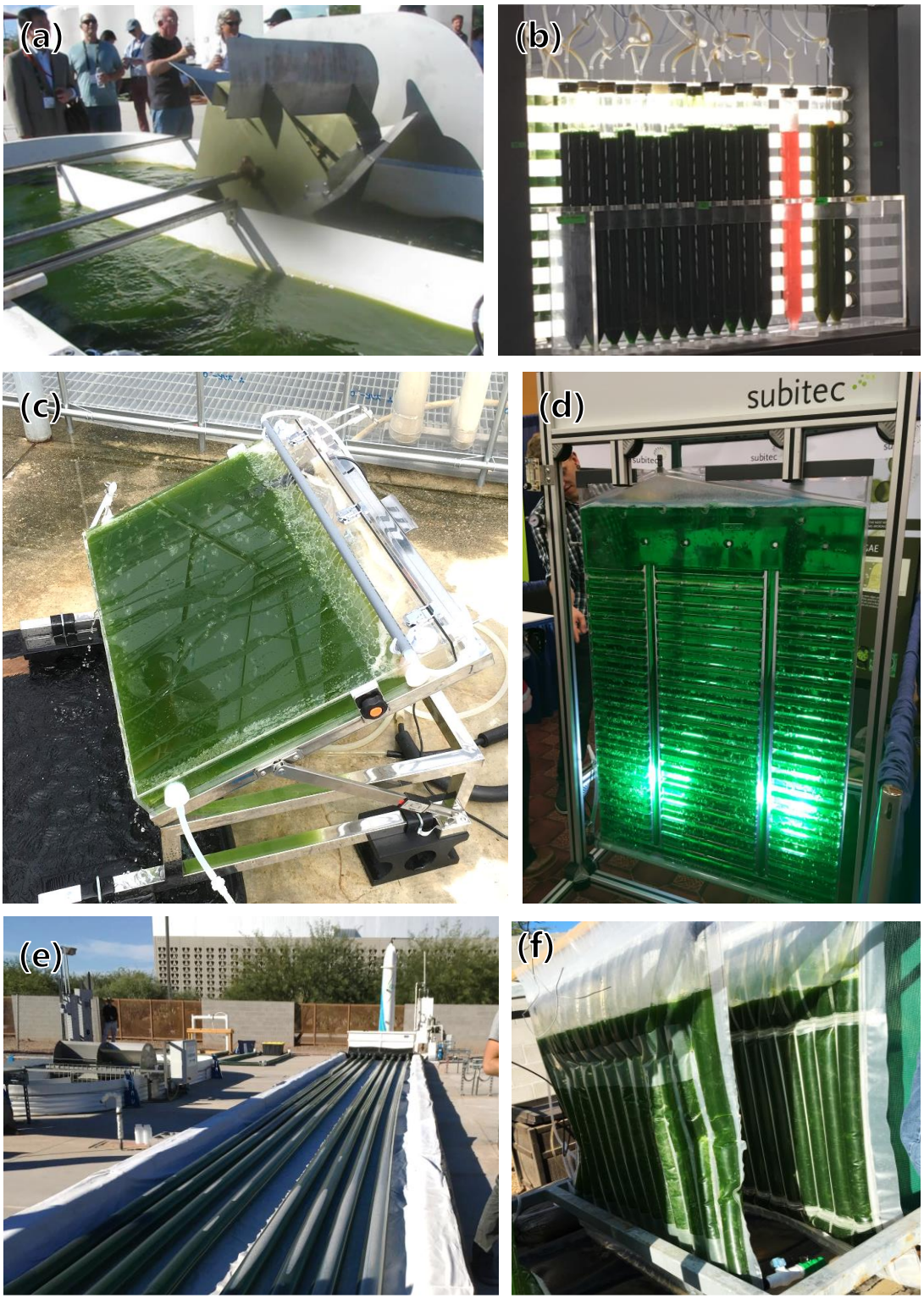

Fig. I-2. Various types of photobioreactors for microalgal culture (a) a raceway pond, (b) lab-scale column reactors, (c) a flat panel reactor, (d) a flat panel airlift reactor, (e) tubular reactors, (f) flat plastic bag reactors. (a,b,e,f: Aztec, Arizona University; d: Subitec Inc.)

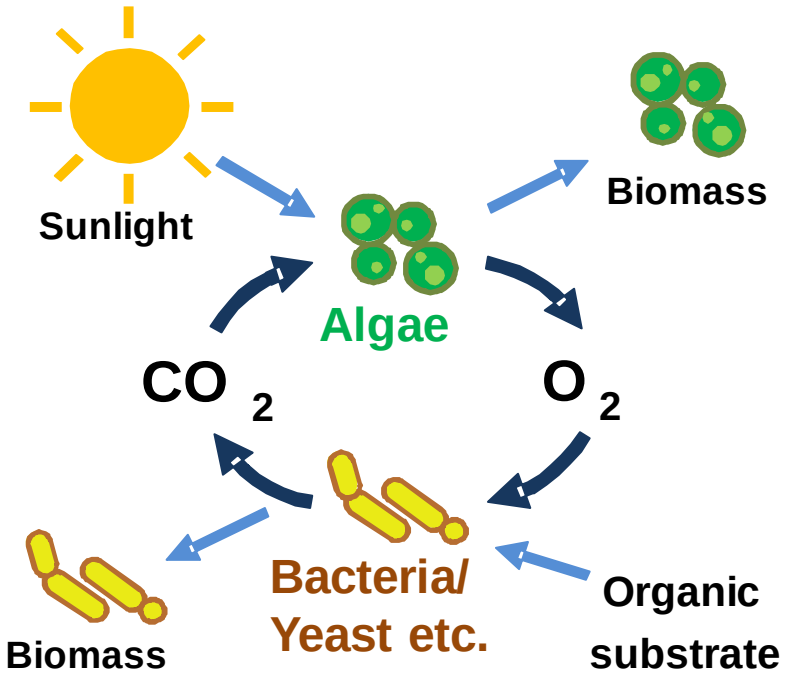

Fig. I-3. Symbiotic oxygen removal and carbon dioxide supply between algae and aerobic microorganisms (modified from Muñoz and Guieysse, 2006).

CHAPTER II

Development of a novel gas-permeating photobioreactor and comparative evaluation of its performance

2.1. Introduction

The proposed novel gas-permeating photobioreactor has the following targeted characteristics: (1) the reactor surface is made of the gas-permeating film; (2) the oxygen produced within the reactor is diffusively removed through the gas-permeating film; and thus (3) aeration in the culture is reduced. To achieve these targets, characteristics of gas-permeating films need to be studied.

A gas-permeating film commonly indicates a thin (< 1mm) film made of single or complex materials that permeate gases such as oxygen, carbon dioxide, and water vapor. Those gas-permeating films with little water permeability are widely applied to commercial products that require separation of liquids and gases, such as rain clothes, dehumidifying agents, and disposable heat packs. Other industrial applications include removal of volatile compounds from products through a process called “pervaporation”, such as organic solvents from industrial wastewater, water content from an organic solvent, and oxygen from fuel or drinking products (Uragami and Takigawa, 1990; Ito et al., 1998; Kujawski, 2000; Solak and Şanlı, 2008). While the materials of gas-permeating films are diverse, this study will focus on polymers owing to its inexpensiveness and relative easiness of handling. Gas-permeating polymer films can be further categorized into two groups: nonporous or porous. Nonporous films are made of dense material, such as silicone, polytetrafluoroethylene (PTFE), and butyl rubber, and the permeants are transported through the film by diffusion between polymer molecules (Balgobin, 2012). On the other hand, porous films can be made of various types of materials such as polyethylene (PE), polypropylene (PP), polycarbonate, and nylon. Gas permeation is mainly through the convective flow through the pores of the film. The pore sizes of the microporous film range between several nanometers to several

hundred micrometers.

The oxygen removal characteristics of the reactor should be comparably evaluated with other conventional oxygen removal technologies. While aeration is the most classical method to be compared, algal co-culture with heterotrophic microorganisms such as bacteria has a high potential. However, information regarding oxygen removal and growth enhancement by co-culture is not clearly evaluated so far. To correctly evaluate the symbiotic effect of bacteria onto algae, ethylene glycol (EG) was chosen as the substrate, since it has been reported that most algae, including *Chlorella fusca*, does not heterotrophically utilize EG (Kishi et al., 2015). By evaluating the algal-bacterial system with EG as a substrate, simple effects of O_2 removal and CO_2 supply between algae and bacteria can be rated.

In this study, a novel gas-permeating bag reactor was developed under the concept of a large interfacial area between the culture media and gaseous phase by making the outer layer of the bag reactor with a gas-permeating film. The oxygen removing characteristics and optical characteristics were evaluated for various gas-permeating films to be selected for the bag reactor material. The reactor design was determined by the empirical calculation of the oxygen removal characteristics. Finally, the oxygen removal characteristics were comparably evaluated with other oxygen removal technologies, especially with experimental results of the algal-bacterial system.

2.2. Materials and methods

2.2.1. Development of gas-permeating photobioreactor

2.2.1.1. Gas-permeable films

The oxygen permeability of various gas-permeating films (silicone, fluoropolymer, and microporous film) and non-permeating films (PE and PP) sheets were evaluated. Silicone rubber sheet (300 × 300 × 0.5 mm) was obtained from As One Corporation. Two types of fluoropolymers, Neoflon perfluoroalkoxy polymer (PFA) and fluorinated ethylene-propylene (FEP) were obtained from Daikin Industries, Ltd. The thickness of both PFA and FEP were 0.025 mm. Microporous film

was obtained from 3M, consisting mainly of polypropylene with a thickness of 0.038 mm and pore size of fewer than 0.3 μm. The polyethylene film was obtained from commercial PE bag (linear low-density PE; LLDPE) with a thickness of 0.025 mm. Polypropylene film, Piren P8128, was a one side heat-sealable oriented PP (OPP) film and was obtained from Toyobo Co. Ltd. Other than the microporous film from 3M, all other tested films were non-porous.

2.2.1.2. Evaluations of gas-permeable films as reactor material

The gas-gas oxygen exchange was measured with a differential pressure method (Fig. II-1), with a maximum pressure difference between above and below films being 0.24 MPa. In this method, the tested material was attached to the attachment with O rings tightly, and the bottom gas tank was vacuumed with a pump. The head pressure above the film was adjusted with oxygen gas cylinder at 0.24 MPa. The bulb toward the gas tank was firstly closed until the pressures above and beneath the film stabilized. After opening the bulb, the pressure change in the gas tank was observed and analyzed for the gas permeability of the films.

The liquid-gas oxygen permeation was measured using an acrylic reactor consisting of a liquid container filled with oxygen-saturated water and a gas container separated by the respective films (Fig. II-2). After filling the liquid container, bubbles were carefully removed from the liquid container. Dissolved oxygen (DO) was then continuously measured while it was being released from the surface of the film. The liquid was continuously stirred by a magnetic stirrer.

2.2.1.3. Bag reactors

Two types of bag reactors were created, (1) the gas-permeating bag reactor and (2) a conventional polypropylene (PP) bag reactor as a control under the same configuration except for the bag material. The reactor was made into 600 × 450 × 20 mm (height × width × thickness) with the microporous film and 0.02 mm PP film (Fig. II-3). The microporous film was heat-sealed to a PP film (thickness 0.02 mm) to construct a reactor.

Dissolved oxygen removal characteristics were evaluated with a decrease in DO

concentration from oxygen-saturated water under (1) continuous aeration, (2) continuous mixing of the water with a centrifugal pump, and (3) intermittent mixing for 12 secs in every 120 secs.

2.2.2. Algal-bacterial symbiosis

2.2.2.1. Microorganisms and pre-culture

Chlorella fusca Shihira et Krauss var. vacuolata NIES-2151, currently known as *Graesiella emersonii* (Shira & Krauss) Nozaki et al., was obtained from the National Institute of Environmental Studies Collection (Tsukuba, Japan). Bacterial inoculum was prepared by filtering activated sludge (Kitano Sewage Treatment Plant, Tokyo, Japan) with GF/C (Whatman, UK) filter so that it does not contain bacterivorous or algivorous protist. Both inoculums were cultured with mineral salt medium (MSM) (Muñoz et al., 2004) with 14,000 mg L^{-1} of ethylene glycol (EG). The experimental cultures were inoculated with the both organisms at their late log-growth phases.

2.2.2.2. Experimental setup

Four experimental conditions were prepared in triplicates: (1) *C. fusca,* (2) bacteria, (3) algal-bacterial consortium, and (4) *C. fusca* without EG (*C. fusca*-EG) (Table II-1). The condition 4 was tested to identify potential growth inhibition by EG on *C. fusca* by comparing its growth with condition 1. In the all conditions, microorganisms were cultured with MSM, and conditions 1-3 received 14,000 mg L^{-1} of EG. All microorganisms were cultured in 1-L cylindrical glass bottles. To simulate a non-aerated outdoor condition, headspaces were continuously replaced with aseptic air at 0.5 L min-1. The cultures were continuously agitated with magnetic stirrers. The bottles were incubated with temperature 25°C and photosynthetic photon flux density (PPFD) 300 μmol m-2 s-1 at 12-h:12-h light and dark cycle.

2.2.3. Analytical parameters

Ethylene glycol concentration was determined using a gas chromatograph equipped with a packed column (Shincarbon A) and flame ionization detector (GC-9A, Shimadzu, Japan). The column was maintained at 140°C, and both injector and detector temperatures were 280°C. The

carrier gas was helium and was introduced at 40 mL min^{-1}. Dissolved oxygen (DO) was measured using a portable DO meter (SG68 and Seven2Go S9, Mettler Toledo AG, Switzerland), and pH was measured with a portable pH meter (D-51S, Horiba, Japan). Algal cells and bacterial cells were counted with a fluorescent microscope (Zeiss, Germany) using epifluorescence and a fluorescent dye (SYBR Gold, Thermo Fisher, USA) as previously reported (Shibata *et al.*, 2006), respectively. To separate algal-bacterial flocs, samples were sonicated for about 5 mins before measurements. The optical characteristics of the films were evaluated with a spectrophotometer equipped with an integrating sphere.

2.2.4. Calculations

Gas-gas transfer rate (GTR; mol m^{-2} Pa^{-1}) was calculated using the following equation:

$$GTR = \frac{V_c}{R \times T \times A(P_1 - P_2)} \times \frac{dP_2}{dt} \quad (1)$$

where V_c is the gas tank volume (0.001 m^3), R is the gas constant (8.31 Pa m^3 K^{-1} mol^{-1}), T is temperature (K), A is the area of tested film (m^2), P_1 and P_2 are pressure above and below the film, respectively. The Eq. 1 was integrated to obtain the following equation:

$$-\frac{V_c \ln(P_1 - P_2)}{R \times T \times A} = GTR \times t \quad (2).$$

The slope of the graph between the left side of Eq. 2 and time t was estimated with the linear regression to obtain the GTR. The gas permeability coefficient (P) of the film was obtained by the following equation:

$$P = GTR \times d \quad (3)$$

where d is the thickness of the film (m).

The DO change during the liquid-gas dissolved oxygen removal test was used to calculate the oxygen transfer rates of respective films. For the estimation of K_La, Eq. 6. was integrated to obtain the following equation:

$$\ln \frac{C^* - C}{C^* - C_0} = -K_L a \times t \quad (4).$$

Oxygen removal rate in the algal-bacterial symbiosis was estimated by summing the oxygen transfer rate from the atmosphere and the photosynthetic oxygen production rate (P_{O_2}) calculated based on algal biomass production rate using the following equation:

$$P_{O_2} = \frac{P_x}{Y_o} \quad (5).$$

where P_x is the biomass production rate (gDW L^{-1} d^{-1}) and Y_o is the ratio between biomass and produced oxygen (1.97 g oxygen per 1 g of biomass; Torzillo et al., 1998).

2.3. Results and discussion

2.3.1. Development and evaluation of gas-permeating photobioreactor

2.3.1.1. Evaluation of gas-permeable films and selection for photobioreactor

The gas-gas oxygen permeabilities of each film exhibited large differences. The two dense non-porous gas-permeable films, silicone and PFA, exhibited approximately 80 times higher oxygen permeability coefficient than PE films, which is known to be relatively less permeable (Fig. II-4). There was an apparent contradiction with some previous studies (Côté et al., 1989; Balgobin, 2012), which reported low oxygen permeabilities of fluoropolymers unlike the current study. The reason seemed to be the vague naming of various fluoropolymers using the trademark “Teflon”. Common names such as Teflon and Neoflon include various fluoropolymers including highly permeable PTFE, PFA, and FEP, as well as hardly permeable PCTFE. On top of the non-porous gas-permeable film, microporous film exhibited approximately 3,000 times higher permeability coefficient than silicone and PFA (Fig. II-4). The reason for this extremely high permeability could be attributable to the large pore size (< 300 nm) compared with the molecular size of oxygen, approximately 0.63 nm; calculated from Van der Waals radius of 0.158 nm (Batsanov, 2001). In a porous membrane with relatively large pores (0.1 to 10 μm), convective flow (Fig. II-5-a) would be the dominant movement of the molecules (Barker, 2000; Balgobin, 2012). On the other hand,

with dense permeable polymers, such as silicone rubber, diffusion within the film becomes the rate-limiting factor (Fig. II-5-b). It was therefore suggested that microporous film should be the most potent material for the gas-permeable bag reactor owing to its high oxygen transfer coefficient.

In order to design an gas-permeating bag reactor that possess sufficient oxygen removal characteristics, the oxygen transfer needs to be studies. The oxygen transfer rate (OTR) from liquid to gaseous phase is determined by the volumetric mass transfer coefficient $K_L a$ and the concentration gradient between the two phases:

$$OTR = \frac{dC}{dt} = K_L a(C^* - C) \quad (6)$$

where C is the oxygen concentration in the liquid phase, and C* is the equilibrium concentration of oxygen between the gaseous phase and the liquid phase. The volumetric mass transfer coefficient, $K_L a$, is a product of the overall mass transfer coefficient K_L (time^{-1}) and the total specific interfacial area available for mass transfer a (m^{-1}). The overall resistance of permeation (reciprocal of K_L) is the sum of several resistance parameters:

$$\frac{1}{K_L} = \frac{1}{Hk_g} + \frac{1}{Hk_m} + \frac{1}{k_L} \quad (7)$$

where H is Henry's coefficient, and kg, km, and kL are mass transfer coefficient in the gas film, within membrane, and liquid boundary layer, respectively (Carvalho and Malcata, 2001). Increase in a would proportionally increase the oxygen transfer rate, and therefore, the surface area of gas-permeable film should be designed to be large enough to remove oxygen produced by algal photosynthesis.

The liquid-gas oxygen transfer rate was then measured using the microporous film and PE as a control. As a result, $K_L a$ of the microporous film was 0.0252 min^{-1}, which was close to 30 times higher value than that of PE (Fig. II-6). Interestingly, the difference of $K_L a$ was not as large as the difference in the permeability coefficient P in gas-gas permeability test. The underlying mechanism could be the difference in the rate limiting factors of oxygen transfer. With a

hydrophobic microporous film, such as that used in this experiment, pores are filled with gases, and the liquid boundary layer exists at the end of the pore (Fig. II-5-c). According to a previous study, the resistance imposed by the microporous membrane material ($1/k_m$) becomes much less than those by gas and liquid boundary layer ($1/k_g$ and $1/k_L$) in Eq. 7 (Carvalho and Malcata, 2001). Therefore, unlike the case of gas-gas permeation, gas diffusion through the liquid-gas boundary layers becomes the rate limiting factor. On the other hand, the resistance from PE film ($1/k_m$) was much larger than the $1/k_g$ and $1/k_L$ that overall resistance ($1/K_L$) became larger than the microporous film. Although many gas-permeation studies have used silicone rubber, it is more expensive, thicker, and exhibit a higher mass transfer resistance than microporous membranes (Duan et al., 2010). Thus, the liquid-gas oxygen transfer again suggested that microporous film was a suitable material for creating gas-permeating bag reactor.

However, the optical properties of the microporous film indicated difficulty of using the microporous film for a wide area of surface of a bag reactor. While the transmittance of silicone and PE films were high (above 80%), the average transmittance of the microporous film was less than 20% (Fig. II-7). For algal culture, light transmittance is a crucial parameter to maintain high photosynthetic activity of microalgae, if the material is placed on the front surface of the bag reactor. On the other hand, the optical reflectance of the film was close to 80%, indicating that most light exposed to the film is not absorbed but reflected. A bag reactor design with consideration to this optical property may enable an efficient use of the microporous film.

2.3.1.2. Design and construction of gas-permeating photobioreactor

The novel gas-permeating photobioreactor was designed based on the evaluation of the microporous film (Fig. II-3). Firstly, the specific interfacial area of the bag reactor was designed based on the liquid-gas oxygen transfer coefficient (c.f. 2.3.1). The K_L of the microporous film was calculated based on K_La 0.025 min^{-1} and the specific interfacial area 16.7 m^{-1}, which resulted in the K_L to be 0.0015 m min^{-1} in this setting. Based on assumption that the same moles of O_2 are produced

as much as the moles of CO_2 fixed by the cyanobacteria, the required specific surface to maintain relatively less inhibitory DO 200% with biomass production rate 1.0 gDW L^{-1} d^{-1} was calculated to be 88 m^{-1}, which was assumed to increase K_La to 0.13 min^{-1}. Secondly, based on the optical characteristics of the microporous film, the bag reactor was deigned to have the microporous film on its backside (Fig. II-3). This configuration was suggested to be effective in fully utilizing the light provided to it, since the film can return the unutilized light back to the algal culture.

The DO removal efficiency of the constructed gas-permeating reactor was tested with oxygen-saturated water. The K_La of the gas-permeating reactor and the non-gas-permeable PP reactor were evaluated under three conditions: aeration, continuous mixing, and intermittent mixing. Well-fitted regression lines were able to be drawn even with intermittent mixing (Fig. II-8). The K_La of the gas-permeating reactor increased from 0.025 to 0.084 ± 0.006 min^{-1} under the continuous mixing (Fig. II-9). Although the K_La was lower than the target value (0.13 min^{-1}), probably due to the difference in mixing condition from the preliminary DO removal experiment, the value was almost 20 times higher than that of the conventional PP bag reactor (0.0033 ± 0.0001 min^{-1}). Furthermore, the decrease in mixing frequency from continuous to 12 sec every 120 sec (10-fold decrease) was found to only decrease the K_La to 0.045 ± 0.005 min^{-1}, probably owing to the continued oxygen diffusion even without mixing. It was demonstrated that the gas-permeating reactor constituting the microporous film was effective in removing DO without aeration.

2.3.2. Oxygen removal with algal-bacterial system

2.3.2.1. Growth and EG utilization

Algal cell counts of *C. fusca* and *C. fusca*-EG were similar (Fig. II-10-a), and there was no significant difference between the two (Student's t-test; $P > 0.05$) except for Day 14.5 ($P = 0.04$). It was shown again that *C. fusca* does not heterotrophically utilize EG for growth. On the other hand, both algal cell count and bacterial cell count increased in algal-bacterial consortium (Fig.

II-10-a,b) compared with algae-only or bacteria-only cultures. While the maximum algal specific growth rate of *C. fusca* was 0.46 d^{-1}, that of consortium was enhanced by more than 2-fold to 0.96 d^{-1}. Similarly, the maximum bacterial specific growth rate increased in the consortium (1.94 d^{-1}) compared with the bacteria monoculture (1.45 d^{-1}). The underlying mechanism of the growth enhancement both in algal and bacterial production should be the exchange of photosynthetic O_2 and respiratory CO_2 from EG decomposition. EG was most rapidly utilized in the consortium (Fig. II-11). During decomposition, oxygen was rapidly depleted (Fig. II-12-b) even with a relatively high algal oxygen generation, and DO dropped to less than 0.1 mg L^{-1} and remained near 0 mg L^{-1} till the end of the experiment. Even in the consortium, despite the highest photosynthetic oxygen supply, bacteria consumed most of the oxygen. Since the lower O_2/CO_2 ratio enhances CO_2 fixation by RubisCO (Peng et al., 2013), the enhancement of algal growth can be attributable to both lowered O_2 concentration and increased CO_2 availability. The growth of algae, however, eventually ceased its growth in the consortium probably because of the nutrient depletion. Nitrate (NO_3^-) concentrations reached near depletion both in bacteria and consortium culture on Day 6.5 (Fig. II-13).

As previous studies have suggested (Oswald et al., 1953; Bell, 1980; Imase et al., 2008), this study confirmed that microalgae and bacteria can create a symbiotic relation, in which growth is enhanced through the accelerated exchange of O_2 and CO_2 within the small community of microorganisms. Since the gas exchange occurs in a microscale, algal-bacterial consortium does not require vigorous mixing to achieve the O_2/CO_2 exchange between algae and bacteria. Therefore, algal-bacterial consortium is an effective energy-saving measure to oxygen accumulation inside reactors.

2.3.3. Comparative evaluations of various oxygen-removing technologies

The oxygen removal ability, energy and mixing requirement, and applicability of (1)

aeration, (2) algal co-culture, and (3) the gas-permeating reactor were compared (Table II-2). In this study, the oxygen removal was higher for aeration and gas-permeating reactor than co-culture. Both aeration and gas-permeating film are more efficient when there is a large difference between the DO and gas O_2 concentration. On the other hand, algal-bacterial oxygen removal is rather constant, since it depends on bacterial respiratory activity. Assuming a relatively high biomass production rate of 1 gDW L^{-1} d^{-1}, the O_2 production rate can be estimated to be approximately 1.97 gO_2 L^{-1} d^{-1} (Torzillo et al., 1998). Based on K_La for aeration and gas-permeating reactor of 0.27 and 0.084 min^{-1} (Fig. II-9), respectively, the equilibrating DO concentrations with the above O_2 production rate were calculated to be 135% and 213%, respectively. On the other hand, the oxygen consumption rate by bacteria in algal-bacterial consortium was 0.24 gO_2 L^{-1} d^{-1}, exhibiting much lower oxygen consumption than the assumed oxygen production. If this rate is maintained, it would only take 10 mins for the culture DO to reach 300%, and the DO would increase further until the algal photosynthetic O_2 production decreases with O_2 inhibition. The O_2 consumption rate by bacteria may have been limited by O_2 availability, in this study and may increase with greater O_2 supply.

In terms of energy consumption, co-culture and the gas-permeating reactor are advantageous over aeration. It was demonstrated for the gas-permeating reactor that an intermittent mixing of culture (1:10 interval) would only reduce the oxygen mass transfer coefficient by half. Similarly, co-culture only required moderate magnetic stirrer for oxygen removal. Some disadvantages of the algal co-culture, however, are (1) shading of algal cells by symbiotic organisms especially with high-density culture, (2) potential growth of unwanted microorganism due to substrate addition, and hence (3) limited applicability. Therefore, the gas-permeating reactor seems to be a good energy-efficient algal culture method especially for high-density pure culture.

2.4. Conclusions

The present study demonstrated the effectiveness of the microporous-based oxygen-permeable bag reactor removal of dissolved oxygen inside a reactor. The microporous film was found to have higher mass transfer coefficient than dense films such as silicone. The performance and applicability of the developed reactor was found to be superior to algal co-culture system. Since the cost of the microporous film is relatively cheap compared to silicone rubber and fluororesin, the application of the method in this study may improve the cost-effectiveness of high-value microalgae biomass production.

Tables

Table II-1. Experimental setup of algal-bacterial experiment

Run	Organisms	Ethylene glycol (mg L^{-1})
Consortium	*C. fusca* + Bacteria	14,000
Bacteria	Bacteria	14,000
C. fusca	*C. fusca*	14,000
C. fusca -EG	*C. fusca*	0

Table II-2. Comparative evaluations of different oxygen-removing technologies for microalgal culture.

	Oxygen removal	Energy	Mechanical mixing	Applicability
Aeration	High	High	Not necessary	Wide
Co-culture	Low ~ medium	Low	Moderate	Limited
Gas-permeating	Medium	Low~Medium	Necessary	Wide

Figures

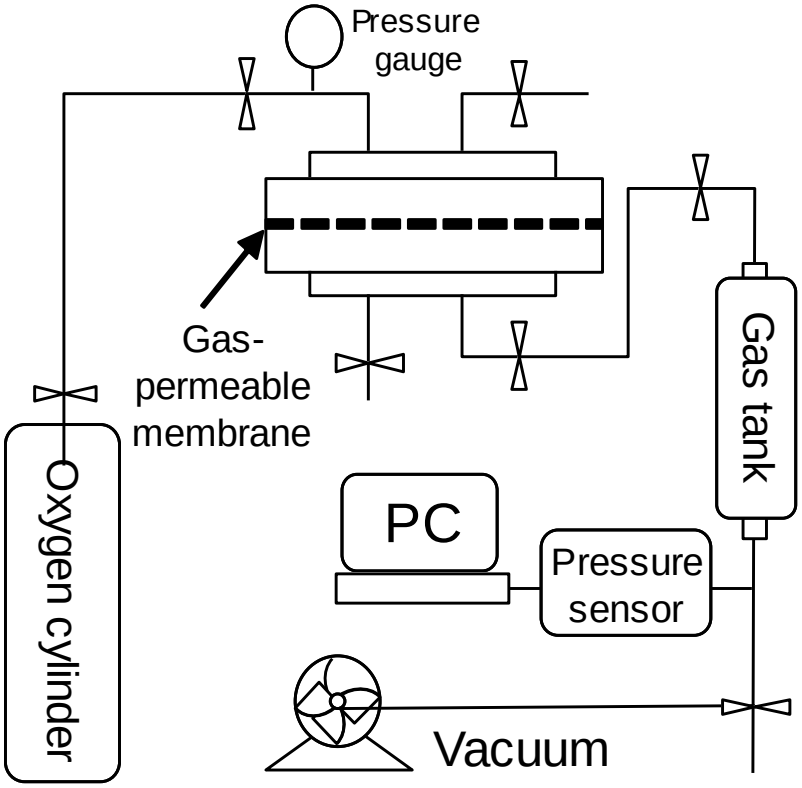

Fig. II-1. Analytical apparatus for the gas-gas oxygen permeability measurement.

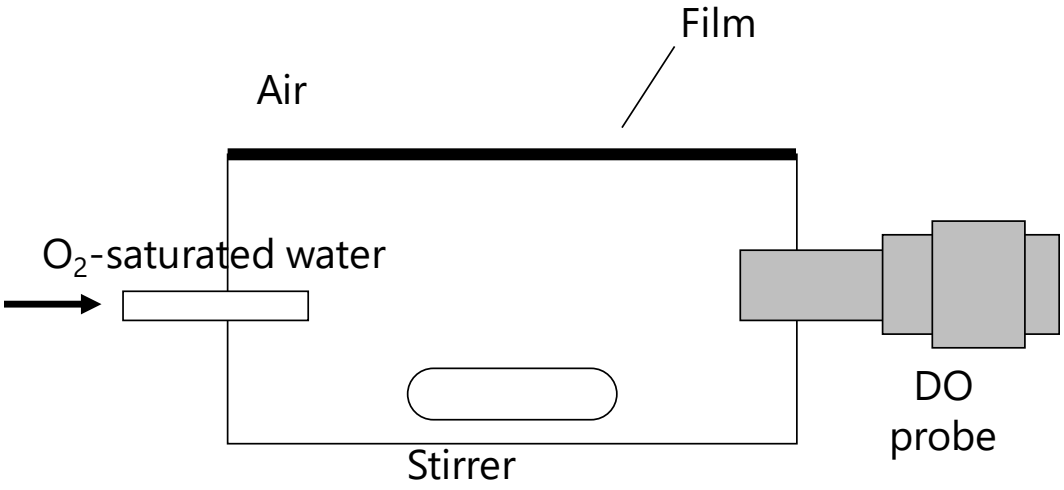

Fig. II-2. Analytical apparatus for the liquid-gas oxygen permeability measurement.

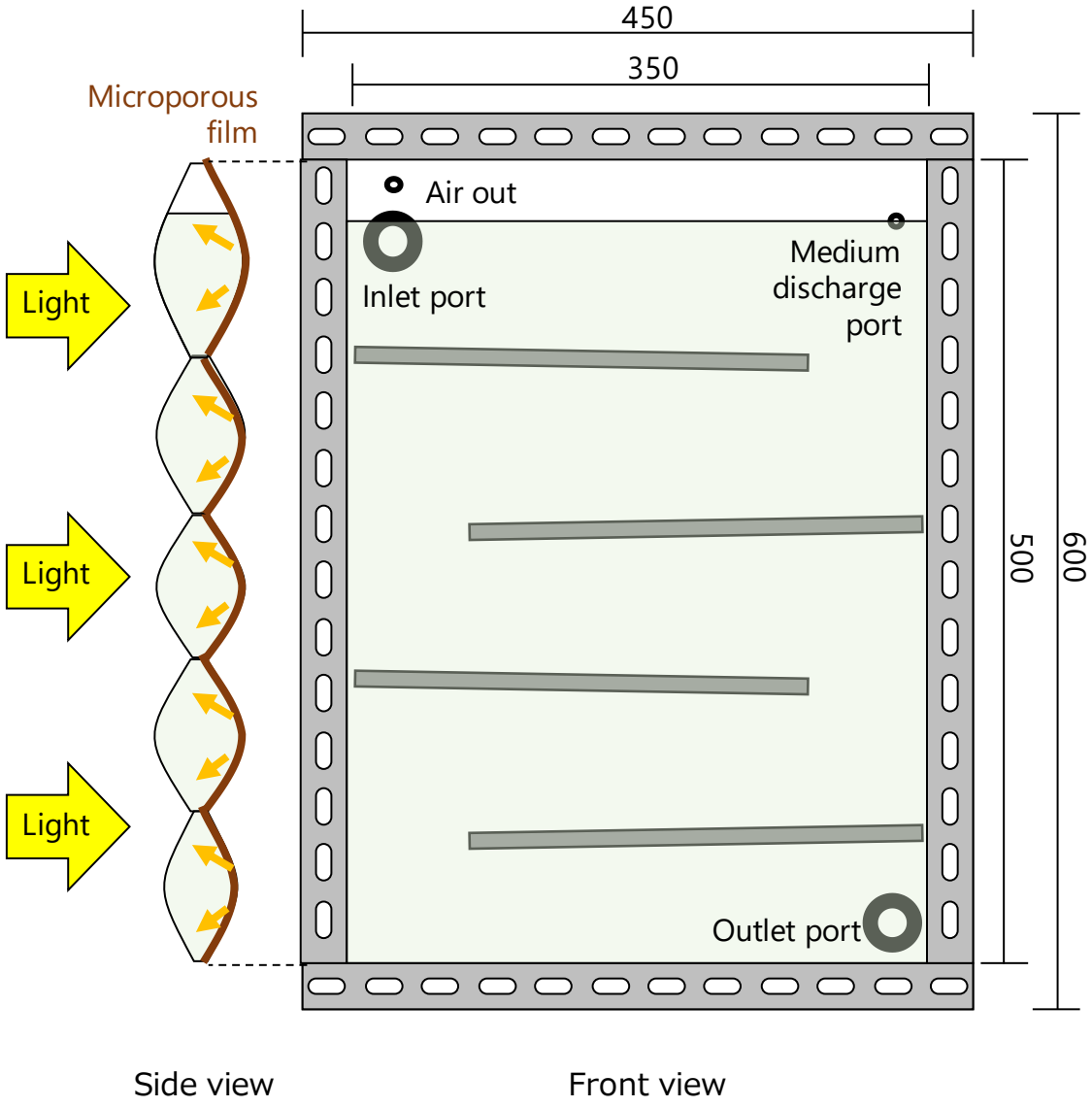

Fig. II-3. Schematic diagram of the constructed bag reactor. The gas-permeable bag reactor was created by attaching the microporous film to polypropylene film on the backside of the reactor. The polypropylene and microporous bag reactors were designed to be horizontally flipped. All units are in millimeters.

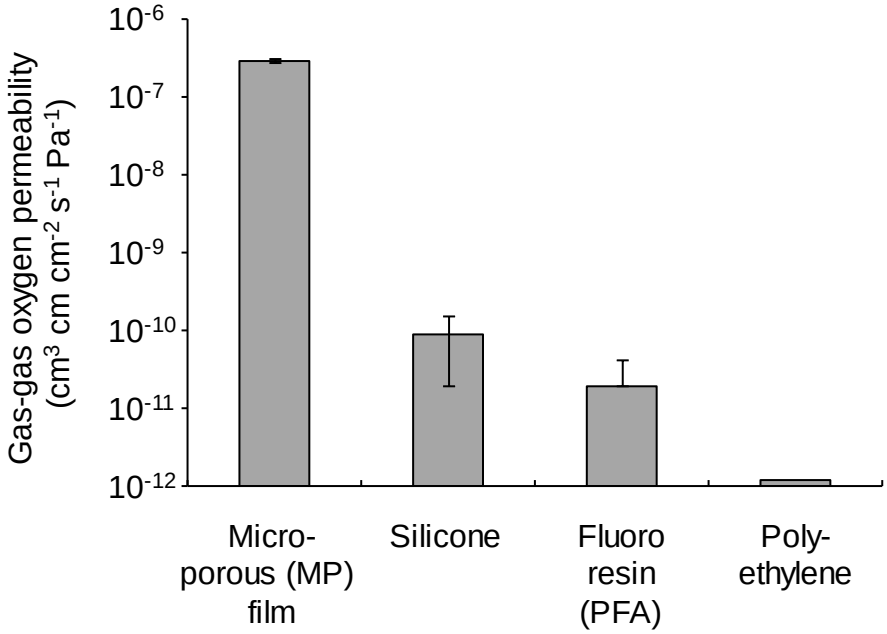

Fig. II-4. Gas-gas oxygen permeability of various plastic materials under the pressure difference method.

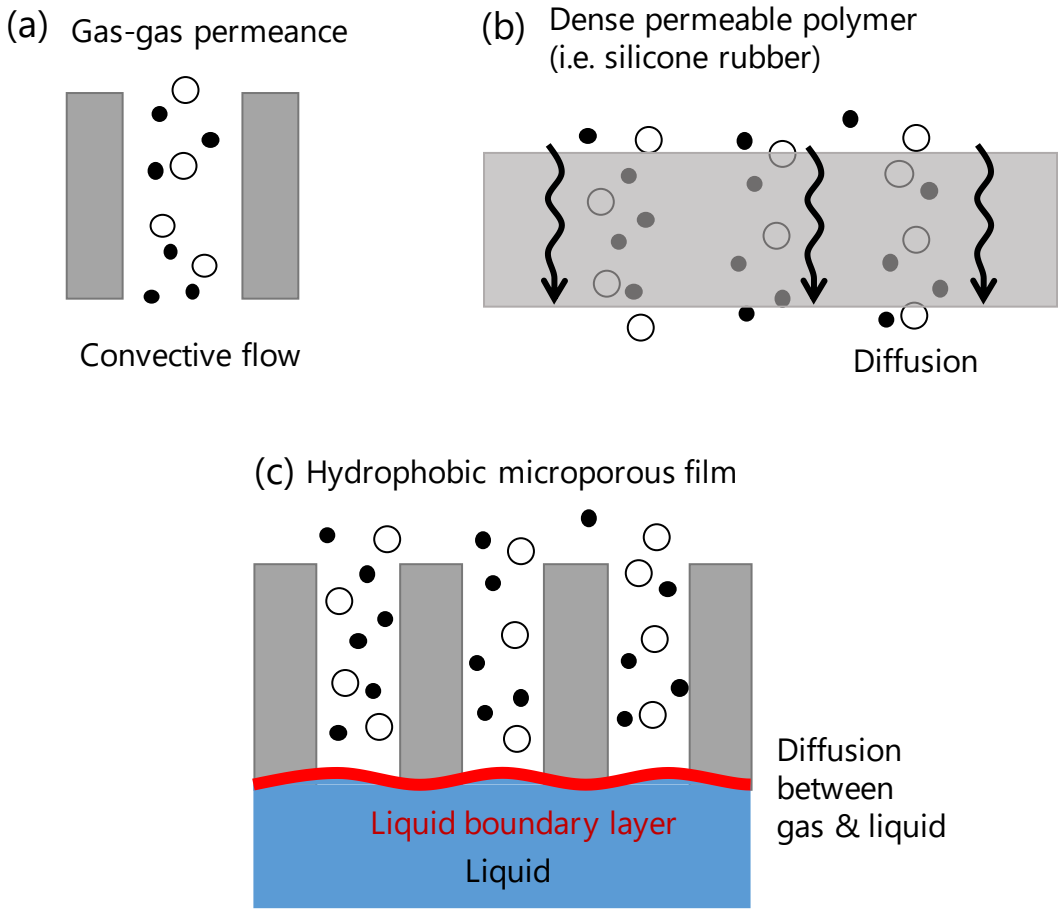

Fig. II-5. Various types of transfer of gases through gas-permeable membrane (Barker, 2000; modified from Balgobin, 2012).

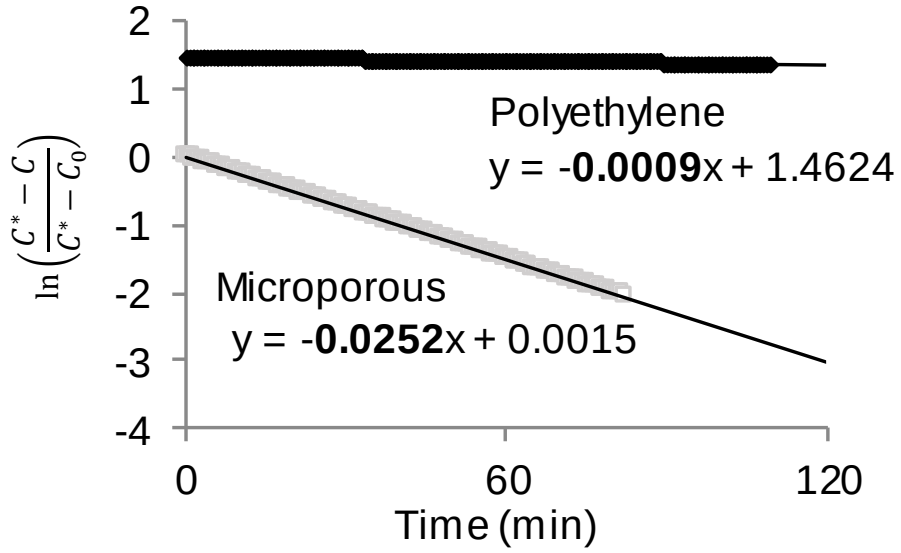

Fig. II-6. Dissolved oxygen removal properties of microporous film and polyethylene film. The slopes of the fitted lines indicate the K_La. C: dissolved oxygen (DO) concentration; C*: dissolved oxygen saturation concentration at gas-liquid interface; C_0: initial dissolved oxygen concentration.

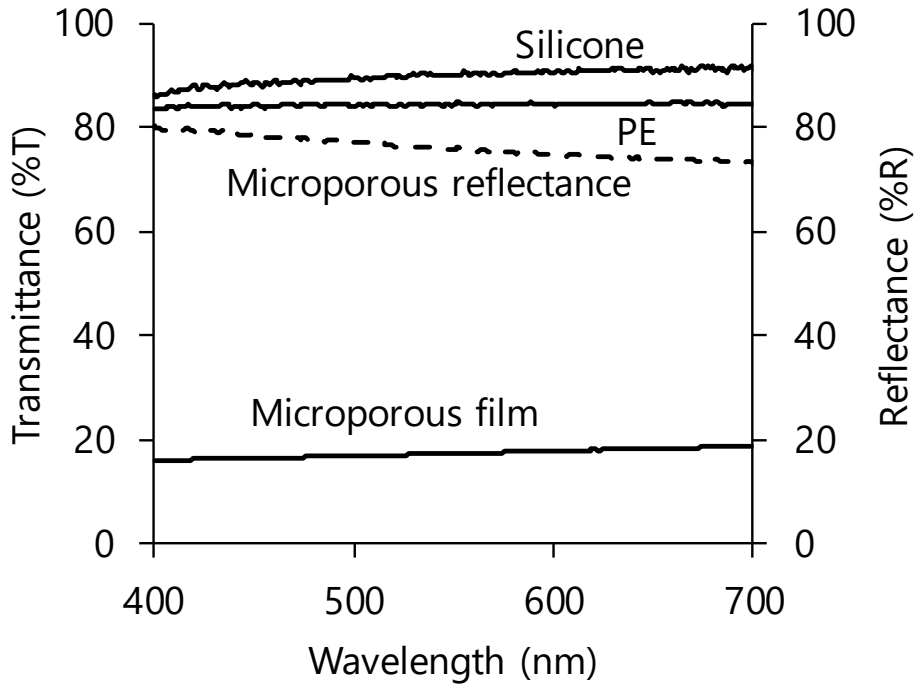

Fig. II-7. Optical properties of selected films. Solid lines are transmittance of silicone, polyethylene (PE) and microporous film. The dashed line is the reflectance of the microporous film.

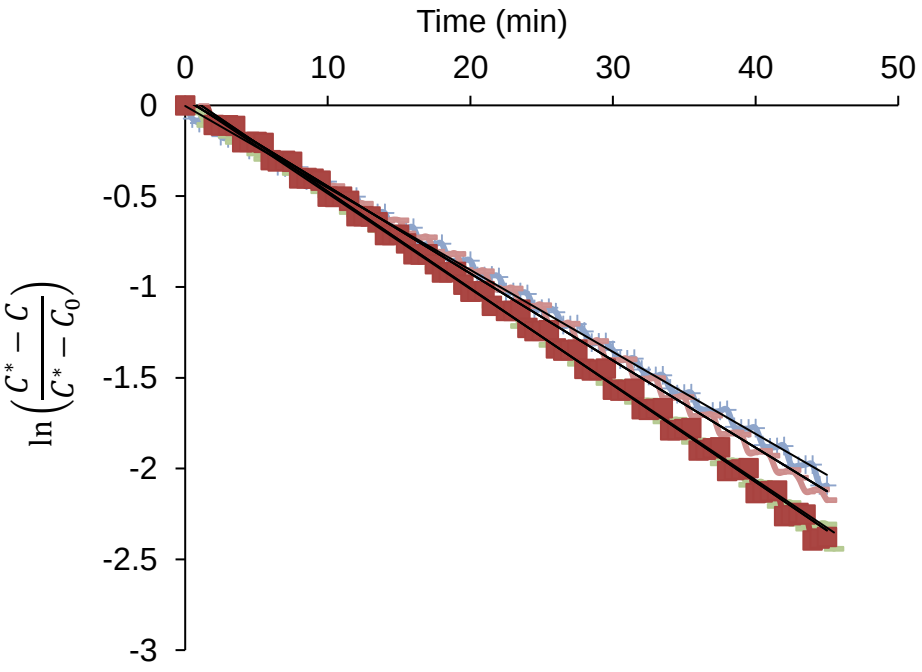

Fig. II-8. Typical oxygen removal curves of intermittent aeration (12 sec in 2 mins) in the developed gas-permeating photobioreactor. Each symbol represents replicates of the same condition (N = 4). *C*: dissolved oxygen (DO) concentration; *C**: dissolved oxygen saturation concentration at gas-liquid interface; C_0: initial dissolved oxygen concentration.

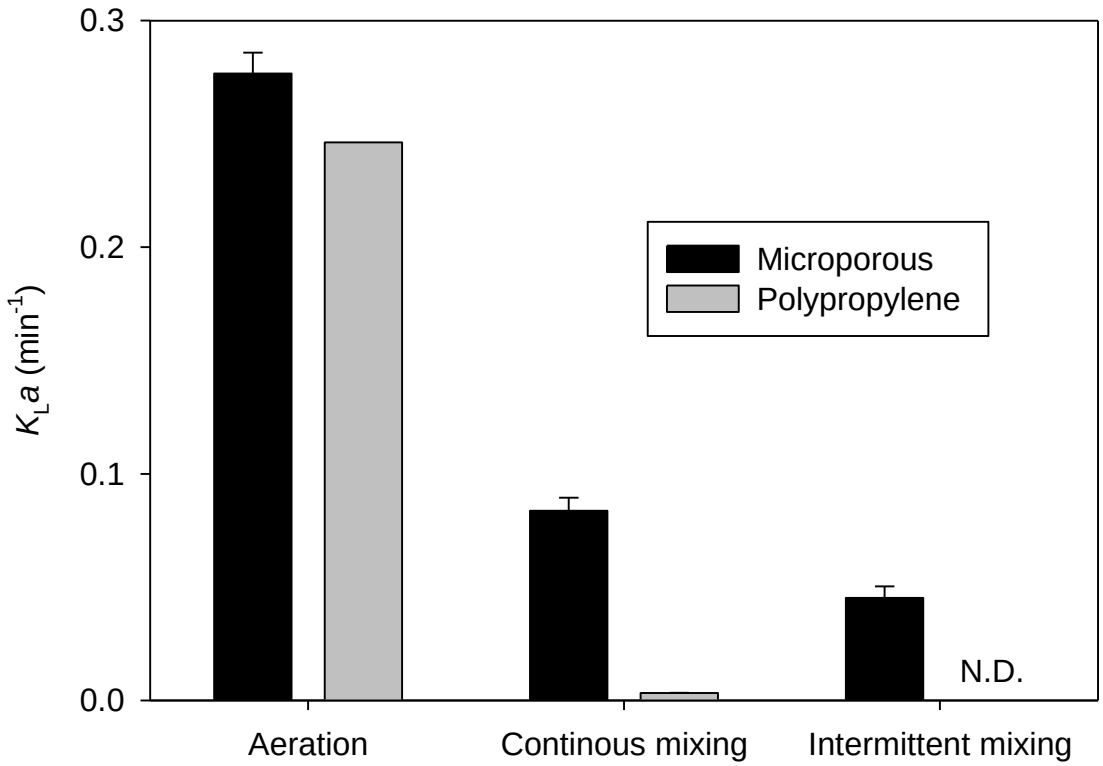

Fig. II-9. Oxygen mass transfer coefficients (K_La) of bag reactors composed of microporous films (black) and polypropylene (grey). Aeration: continuous aeration. Continuous mixing: mixing by centrifugal pump within reactor continuously. Intermittent mixing: mixing by centrifugal pump for 12 secs in every 120 secs. N.D.: no data.

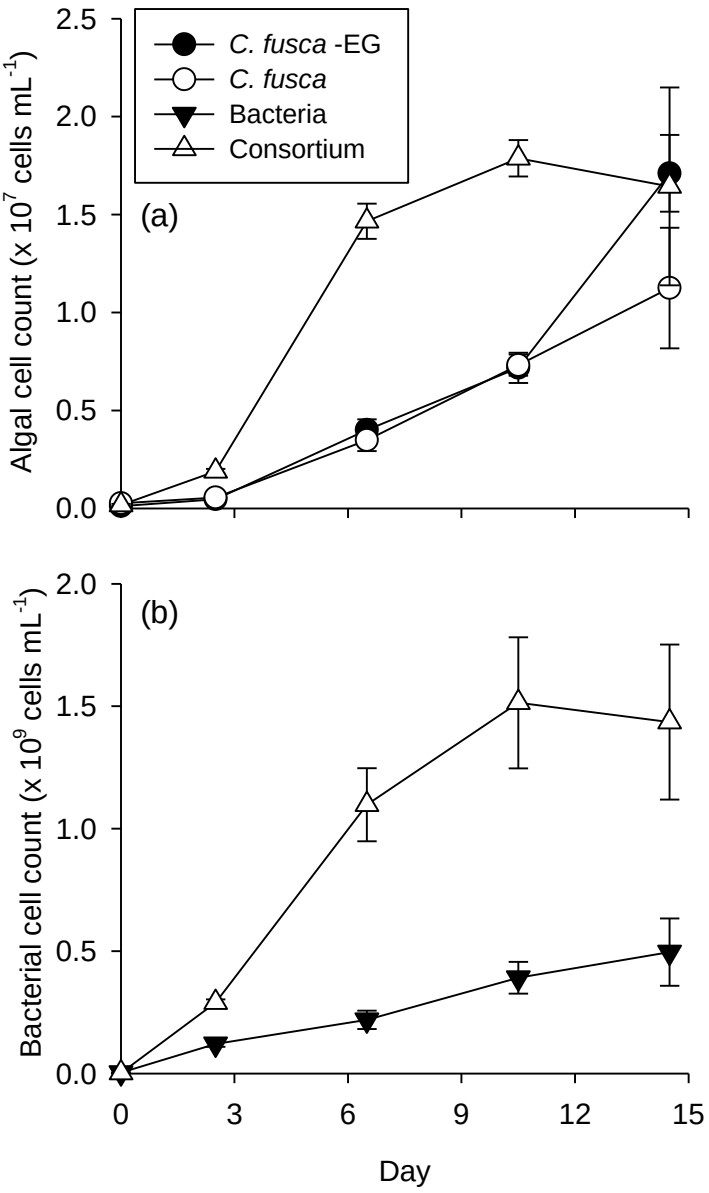

Fig. II-10. Enhancement of the growth of a green alga *Chlorella fusca* oxygen removal by bacterial consortium: (a) algal cell count and (b) bacterial cell count (modified from Kishi et al., in press).

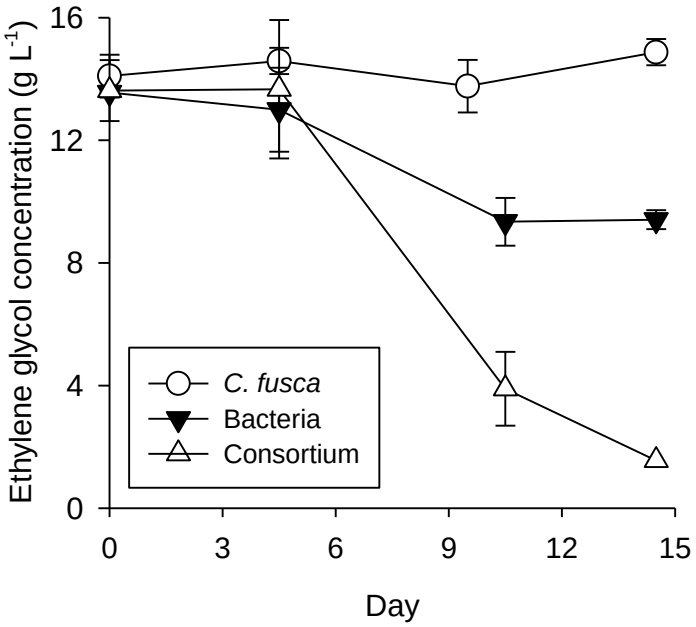

Fig. II-11. Ethylene glycol utilization (modified from Kishi et al., in press).

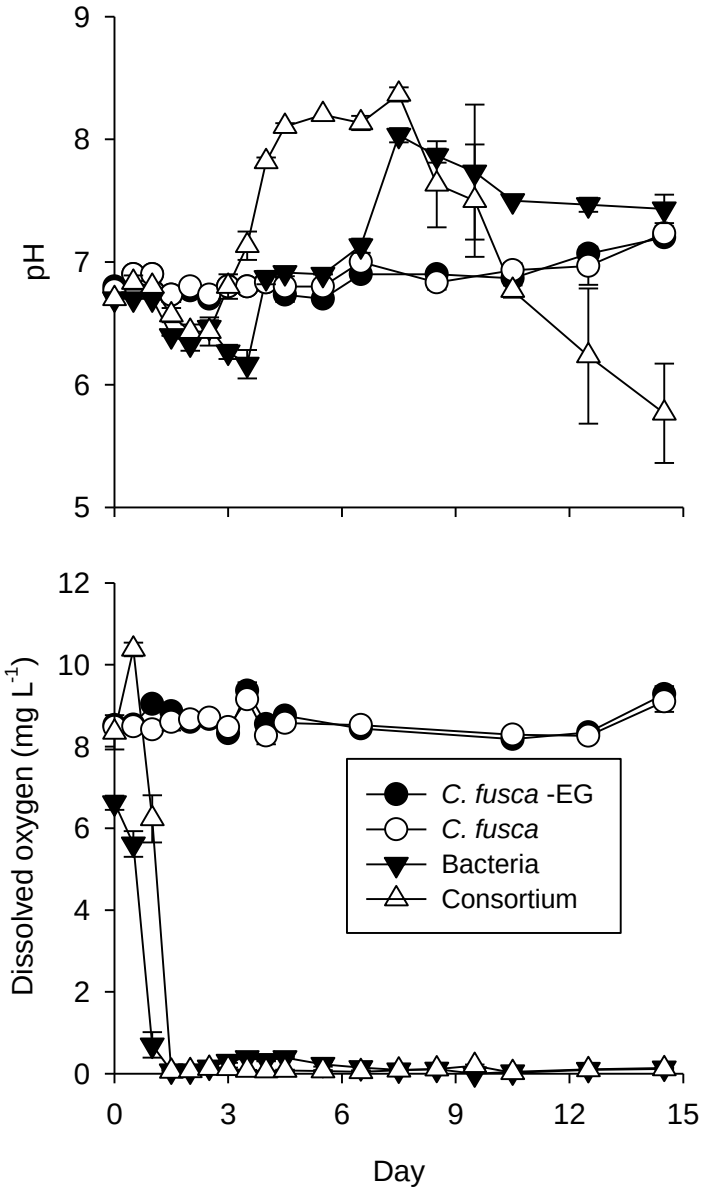

Fig. II-12. Enhancement of the growth of a green alga *Chlorella fusca* oxygen removal by bacterial consortium: (a) pH, (b) dissolved oxygen (DO) (modified from Kishi et al., in press).

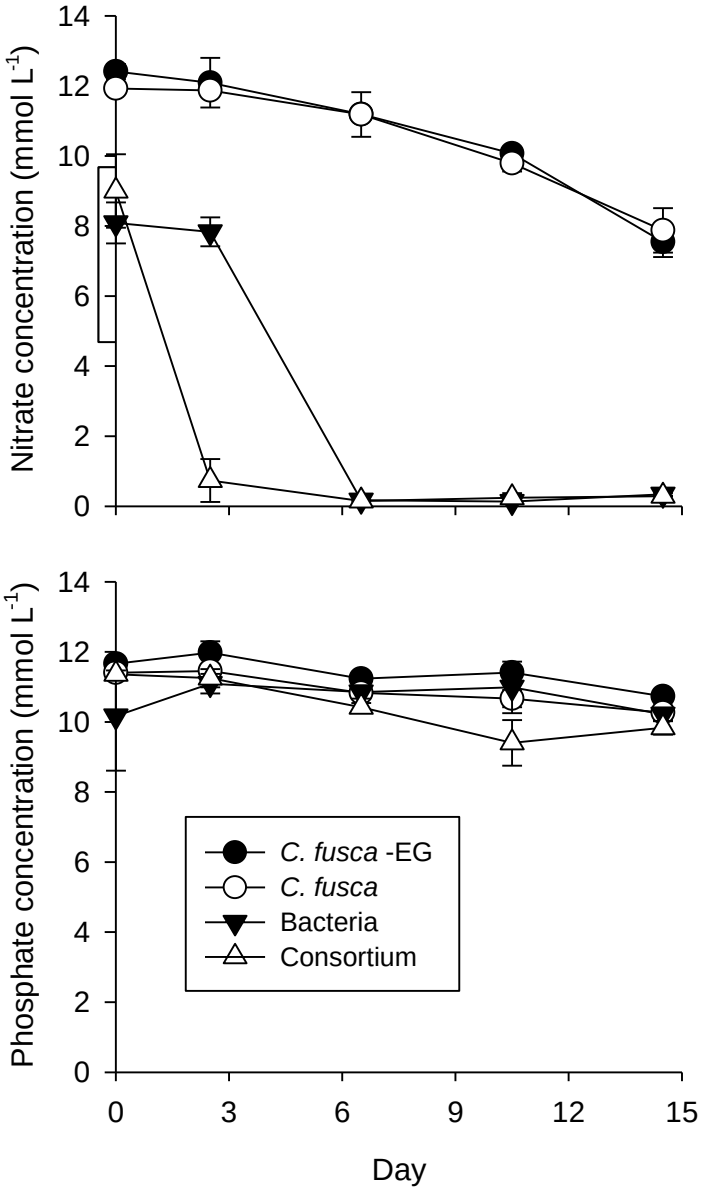

Fig. II-13. Nutrient concentration: (a) nitrate (NO_3^-) and (b) phosphate (PO_4-) (modified from Kishi et al., in press).

CHAPTER III

Application of gas-permeating bag reactor: development of aeration-free operational model

3.1. Introduction

The gas-permeating bag reactor can improve the energy efficiency of microalgal cultivation by reducing the necessity of aeration. In an ideal case, aeration-free cultivation system can be developed if the culture is well mixed by constant flow of the medium as in the case for tubular photobioreactors (Fig. I-2). However, since aeration normally has another important role of carbon dioxide (CO_2) supplementation, the culture may become carbon-limited if no aeration is implemented. One countermeasure to this problem is the use of bicarbonate (HCO_3^-) as inorganic carbon source. Bicarbonate has nearly 10,000 times higher solubility to water than CO_2 does (Chi et al., 2011), and a number of microalgal and cyanobacterial species are capable to directly utilize bicarbonates for carbon assimilation (Devgoswami et al., 2011; Canon-Rubio et al., 2016). With a relatively small CO_2 absorption unit that efficiently converts high-concentration of CO_2 into HCO_3^-, inorganic carbon source can be provided to the entire aeration-free photobioreactors.

This bicarbonate-based carbon supply system is especially favorable with alkalihalophilic species. Alkalihalophiles grow well with high alkalinity and high dissolved inorganic carbon (DIC) concentration, at which CO_2 is efficiently absorbed and retained in the medium owing to its buffer capacity. A commercially important alkaliphilic cyanobacteria, *Arthrospira platensis*, for example, grows well in high pH (8-10) and high DIC (0.1 to 0.4 mol L^{-1}) (Belkin and Boussiba, 1991; Belay, 2013; Kishi and Toda, 2017). *A. platensis* is known to possess high activity of carbonic anhydrase, which converts assimilated HCO_3^- into CO_2 inside its cell (Ramanan et al., 2010; Klanchui et al., 2017). *A. platensis* is also an important commercial cyanobacterium as a source of natural blue food colorant and health supplement (Vonshak, 1997; Spolaore et al., 2006), and now it is the most produced microalgae/cyanobacteria (Borowitzka, 1999; Spolaore et al., 2006). Therefore, *A. platensis* is suitable for the evaluation of the bicarbonate-based CO_2 supply process with the gas-

permeating reactor.

The bicarbonate-based carbon supply has various other advantages over conventional CO_2 supply system. Conventional CO_2 supply for microalgal culture is realized by bubbling of pure gas into the culture ponds. Diverse types of CO_2 supply system have been implemented. For example, Becker (1994) reported CO_2 supplementation with air stones and perforated PVC columns. Another *in situ* supplementation is realized with an aeration ditch with 30 – 100 cm deep hole (Fig. III-1) (Bao et al., 2012). These methods, however, do not always allow the maximum available utilization of CO_2, due to several reasons. First reason is that many microalgal medium is neutral to slightly basic pH, and CO_2 solubility is not very high. Secondly, the depth and mixing in the aeration ditch needs to be optimized for gas dissolution (deeper, more mixing and longer gas retention), while it complexes the structure and increases the construction cost or damages microalgae. Thirdly, utilization of flue gases or biogas induces a low CO_2 dissolution, owing to the lower CO_2 concentrations (10-40%) compared to the pure CO_2.

The first problem is mostly solved with *A. platensis* culture, since it prefers high pH and high alkaline condition, at which pH buffer supports higher CO_2 dissolution. However, the optimum pH and DIC combinations for growth need to be established, and physicochemical characteristics of the optimized medium during CO_2 absorption need to be studied to comprehensively analyze the process since CO_2 absorption is greatly influenced by medium composition. The pH and the dissolved inorganic carbon concentration especially have crucial role in controlling the CO_2 absorption (Bao et al., 2012; Chi et al., 2013). The second and the third problems could be solved by using the two-phase CO_2 supply process and optimizing the CO_2 absorption column for the recovery of CO_2 from supplied gases, separately from the algal bioreactor.

The combination of the two-phase CO_2 recovery process with the developed gas-permeating plastic bag reactor may meet the above demands. The two-phase CO_2 recovery process has been proposed as a method to efficiently remove CO_2 from gases and supply it to algal medium

(Chi et al., 2011; González-López et al., 2012). In the two-phase CO_2 recovery process, CO_2 is immediately converted into bicarbonate (HCO_3^-) in a CO_2 absorption column (Eq. 1), which is filled with carbonate (CO_3^{2-})-rich alkaline solution. The CO_3^{2-} acts as a pH buffer in the absorption column and prevents pH decrease (Eq. 2):

$$CO_2 + H_2O \rightleftharpoons HCO_3^- + H^+ \quad (1).$$

$$CO_3^{2-} + H^+ \rightleftharpoons HCO_3^- \quad (2).$$

The carbon fraction converted into HCO_3^- is then transferred to an algal photobioreactor (PBR), in which HCO_3^- is utilized by algal photosynthesis (Eq. 3):

$$HCO_3^- \rightarrow CO_2(\text{algal fixation}) + OH^- \quad (3)$$

and used for pH counterbalancing (Eq. 4):

$$HCO_3^- + OH^- \rightleftharpoons CO_3^{2-} + H_2O \quad (4).$$

Note that the CO_3^{2-} used in Eq. 2 to buffer pH reduction is regenerated with the OH^- (Eq. 4) produced by photosynthesis (Eq. 3). The photosynthetic regeneration of CO_3^{2-} enables low-energy operation, unlike physicochemical processes in which absorbent is regenerated with heat (100-150°C). The two-phase CO_2 recovery process may enable a high CO_2 recovery efficiency from waste gases such as flue gases from power plants, steel mills, and chemical plants. Furthermore, the process may also be applied for enhancing the gas quality of methane gas from anaerobic digestion, which contains CO_2 up to its 60%. In addition, the high medium DIC enables reduction of frequent costly aeration for CO_2 supply.

The current challenge with the two-phase CO_2 recovery process is the shortage of empirical information of physicochemical modeling and its application to *A. platensis* culture. Therefore, in this study, *A. platensis* culture medium was firstly optimized, and the physicochemical characteristics during two-phase CO_2 absorption was evaluated, and generalized operational parameters for a successful CO_2 recovery was elucidated. Consecutively, the growth of *A. platensis* was evaluated to elucidate the effect of the oxygen-removal reactor compared with a

conventional polypropylene (PP) bag reactor. Lastly, the developed two-phase CO_2 supply model was applied to the gas-permeating reactor to test the feasibility.

3.2. Materials and methods

3.2.1. Algal strain, growth medium, and inoculum preparation

An alkali-halophilic cyanobacterium, *A. platensis* NIES-39, was obtained from National Institute of Environmental Studies (Tsukuba, Ibaraki, Japan). The algal strain was cultured with modified SOT medium (Ogawa and Terui, 1970) containing (mg L^{-1}): Na_2CO_3, 12,189; $NaHCO_3$, 9,660; K_2HPO_4, 500; $NaNO_3$, 2,500; Na_2SO_4, 815; NaCl, 1,000; $MgSO_4 \cdot 7H_2O$, 200; $CaCl_2$, 30; $FeSO_4 \cdot 7H_2O$, 10; Na_2EDTA, 72; H_3BO_3, 2.86; $MnSO_4 \cdot 7H_2O$, 2.5; $ZnSO_4 \cdot 7H_2O$, 0.222; $CuSO_4 \cdot 5H_2O$, 0.079; $Na_2MoO_4 \cdot 2H_2O$, 0.021. The absolute salinity of the medium was 27.0 g kg^{-1}.

For the preparation of inoculum, *A. platensis* was grown in an Erlenmeyer flask filled with autoclaved SOT medium. In order to avoid precipitation during autoclave sterilization, the medium was separated into two batches; the first consists of $NaHCO_3$ and K_2HPO_4 and the second of the others. Both batches were autoclaved at 121°C for 20 minutes and mixed after cooling down to the room temperature. The medium was stirred with a magnetic stirrer continuously at 350 rpm to avoid flocculation. Cool-white fluorescent light at 150 μmol photons m^{-2} s^{-1} was continuously irradiated. Algal cells at a late log-growth phase were used as inoculum for the experiment. In the semi-continuous cyclic operation, after adjustment of pH, modified SOT medium was filter-sterilized with 0.22 μm membrane filter (Millipore, USA) instead of autoclaving.

3.2.2. Optimization of A. platensis *culture conditions*

A preliminary batch growth optimization study was conducted based on the central composite design (CCD). Design-Expert 9 (Stat-Ease Inc., USA) was used for construction and analysis of the model. The test ranges of temperature, pH, DIC, and NaCl concentration were determined in preliminary experiments (Table III-1). A total of 30 runs were operated with 6

replicates for the center point.

Inoculated medium with respective pH, DIC and NaCl concentrations was transferred to 16-mL glass test tubes. Temperature was controlled with incubators (Biotron, Eyela, Japan) with photosynthetic photon flux (PPFD) 160 μmol m^{-2} s^{-1}. The growth was measured by optical density at 750 nm (OD_{750}) every 24 hour. Consecutively, pH was adjusted with 1-N or 10-N HCl and 1-N NaOH. Specific growth rates (d^{-1}) at log-growth phase were used for optimization.

The following quadratic model was selected for modeling the response:

$$Y = \beta_0 + \sum \beta_i x_i + \sum \beta_i x_i^2 + \sum \beta_{ij} x_i x_j \quad (8)$$

where Y indicates the predicted response, β_i are the coefficients, and x_i is the coded levels of variable i (Table III-1).

3.2.3. Semi-continuous operation of two-phase CO_2 recovery process

Two-phase CO_2 recovery process with a small CO_2 absorption column and an algal photobioreactor (PBR) was conducted to construct an operational model suitable for the gas-permeating reactor. In order to construct and critically evaluate a pH model (cf. 3.2.8), three CO_2 supply rates, 0.4, 0.8, and 1.2 L L-PBR^{-1} d^{-1} were tested so that the pH conditions of both the absorption columns and PBR would vary. The effects of CO_2 supply rates on biomass productivity and CO_2 recovery were also evaluated.

The absorption column was a closed 1-L medium bottle with active volume 0.4 L and headspace approximately 0.7 L. Rather than sparging directly into the medium, CO_2 gas was injected into the headspace every 24 hour, so that the gas and liquid phases reach equilibrium. The column was incubated at 25°C. The PBR was a glass column reactor (active volume 1 L). After inoculation, the PBR was placed in an incubator controlled at 35°C with 24-h continuous light with PPFD 300 μmol m^{-2} s^{-1}. At sampling every 24-h, 0.2-L of algal suspension was firstly removed from PBR, which was then refilled with 0.2-L CO_2 absorbent from the absorption column (Fig. III-2). The 0.15 L of removed algal suspension was filter-sterilized with 0.2-μm filter and

recirculated into the absorption column together with 0.05-L new medium (Fig. III-2). The hydraulic retention times (HRT) of the absorption column, the PBR, and the entire system were 1.8, 4.75, and 18 days, respectively. The experiment was continued for 18 days. Samples of algal suspension were taken before and after medium recirculation every 24 hours.

Based on ionic equilibrium, charge balance, and Fick's law of diffusion, models were created for the pH change during CO_2 absorption and the amount of maximum CO_2 absorption at different CO_2 supply rates. Carbon mass balance was calculated based on the CO_2 supply, DIC, and carbon fixation by *A. platensis* (cf. 3.2.8).

3.2.4. Continuous culture of A. platensis with gas-permeating bag reactor

Continuous culture of *A. platensis* was performed with the gas-permeating bag reactor and the PP bag reactor (Fig. II-3; Fig. III-3-a,b). The reactors were installed inside an incubator, and an LED light was irradiated in the middle of the two reactors (Fig. III-3-c). During the continuous culture, the bag reactors were aerated for 1 minute in every 20 minutes to remove DO and to mix the culture (Fig. III-4). The culture was mixed with a centrifugal pump for 12 seconds in every 2 minutes (Fig. III-4). Medium supply and culture discharge were continuously implemented with a peristaltic pump at the dilution rate of 0.5 d^{-1}. The photosynthetic photon flux density (PPFD) was varied from approximately 100 to 800 μmol m^{-2} s^{-1} (Table III-3). The pH of culture was maintained at 9.8 ± 0.1 with automated CO_2 supply. In order to simply compare the effect of gas-permeability, the backside of PP reactor was covered with white paper of similar optical characteristics so that light reflectance by the microporous film would not create differences.

3.2.5. Two-phase circulating operation with developed gas-permeating photobioreactor

A CO_2 absorption column with the effective volume of 1.9 L and the height of 1 m was designed and constructed with acryl resin (Fig. III-5). Using the column, firstly, the CO_2 absorption characteristics was evaluated by continuous supply of 100% CO_2 gas into the column at 0.28 L min^{-1}. The relationship between pH reduction, DIC increase, and CO_2 gas recovery efficiency over

time was investigated.

Secondly, the absorption column was incorporated into CO_2 supplementation for the gas-permeating reactor. After inoculation, the bag reactor was singly operated until the biomass concentration reached steady-state on Day 5. The absorption column was then connected to the gas-permeating continuous culture system (Fig. III-6). The column was continuously supplied with *A. platensis* culture filtrate through a hollow fiber filter module (PSP-113, AsahiKASEI, Japan), and the same amount of bicarbonate-enriched medium is returned to the gas-permeating reactor. The absorbent inside the reactor was continuously mixed with a centrifugal pump to verify the homogeneity of the liquid and to prolong the bubble retention time. For the first three days of two-phase operation (Day 5-7), the amount of CO_2/N_2 (40/60 v/v) mixture gas supplied from the bottom of the column was determined from the biomass productivity of the previous day. On the next three days (Day 8-11), the gas supply was controlled with the pH of *A. platensis* culture; gas is supplied when the pH is above 9.85. The temperature of the absorbent was controlled at 25°C.

3.2.6. Effects of long operation on oxygen removal

The oxygen removal characteristics and development of biofouling on the microporous film was evaluated after 91 days of continuous culture with the developed gas-permeating reactor. The oxygen mass transfer coefficient was measured with intermittent mixing, as described in section 2.2.1.3. Biofouling was evaluated with scanning electron microscopy (SEM) imaging and chlorophyll *a* on the microporous film. The film samples were obtained from three separate parts of the reactor after moderately mixing the culture medium to remove biomass settled on the wall by gravity. Each filter sample was softly washed with fresh modified SOT medium and distilled water for chl. *a* and SEM analysis, respectively.

3.2.7. Analytical parameters

The algal suspension was used to measure algal dry weight (DW), algal cell carbon and nitrogen content. Algal suspension filtrate was used to measure pH, electrical conductivity,

nutrients (nitrate, nitrite and phosphorous), dissolved inorganic carbon (DIC), and dissolved organic carbon (DOC). The gas sample was used to measure headspace CO_2, N_2, and O_2 concentration.

Algal DW was measured every day using glass fiber filters. Firstly, algal suspensions were filtered through pre-weighed glass fiber filters with pore size of 0.7 μm (GF/F, Whatman, USA) and washed with distilled water three times. Then, filters were dried in an oven at 60°C for over 24 hours and subsequently cooled to room temperature in a desiccator before weighing. Filters were weighed with an ultra-microbalance (XP6U Ultra Micro Comparator, Mettler Toledo, USA). Algal cell carbon and nitrogen contents were measured by measuring particulate organic carbon and nitrogen (POC and PON) of algal cells on the filters using an elemental analyzer (Flash 2000 CHN, Thermo, USA). Dissolved inorganic carbon (DIC) and dissolved organic carbon (DOC) were measured using TOC analyzer (Shimadzu, Japan). Nutrients (nitrate, nitrite, and phosphate) were analyzed with a nutrient analyzer (SWAAN, BL-TEC, Japan).

Gas composition (CO_2, N_2, and O_2) was measured using a gas chromatograph (GC-2014, Shimadzu, Japan) equipped with a packed column (Shincarbon ST, 6.0 m long, 3 mm I.D., Shimadzu, Japan) and a thermal conductivity detector. The temperature of the injector and the detector were maintained at 120ºC and 260ºC, respectively. The column temperature was gradually increased from 40ºC to 250ºC. Helium was used as the carrier gas with the flow rate of 40 mL min^{-1}.

Scanning electron microscopic samples were prepared by water freeze-drying method (Natori et al., 2017). The samples were placed on aluminum specimen stubs with conductive carbon tapes. The samples were then rapidly frozen by pressing a -100°C copper column blocks on the aluminum specimen stubs. The samples were vacuumed to get dried with a freeze-drying system (Freeze Dryer FD-6510, SUN Technologies). The samples were coated with osmium with an osmium coater (HPC-1SW, VACUUM DEVICE, Ibaraki, Japan). The samples were analyzed with

a field-emission electron microscope (JSM-7500F, JEOL).

Chlorophyll *a* was measured with a fluorometer (Model 10-AU, Turner Design, USA) as described by Welshmeyer (1994) after extracting filtered samples with *N*,*N*-dimethylformamide (Suzuki and Ishimaru, 1990).

3.2.8. Calculations

3.2.8.1. Carbonate/bicarbonate equilibrium model

The stoichiometric equilibrium constants, K_1 and K_2, are defined as:

$$K_1 = \frac{[\mathrm{HCO_3^-}][\mathrm{H^+}]}{[\mathrm{CO_2}]} \quad (9)$$

$$K_2 = \frac{[\mathrm{CO_3^{2-}}][\mathrm{H^+}]}{[\mathrm{HCO_3^-}]} \quad (10).$$

In this study, pK_1 = 6.38 (Camacho Rubio et al., 1999) and pK_2 = 9.8 (Chi et al., 2013) were assumed. The molar concentration of dissolved inorganic carbon *DIC* (mol L^{-1}) was the sum of three inorganic carbon species:

$$DIC = [\mathrm{CO_2}] + [\mathrm{HCO_3^-}] + [\mathrm{CO_3^{2-}}] \quad (11)$$

The composition of DIC was calculated based on the following equations derived from Eq. 9-11 (Zeebe and Wolf-Gladrow, 2001):

$$[\mathrm{CO_2}] = \frac{DIC}{1 + \frac{K_1}{[\mathrm{H^+}]} + \frac{K_1 K_2}{[\mathrm{H^+}]^2}} \quad (12)$$

$$[\mathrm{HCO_3^-}] = \frac{DIC}{1 + \frac{[\mathrm{H^+}]}{K_1} + \frac{K_2}{[\mathrm{H^+}]}} \quad (13)$$

$$[\mathrm{CO_3^{2-}}] = \frac{DIC}{1 + \frac{[\mathrm{H^+}]}{K_2} + \frac{[\mathrm{H^+}]^2}{K_1 K_2}} \quad (14).$$

Based on the above equations, pH variations with CO_2 absorption/desorption was modeled. In the current experiment, DIC concentration can be expressed using the initial DIC concentration c_0 (mol L^{-1}) and DIC change ΔDIC (mol L^{-1}) due to CO_2 supply or algal assimilation:

$$DIC = [\mathrm{CO_2}] + [\mathrm{HCO_3^-}] + [\mathrm{CO_3^{2-}}] = c_0 + \Delta DIC \quad (15).$$

Charge balance in the medium can be expressed as:

$$[\mathrm{H^+}] + [\mathrm{Na^+}] = [\mathrm{H^+}] + c_0 + c_b = [\mathrm{OH^-}] + [\mathrm{HCO_3^-}] + 2[\mathrm{CO_3^{2-}}] \quad (16)$$

where c_b is the NaOH concentration that raised medium pH to 10.5 (0.215 mol L^{-1}). Using the ion product constant of water ($K_w = [\mathrm{H^+}][\mathrm{OH^-}] = 1.0 \times 10^{-14}$ mol^2 L^{-2}), Eq. 16 can be expressed as:

$$[\mathrm{H^+}] + c_0 + c_b = \frac{\mathrm{K_w}}{[\mathrm{H^+}]} + [\mathrm{HCO_3^-}] + 2[\mathrm{CO_3^{2-}}] \quad (17).$$

Finally, Eq. 10, 14, 15 and 17 can be formulated into a quartic equation:

$$[\mathrm{H^+}]^4 + (K_1 + c_0 + c_b)[\mathrm{H^+}]^3 + (K_1K_2 + K_1c_b - K_w - K_1\Delta DIC)[\mathrm{H^+}]^2 + K_1(K_2c_b - K_w - K_2c_0 - 2K_2\Delta DIC)[\mathrm{H^+}] - K_1K_2K_w = 0 \quad (18).$$

In the current experiment, all variables in Eq. 18 except for ΔDIC and $[\mathrm{H^+}]$ remained constant. Therefore, with this model, pH variation can be estimated based on changes in DIC concentration (ΔDIC) due to CO_2 absorption or photosynthetic assimilation. The quartic equation was solved with Mathematica 8.0 (Wolfram Research, Champaign, IL).

Buffer capacity, β, can express the strength of pH buffer, and was calculated based on the following approximation for diprotic acids (Stumm and Morgan, 1993):

$$\beta = -\frac{d\mathrm{C_A}}{d\mathrm{pH}} \cong 2.3\left([\mathrm{H^+}] + [\mathrm{OH^-}] + \frac{[\mathrm{CO_2}][\mathrm{HCO_3^-}]}{[\mathrm{CO_2}] + [\mathrm{HCO_3^-}]} + \frac{[\mathrm{HCO_3^-}][\mathrm{CO_3^{2-}}]}{[\mathrm{HCO_3^-}] + [\mathrm{CO_3^{2-}}]}\right) \quad (19)$$

where $d\mathrm{C_A}$ is infinitesimal amount of acids required to decrease dpH. Phosphate and borate were assumed to have negligible effects on buffer capacity owing to their 100-fold lower concentrations than DIC concentration in the SOT medium.

The CO_2 absorption capacity of non-buffered pH 10.5 solution (adjusted with NaOH) was calculated, based on the assumption that no inorganic carbon existed in the solution, using Eq. 18 and Henry's law:

$$[\mathrm{CO_2}]_{\mathrm{sat}} = H^{cp} \times p_{\mathrm{CO_2}} \quad (20)$$

where $[CO_2]_{sat}$ is the saturation concentration of CO_2 (mol L^{-1}), H^{cp} is Henry's law solubility constant (3.30×10^{-7} mol L^{-1} Pa^{-1}) (Sander 2015) and p_{CO_2} is the partial pressure of CO_2 (Pa). The concentration of NaOH was calculated to be 3.16×10^{-4} mol L^{-1} using Eq. 18.

3.2.8.2. Biomass production, carbon fixation, and carbon mass balance

Specific growth rate (μ; day^{-1}) during log-growth phase was calculated using the following equation:

$$\mu = \frac{\ln(x_2/x_1)}{t_2 - t_1} \tag{21}$$

where x_i is biomass concentration (gDW L^{-1}) at time t_i. Algal biomass production rate (P_x; gDW L^{-1} d^{-1}) was calculated with the following equation:

$$P_x = \frac{x_2 - x_1}{t_2 - t_1} \tag{22}$$

where x_i is biomass concentration (gDW L^{-1}) at time t_i (d). In the semi-continuous culture, the steady-state condition of growth was defined as a period with less than 10% variation in the 3-day moving averages of DW, which was found to be Day 10 to 18. In the continuous culture of *A. platensis* with gas-permeating reactor, the steady-state condition of growth was defined as a period with less than 10% variation in the dry weight.

The CO_2 recovery rate, R_{CO2} (gCO_2 L^{-1} d^{-1}), was estimated based on the increase in the total DIC concentration after every 24-hours of CO_2 absorption period using the following equation:

$$R_{CO_2} = \frac{DIC_2 - DIC_1}{t_2 - t_1} \times \frac{V_{abs}}{V_{PBR}} \times \frac{MW_{CO_2}}{MW_C} \tag{23}$$

where DIC_i is the DIC concentration (mol L^{-1}) in the CO_2 absorption column at time t_i (d), V_{abs} and V_{PBR} are the volume of CO_2 absorption column (0.4 L) and PBR (1 L), and MW_{CO_2} and MW_C are the molecular weights of CO_2 (44.01 g mol^{-1}) and carbon (12.01 g mol^{-1}), respectively. While R_{CO2} was the indicator of the total amount of CO_2 absorbed into the medium, algal CO_2 biofixation rate R_{BioCO_2} (gCO_2 L^{-1} d^{-1}) was also calculated in this study:

$$R_{BioCO_2} = C_c \times P_x \times \frac{MW_{CO_2}}{MW_C} \quad (24)$$

where C_c is the carbon content of algal cell (gC gDW^{-1}). The carbon content of the dry cell of *A. platensis* during this experiment was found to be 32 ± 4% from the elemental analysis. For evaluation of literature without information of the carbon content, 0.5 gC gDW^{-1} was used.

The carbon mass balance of the semi-continuous operation was calculated using the following equations:

$$C_{in} = (DIC + DOC)_{ABSi} + (POC + DIC + DOC)_{PBRi} + \sum_{i=1}^{n}(DIC + DOC)_N + \sum_{i=1}^{n} CO_{2in} \quad (25)$$

$$C_{out} = (DIC + DOC)_{ABSf} + (POC + DIC + DOC)_{PBRf} + \sum_{i=1}^{n}(DIC + DOC)_{ABSs} + \sum_{i=1}^{n}(POC + DIC + DOC)_{PBRs} \quad (26)$$

where C_{in} and C_{out} represent the total incoming and outgoing carbon (gC) after 18 days of the experiment, respectively. *ABSi* and *PBRi* refer to the carbon mass in the initial medium of CO_2 absorption column and PBR, respectively. *N* represents carbon mass in the new SOT medium, and CO_{2in} means the carbon dioxide absorbed into the medium. *ABSf* and *PBRf* indicate final carbon mass of each reactor, and *ABSs* and *PBRs* represent the carbon mass in each sample taken every day.

3.2.8.3. Oxygen removal

Oxygen removal rate (R_{O2}; mg L^{-1} d^{-1}) in bag reactors was calculated using the following equation:

$$R_{O2} = \frac{XD}{Y_o} - (C_o^2 - C_o^1) \quad (27).$$

where X is the biomass concentration (gDW L^{-1}), D is the dilution rate (d-1), Yo is the

ratio between biomass and produced oxygen (1.97 g oxygen per 1 g of biomass; Torzillo et al., 1998), $C_o^i$is the oxygen concentration (mg L^{-1}) on day i.

3.2.9. Statistical analysis

Results are expressed as means ± standard deviations of mean, where available. The correlation coefficient was obtained using simple regression analysis (Excel software). Results from different conditions were analyzed using the Tukey-Kramer method. Differences with $P < 0.05$ were considered significant.

3.3. Results and discussion

3.3.1. Optimization of A. platensis *culture conditions*

A significant model was established with the CCD analysis (Table III-4). The CCD analysis revealed the optimal culture conditions of *A. platensis* to be pH 9.8, DIC 0.23 mol L^{-1} (Fig. III-7), and temperature ca. 34°C, which is highly alkalihalophilic compared with common species such as *Chlorella* (pH 6.2, DIC 0.01 mol L^{-1}) and *Haematococcus* (pH 7, DIC 0.02 mol L^{-1}) (Kang et al., 2005; Yeh et al., 2010). Variations in pH and temperature were found to have relatively stronger effects on the growth than NaCl and DIC.

3.3.2. Semi-continuous two-phase CO_2 supply

3.3.2.1. pH variation and CO_2 recovery efficiencies in semi-continuous operation of two-phase CO_2 recovery process

The semi-continuous operation of the two-phase CO_2 recovery process was operated at three different CO_2 supply rates (Run 1: 0.4; Run 2: 0.8; and Run 3: 1.2 L L-PBR d^{-1}) for 18 days. The CO_2 recovery efficiencies in Run 1, 2, and 3 were 115, 94 and 63%, respectively. While most of the supplied CO_2 was recovered in Run 1 and 2, only half was recovered by Run 3, owing to the pH reduction in the absorption column.

The pH of the absorption column and the PBR fluctuated with CO_2 supply and CO_2

utilization by the cyanobacteria (Fig. III-8). In Run 2 and 3 with high CO_2 supply rates, the pH of the absorption column largely decreased with CO_2 absorption during 24-hour of incubation (Fig. III-8-b,c; ●). However, the pH recovered back to over 9.5 with a supply of PBR medium owing to the strong buffer function of the SOT medium (Fig. III-8-b,c; ▲). The pH in Run 1 relatively remained stable, because the CO_2 supply and algal CO_2 fixation were more balanced than the other two. Since the biomass production rate of *A. platensis* remained in the same range (on average 0.27-0.31 gDW L^{-1} d^{-1}) regardless of the CO_2 supply rate, the higher CO_2 supply resulted in the excess of CO_2 supply. The excess CO_2 supply induced accumulation of DIC especially HCO_3^- in Run 2 and 3. The increasing trend of DIC even in Run 1 indicates eventual saturation and decrease of CO_2 recovery efficiency.

The successfully constructed model (Fig. III-9) revealed that the modified SOT medium can buffer pH with the CO_2 absorption of up to 0.17 mol L^{-1} (half of the maximum β; Fig. III-9). When the CO_2 absorption exceeded this buffer range, the pH dropped drastically. The reduction in pH not only interferes the CO_2 recovery but also damages the growth of *A. platensis*; e.g., over 50% decrease with pH reduction from 9.8 to 8. While the balance between CO_2 supply and the carbon fixation rate is highly demanded, the current medium can buffer at least 1.6 and 4.1-fold fluctuations of the CO_2 supply rate and the fixation rate, respectively. Although some other freshwater algal CO_2 recovery studies suffer from large pH fluctuation (Kao et al., 2012; Bahr et al., 2014), the two-phase CO_2 recovery process with *A. platensis* achieved successful CO_2 recovery with high pH stability.

3.3.2.2. Carbon mass flux analysis

The balance between the total incoming carbon mass (Total In; DIC, CO_2, DOC, and POC in initial and additional medium) and outgoing carbon mass (Total Out; DIC, DOC, and POC in the discharged and final medium) was evaluated (Table III-6). There was no difference in the total fixed carbon (DOC + POC) among three CO_2 supply rates: 2.7, 2.8, and 2.6 gC for Run 1, 2 and 3,

respectively. The conversion efficiencies from absorbed CO_2 to DOC + POC decreased with increasing CO_2 supply rates: 58, 38, and 30% for Run 1, 2 and 3, respectively. The difference between CO_2 supply and biological carbon fixation was relatively large in Run 2 and 3, indicating that produced HCO_3^- (Eq. 2) was not fully regenerated back to CO_3^{2-} (Eq. 4). It was suggested that the imbalance between CO_2 supply and fixation was the cause of DIC accumulation and pH decrease (Fig. III-8).

In order to balance the CO_2 supply and fixation, it is necessary to either decrease the CO_2 supply rates or increase the photosynthetic carbon fixation rate. The growth of the *A. platensis* in this study was likely to be limited by the light availability because inorganic carbon and nutrient resources were plenty. In a previous study, with a light-efficient flat panel reactor, *A. platensis* was able to grow at a more than 5 times higher rate (1.9 gDW L^{-1} d^{-1}) (Tredici and Zittelli, 1997) than this study. Modification of culture apparatus may lead to a higher biofixation rate by the same species. To achieve a high volumetric CO_2 fixing rate, the CO_2 supply rate should be adjusted accordingly with the biomass production rate in the PBR, which should be optimized for a high biomass production rate.

The carbon mass flux analysis also revealed that 16-24% of photosynthetically fixed carbon was converted into DOC (Table III-6). This high amount of DOC excretion commonly occur with other algae and cyanobacteria, such as *Aphanothece microscopica* (Jacob-Lopes et al., 2008) and *Chlamydomonas reinhardtii* (Bafana, 2013), in the form of extracellular polymeric substances (EPS) (Delattre et al., 2016). It is therefore necessary to take DOC fraction into consideration in the case of carbon mass balance during algal CO_2 recovery process.

Excretion of DOC in an algal CO_2 absorption process also holds several disadvantages. Firstly, excretion of viscous EPS may lead to formation of biofilm on the surface of gas-permeating film, and therefore deteriorating the oxygen-removing properties. Secondly, DOC may induce

bacterial contamination, which would not only promote biofilm formation, but also depreciate the quality of biomass. Although the high alkalinity limits the growth of some microbes, bicarbonate was tested to be not an effective antibacterial agent (Miyasaki et al., 1986; Karapinar and Gönül, 1992). Thirdly, certain types of excreted DOC can inhibit algal growth. For example, over 60 mg L^{-1} of DOC was reported to decrease the content of chlorophyll *a* of *A. platensis* (Zengling et al., 2006). The final DOC concentration in this study ranged between 260 and 370 mgC L^{-1}, and there could have been a certain degree of growth inhibition. Hence, in common algal mass culture, except for the cases where extracellular DOC is the target product, it is preferred to reduce DOC production.

The amount of DOC excretion varies depending on culture conditions. In a culture of *A. platensis*, for example, DOC release was the most substantial during the stationary-phase (> 30% primary production), but it was below 5% during the exponential phase (Gordillo et al., 1998). By maintaining the dilution rate of the PBR at high rate, and keeping the cell condition active. extracellular DOC production may be reduced.

The carbon mass flux analysis suggested that the CO_2 supply rate and fixation rate were not in balance in this semi-continuous operation, although the reactors were able to recover nearly 100% CO_2, owing to the high CO_2 absorptivity of the medium. For the long-term stability of the two-phase CO_2 recovery process, the appropriate operating parameters, such as CO_2 supply rates, circulating frequency, and reactor volumes of the absorption column and PBR, should be therefore estimated from empirical models.

3.3.2.3. Generalization of the two-phase CO_2 recovery process

In order to balance the supply and utilization of CO_2, the following equation was considered:

$$D_{CO_2} = x(F_{POC} + F_{DOC}) \quad (28)$$

where D_{CO_2} is the CO_2 demand (gC L^{-1} d^{-1}), x is the biomass production rate (gDW L^{-1} d^{-1}),

F_{POC} and F_{DOC} are the fractions of POC and DOC in the algal dry cells.

On top of the total carbon supply, volume ratios of CO_2 absorption column and PBR, as well as circulation frequency between them need to be modelled:

$$\frac{V_{PBR}}{V_{CO_2}} \times \frac{D_{CO_2}}{C_{DIC}} = \text{frequency of circulation} \quad (29)$$

where V_{PBR} and V_{CO2} indicate the volume of PBR and CO_2 absorption column, C_{DIC} indicate the capacity of the medium to absorb CO_2 without hindering CO_2 recovery. By determining the above parameters, a successful two-phase CO_2 recovery process would be achieved.

3.3.3. Continuous operation of gas-permeating photobioreactor

3.3.3.1. Biomass production rates at different light intensities

From Phase 1 to 3, the PPFD was increased step-wise from 100 to 800 μmol m^{-2} s^{-1} (Table III-3). In Phase 1, the biomass concentration between the microporous bag reactor and the PP reactor were comparable (Fig. III-10). However, the biomass concentration substantially increased in Phase 2, and the steady-state biomass concentration in the microporous reactor was approximately 1.6 times that of PP reactor (Fig. III-10). The average biomass concentrations of the microporous reactor were significantly higher in Phase 2 and 3 (Fig. III-11). The difference became even larger in Phase 3; while the biomass concentration in the PP reactor gradually decreased, that of microporous reactor remained relatively stable. The volumetric biomass production rate reached 2.0 gDW L^{-1} d^{-1} in the microporous reactor, while that remained less than 1.3 gDW L^{-1} d^{-1} in the PP reactor (Fig. III-12 and Fig. III-13). This figure is comparable to 2.1 gDW L^{-1} d^{-1} obtained by the continuously mixed flat panel cultivation of *A. platensis* (Tredici and Zittelli, 1997). The present study demonstrated the effectiveness of the novel gas-permeating bag reactor in maintaining a high biomass productivity with less energy for aeration and mixing.

The cause of the difference should be attributable to the gas-permeability of the microporous reactor, since other factors such as temperature (Fig. III-14 and Fig. III-15), dilution

rates, and light reflectance were set at the same level. However, the apparent DO did not exhibit clear trends (Fig. III-16 to Fig. III-18). While the average DO was lower for the microporous reactor in Phase 1, there was no apparent difference in Phase 2 (Fig. III-18). It is reasonable to assume that removal of DO results in increased biomass production and oxygen production, compensating the decrease of DO due to the gas permeation. In this line, the significantly lower DO in Phase 1 can be explained by the light limitation, at which oxygen concentration was not limiting the growth. The similar biomass production as well as the lower DO in the microporous film indicate that a certain portion of the DO is being removed.

The oxygen removal rate was calculated based on the assumption that biomass production rate is proportional to the net oxygen production (photosynthetic oxygen production - respiration), and other oxygen removal was either by aeration or diffusion from the microporous film surface (Fig. III-19). The oxygen removal rates were significantly higher in the microporous film in Phase 3, and relatively higher in Phase 2, indicating the effectiveness of the microporous film for gas-permeation.

In Phase 3 despite the increase in the PPFD by more than twice from Phase 2, both the biomass concentration and production rate did not increase in gas-permeable reactor, but rather decreased in the PP reactors. This result indicates that both reactors suffered from photoinhibition. According to a previous study, most *Arthrospira platensis* strains have light saturation intensities of between 200 and 300 μmol m^{-2} s^{-1} (Belay, 2013). When the culture is mixed well, the cells on the surface can immediately be shaded in a high-density culture (Grobbelaar et al., 1996). However, the present study implemented intermittent mixing, which may have hindered the photoprotective effect of high-density culture. Moreover, high oxygen condition further intensifies the photodamage (Vonshak et al., 1996). The low biomass in the PP reactor may be because of the combined effect of oxygen and high light stress. Similarly, the increased oxygen concentration in the microporous reactor may have relatively lower growth in Phase 3.

High photosynthetic efficiencies (PE) were also achieved by the microporous reactors especially at lower PPFDs. The PE was the highest with the lowest PPFD in Phase 1 (Table III-7), especially for over 10% in the microporous reactor. This value was comparably higher than many outdoor cultures, which range between 2% to 9% (Tredici and Zittelli, 1998; Hall et al., 2003; Janssen et al., 2003). The PE slightly decreased to 9.1% in Phase 2. The possible reasons for the decrease are (1) damage to photosynthetic systems by oxygen buildup and (2) light saturation owing to insufficient mixing of the cells. The damage to photosynthetic system is apparent for the PP reactor, in which PE was lower than microporous reactor even at the lowest light intensity in Phase 1. On top of the oxygen damage, mixing is extremely important for maintaining high PE at high PPFD (Qiang and Richmond, 1996; Richmond, 2013). Since the light saturation intensities are in the range of 200-300 μmol m^{-2} s^{-1} with *A. platensis* (Belay, 2013), higher PPFDs can be only utilized when the surface and the mid of the reactor are continuously turned over. In fact, at a very high PPFD of 1800 μmol m^{-2} s^{-1} radiated, an increase in aeration from 0.6 to 4.2 L L^{-1} min^{-1} enhanced *A. platensis* biomass production rate from 200 to 400 mg L^{-1} h^{-1} (Qiang and Richmond, 1996). The infrequent mixing of the current reactor had an advantage in reducing the energy intensity but limited the PE at higher PPFD than 325 μmol m^{-2} s^{-1}. Instead of the increase in mixing, spatial light dilution can be incorporated to the reactor operation to solve the issue with lowered PE. To fully utilize the high outdoor PPFD, which can reach higher than 2000 μmol m^{-2} s^{-1}, light dilution has been proposed as the countermeasure (Burlew, 1953; Tredici and Zittelli, 1998; Dye and Sims, 2010; Norsker et al., 2011). While mixing is considered as temporal dilution of light, spatial dilution of light can be achieved by increasing the irradiated surface over culture volume of the reactor and creating angle towards the light source (Tredici and Zittelli, 1998; Dye and Sims, 2010). For example, tubular or dome reactors have curved surfaces, increasing the surface area and the angle towards the light. Compared with a rectangular reactor facing perpendicular to the light, curved surface has 60% increase in illuminated surface area, thus diluting the light intensity.

Similarly, vertical flat panel reactors can dilute light spatially owing to the sharp angle of reactor towards the sun (Norsker et al., 2011), especially around the seasons of stronger light intensity in solstice. The diluted light intensity (L_d) of a vertical flat panel can be calculated with the following equation (Fig. III-21):

$$L_d = L_p \times \sin\left(\frac{1}{2}\pi - \theta\right) \quad (30)$$

where *Lp* is the PPFD measured perpendicular to the sun, θ is the sun angle in radian. For instance, with summer solstice sun angle of 78° (radian 1.36) in Tokyo, PPFD of 2000 μmol m^{-2} s^{-1} would be diluted to 416 μmol m^{-2} s^{-1}, which is close to the saturating light intensity of *A. platensis*. Therefore, the newly-developed gas-permeating reactor will be an effective tool to improve decrease energy consumption without decreasing the productivity by applying it to vertical flat reactors or to low-light indoor applications.

3.3.3.2. Effect of long-term operation on oxygen-permeability of the reactor

The K_La of the gas-permeating photobioreactor after 91 days of *A. platensis* culture was 0.040±0.002 min^{-1} with intermittent circulation. There was no significant difference in K_La between before (0.045±0.005 min^{-1}) (Fig. II-9) and after the long operation, although the value was slightly (ca. 10%) lower. This result indicates that the effects of long-term operation, such as by biofouling and physical damage on the film, on oxygen removal efficiency is negligible.

Microscopic imaging with SEM revealed slight adhesion of white crystals, probably constitute of extracellular polymers and biomass after the long-term operation (Fig. III-20-a,b). However, most pores were not covered with such crystals (Fig. III-20-c,d) except for the smaller portions of the surface. The chl. *a* attached on the microporous film was 5.74 ± 5.28 μgChl.a m^{-2}. Assuming 1% chl. *a* content in 1 g of algal DW, the biomass attached to the microporous film was approximately 0.57 mgDW m^{-2}, which was fairly negligible. These results suggest that a long-term operation of gas-permeating reactor with *A. platensis* does not deteriorate the oxygen-removal properties of the reactor at least up to 91 days.

3.3.4. Incorporation of two-phase CO_2 supply into gas-permeating reactor

With a continuous supply of CO_2 gas into the absorption column, simulating 100-times faster supply rate than the current bag reactor, a rapid drop in pH was observed (Fig. III-22). However, the headspace CO_2 gas remained low until the pH becomes less than around 8.5 even with this high supply rate. This result indicates that, with a constant mixing in the absorption column, the gas and liquid phase was nearly in equilibrium. Hence, the calculated and measured CO_2 gas concentrations were in good agreement (Fig. III-22 and Fig. III-23). These results suggest that two-phase CO_2 supply with *A. platensis* culture can absorb CO_2 gas at high efficiency.

In the two-phase CO_2 recovery process with the gas-permeating reactor, the average biomass production rate was 1.58±0.09 gDW L^{-1} d^{-1} (Fig. III-24). Between Day 5 and 7, the amount of CO_2 supply was calculated based on Eq. 22 and 23. With the beginning of the two-phase CO_2 supply on Day 5, the PBR pH gradually increased to 10.1 (Fig. III-25), but stabilized on Day 7. This rise in pH indicates slight shortage of CO_2 supply. In order to confirm the require quantity of CO_2, pH-stat operation was continued Day 8 through 11. After the rapid reduction of pH both in the PBR and the absorption column, it stabilized after Day 9. The consumed CO_2 gas on Day 9 and 10 were slightly higher than that between Day 5 and 8 (Fig. III-25). Throughout the experiment, the CO_2 gas concentration in the headspace was constantly low, and it maintained less than 0.2%. The high CO_2 absorptivity enabled nearly complete CO_2 recovery from 40% CO_2 gas.

Although constant monitoring or automatic control of pH was found to be necessary, this experiment demonstrated the high CO_2 recovery efficiency of the two-phase CO_2 supply process. The combination of the two-phase CO_2 supply and the gas-permeating reactor successfully achieved aeration-reduced culture of *A. platensis*.

3.4. Conclusions

The present study demonstrated the effectiveness of the gas-permeating bag reactor for improving biomass production rate with less intensive mixing and aeration. Although the DO

difference was not apparent, intrinsic oxygen removal of the gas-permeable reactor enabled a high biomass productivity of *A. platensis*. The pH, CO_2 absorption, and carbon flux models developed in this study provided necessary insights for determination of optimum operation conditions of two-phase CO_2 supply. The incorporation of the two-phase CO_2 supply into the gas-permeating reactor achieved a successful operation of aeration-reduced *A. platensis* culture.

Tables

Table III-1.Coded levels and actual values of culture conditions of face-centered central composite design of *Arthrospira platensis*

Algal Strain	Code levels	Temperature (°C)	pH	DIC [a] (mol L^{-1})	NaCl (mol L^{-1})
A. platensis	-1	30	9.0	0.02	0
	0	35	10.0	0.16	0.085
	1	40	11.0	0.3	0.17

[a] Dissolved inorganic carbon (DIC).

Table III-2. Gas supply configuration for CO_2 absorption column.

Run	CO_2 supply rate		Headspace	Headspace CO_2	Headspace CO_2	Headspace N_2	CO_2 in gas bag	N_2 [a] in gas bag
	(L d^{-1})	(mol $L_{absorbent}^{-1}$ d^{-1})	(L)	(%)	(L)	(L)	(L)	(L)
1	0.4	0.041	0.73	55	0.4	0.33	0	0.4
2	0.8	0.081	0.72	100	0.72	0	0.07	0.74
3	1.2	0.123	0.74	100	0.74	0	0.45	0.75

[a] Nitrogen was prepared in order to prevent negative pressure inside the column.

Table III-3. Operational conditions of each phase for each reactor.

Phase		Average PPFD* ($\mu mol\ m^{-2}\ s^{-1}$)	Average temp. (°C)	Average dilution rate (d^{-1})
1	Microporous	97	34.4 ± 0.9	0.42 ± 0.11
	Polypropylene	115	34.8 ± 0.5	0.43 ± 0.07
2	Microporous	326	34.3 ± 2.3	0.45 ± 0.09
	Polypropylene	320	35.2 ± 0.4	0.49 ± 0.13
3	Microporous	851	33.6 ± 2.1	0.49 ± 0.05
	Polypropylene	743	35.6 ± 1.5	0.52 ± 0.07

*PPFD: photosynthetic photon flux density. Average of 9 points on the reactor surface.

Table III-4. Variables, coefficients and statistic parameters of central composite design model

	A. platensis	
Variable	Coefficient	*P*
Intercept	0.43	
A-Temperature	**-0.062**	**0.002**
B-pH	**-0.043**	**0.018**
C-DIC	**0.045**	**0.014**
D-NaCl	0.007	0.668
AB	-0.009	0.603
AC	0.012	0.484
AD	0.007	0.679
BC	**-0.041**	**0.032**
BD	-0.002	0.92
CD	-0.005	0.764
A^2	**-0.092**	**0.047**
B^2	**-0.17**	**0.001**
C^2	-0.043	0.329
D^2	0.016	0.716
Model		**<0.001**

Coefficients are for coded values. Bold indicates significant parameters ($P < 0.05$). The coefficient of determination of was R^2=0.906.

Table III-5. Average CO_2 fixing rate and pH before and after CO_2 supply in absorption columns [a].

Run	CO_2 supply rate ($L\ d^{-1}$)	CO_2 fixing rate, R_{CO_2} [b] ($L\ d^{-1}$)	($gCO_2\ L^{-1}\ d^{-1}$)	CO_2 recovery efficiency (%)	pH before CO_2 supply	pH after CO_2 supply
1	0.4	0.46 ± 0.11	0.83 ± 0.19	115	9.85 ± 0.08	9.43 ± 0.09
2	0.8	0.75 ± 0.12	1.35 ± 0.21	94	9.35 ± 0.11	8.33 ± 0.17
3	1.2	0.75 ± 0.11	1.35 ± 0.20	63	9.34 ± 0.05	8.13 ± 0.16

[a] Values from steady-state (Day 10-18) were averaged. [b] CO_2 fixing rate (R_{CO_2}) was calculated per PBR (1 L) basis.

Table III-6. Carbon mass balance analysis of the experiments.

Carbon species* (g-C)	Run 1		Run 2		Run 3	
	In	Out	In	Out	In	Out
Supplied CO_2	3.6	-	6.4	-	7.3	-
Dissolved inorganic carbon (DIC)	8.5	10.6	8.6	12.3	8.5	12.9
Dissolved organic carbon (DOC)	0.2	0.7	0.2	0.7	0.2	0.5
Algal biomass	0.4	2.0	0.3	2.1	0.2	2.1
Sum	12.6	13.3	15.4	15.2	16.2	15.5

*Cumulative amounts over 18 days of experiment.

Table III-7. Biomass productivities and photosynthetic efficiencies[1].

Phase		Volumetric productivity ($gDW\ L^{-1}\ d^{-1}$)	Areal productivity. ($gDW\ m^{-2}\ d^{-1}$)	Photosynthetic efficiencies (%PAR[2])
1	Microporous	0.67±0.19	9.6 ± 2.7	10.3 ± 2.9
	Polypropylene	0.64±0.17	9.2 ± 2.5	8.3 ± 2.2
2	Microporous	1.98±0.62	28.5 ± 8.9	9.1 ± 2.8
	Polypropylene	1.32±0.44	19.0 ± 6.4	6.1 ± 2.1
3	Microporous	1.90±0.24	27.4 ± 3.5	3.3 ± 0.4
	Polypropylene	0.97±0.20	13.9 ± 2.8	1.9 ± 0.4

[1]The presented data are average of the last three days of each phase.

[2]PAR: photosynthetically available radiation (400-700 nm).

Figures

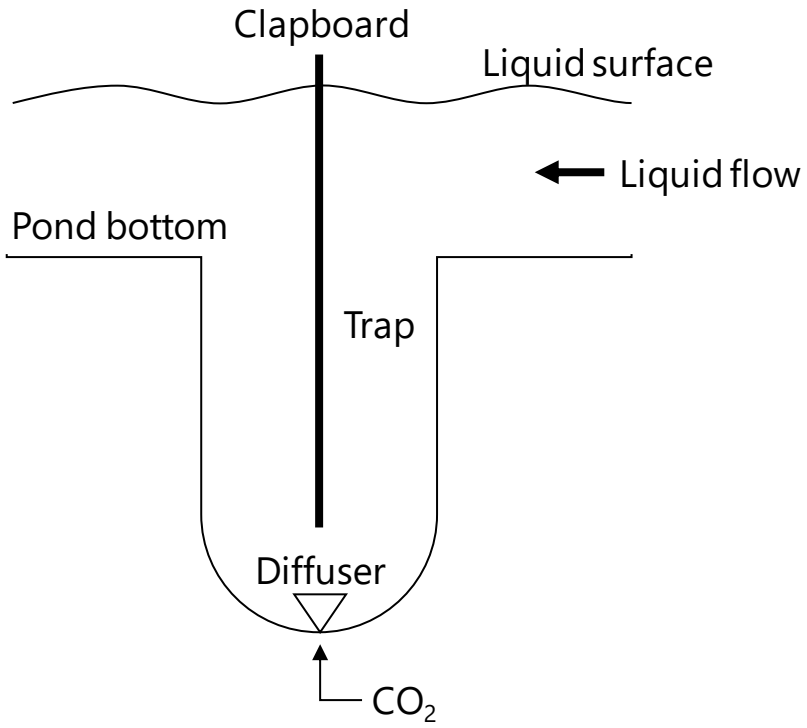

Fig. III-1. Schematic diagram of CO_2 supplementation ditch in an open raceway pond (modified from Bao et al., 2012). The depth of a common ditch is 1 m.

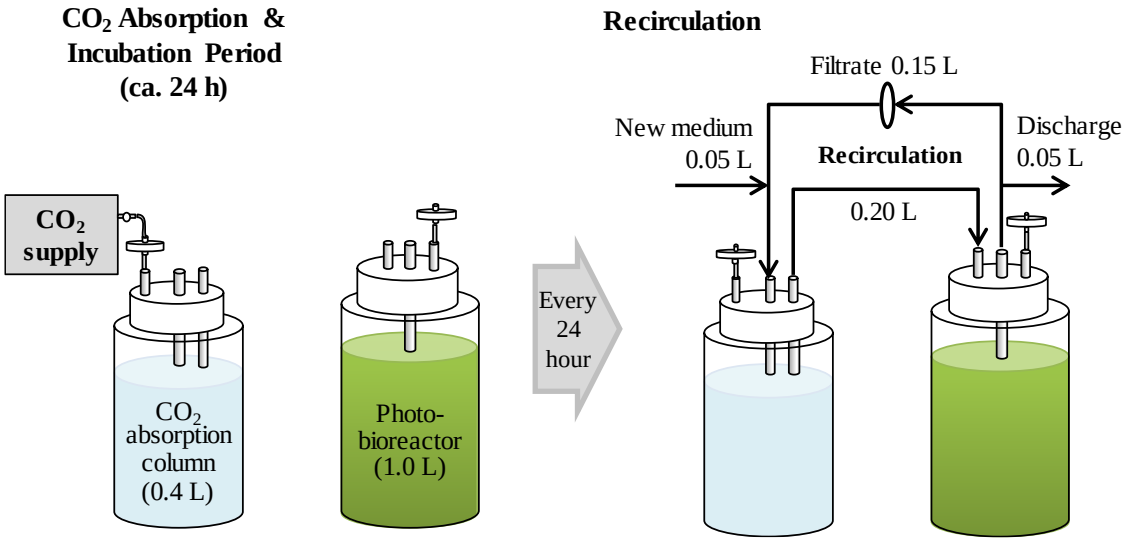

Fig. III-2. Experimental set-up of the semi-continuous operation of BICCAPS process. After 23.5 hours of CO_2 absorption and algal incubation period, circulation of the medium was implemented. After circulation, the headspace of the absorption column was replaced with CO_2 containing gas (Table 1) and a newly filled gas bag was attached.

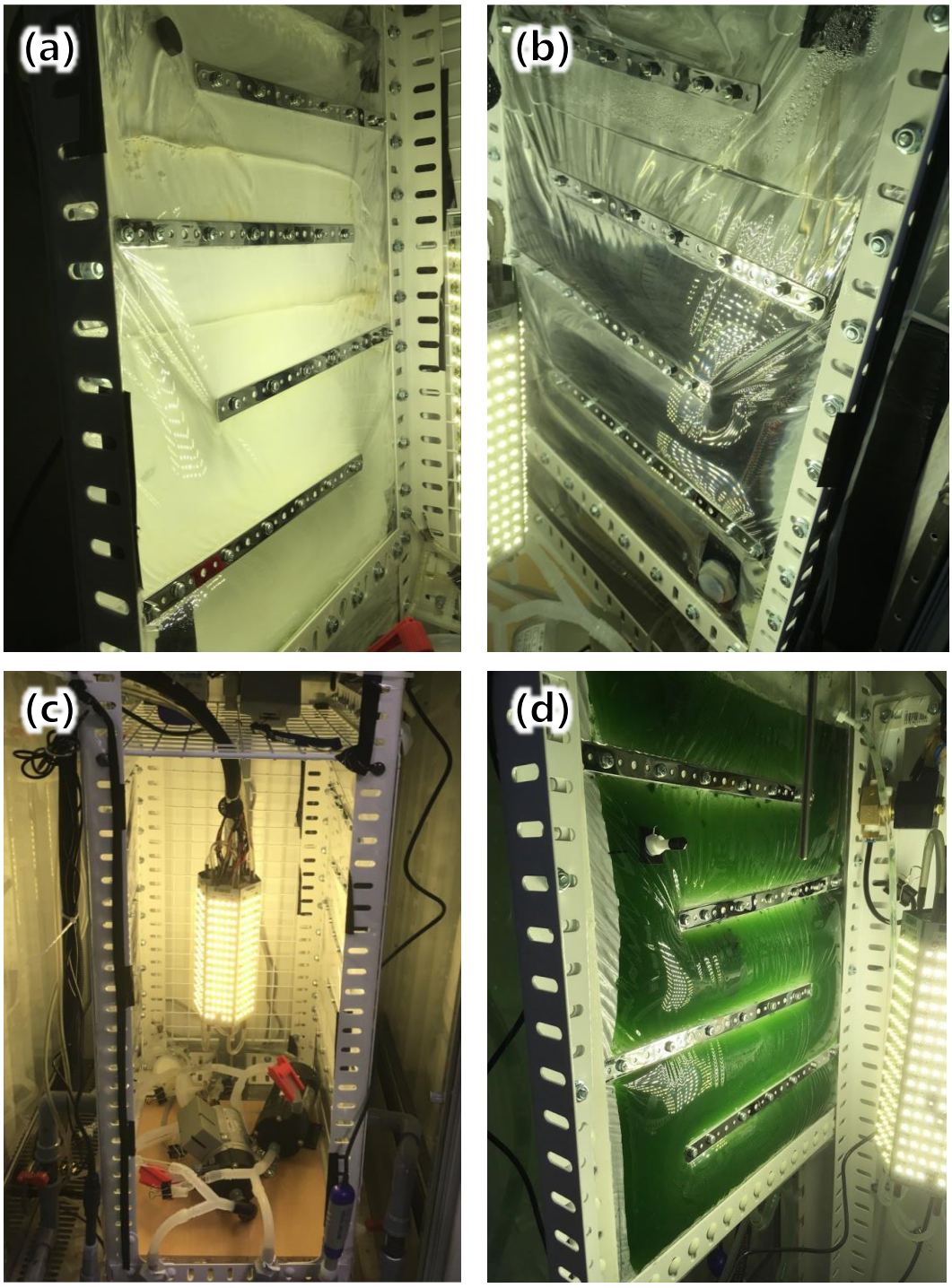

Fig. III-3. Photographs of the created (a) microporous and (b) polypropylene reactors, as well as (c) placement in an incubator with LED light, and (d) oxygen permeable reactor with *Arthrospira platensis*.

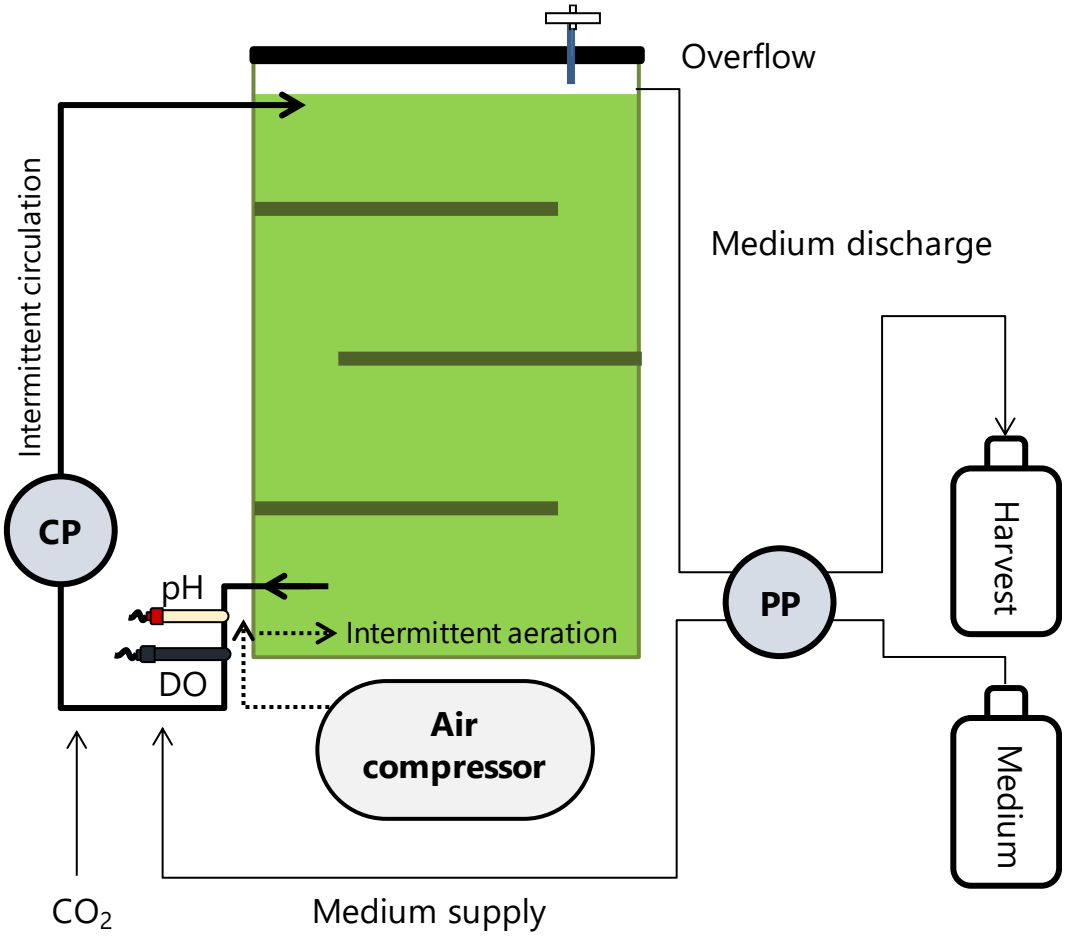

Fig. III-4. Operational condition of bag reactors. PP peristaltic pump; CP: centrifugal pump.

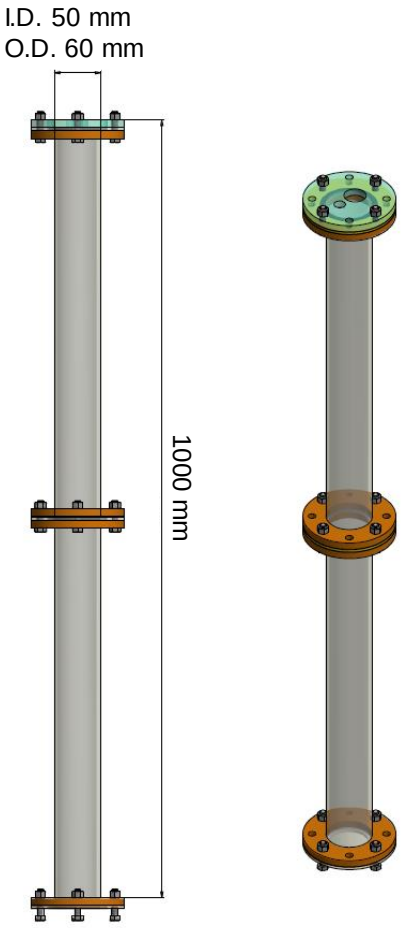

Fig. III-5. Schematic diagram of the CO_2 absorption column made of acryl resin.

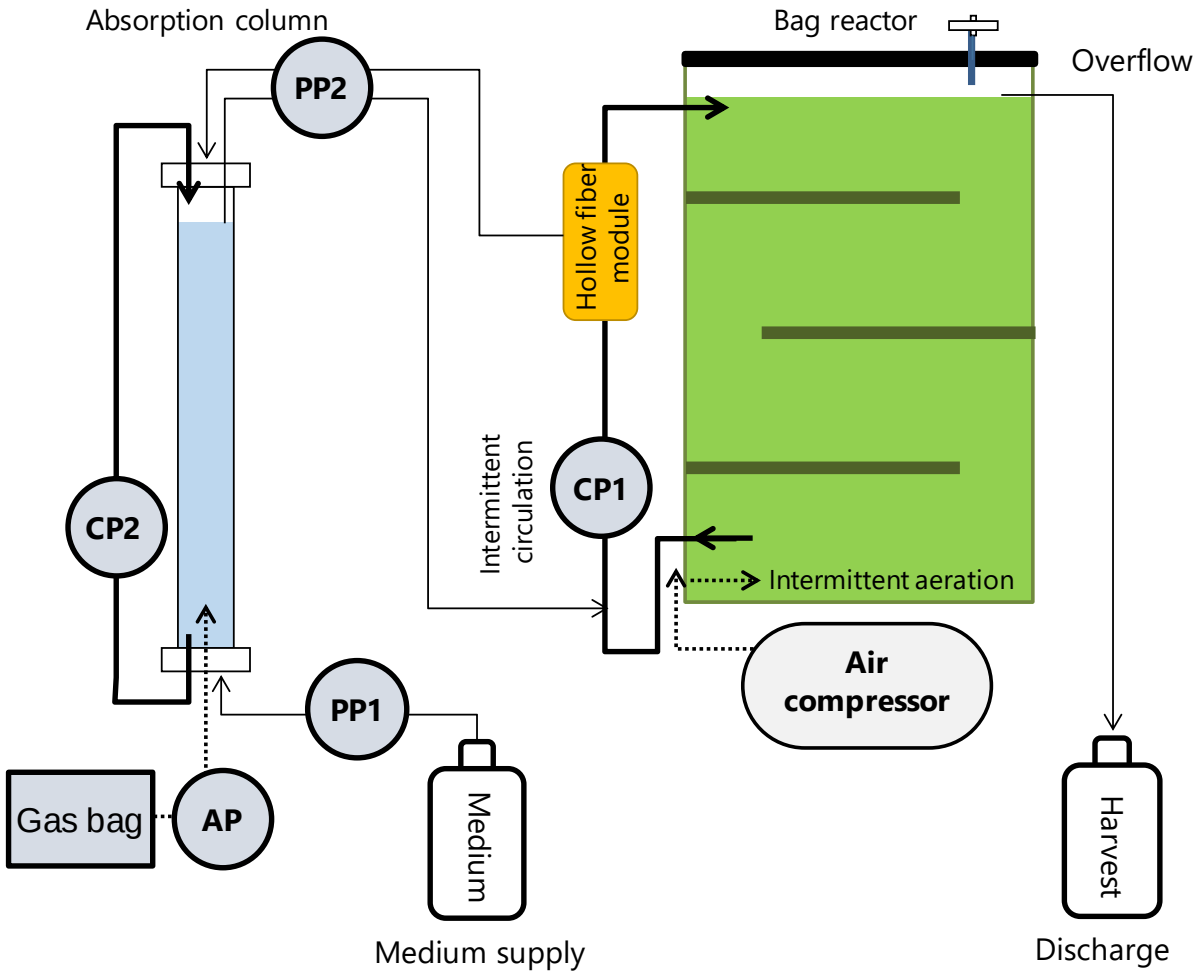

Fig. III-6. Operational condition of two-phase circulating CO_2 supply with the bag reactor. CP: centrifugal pump, AP: air pump, PP: peristaltic pump.

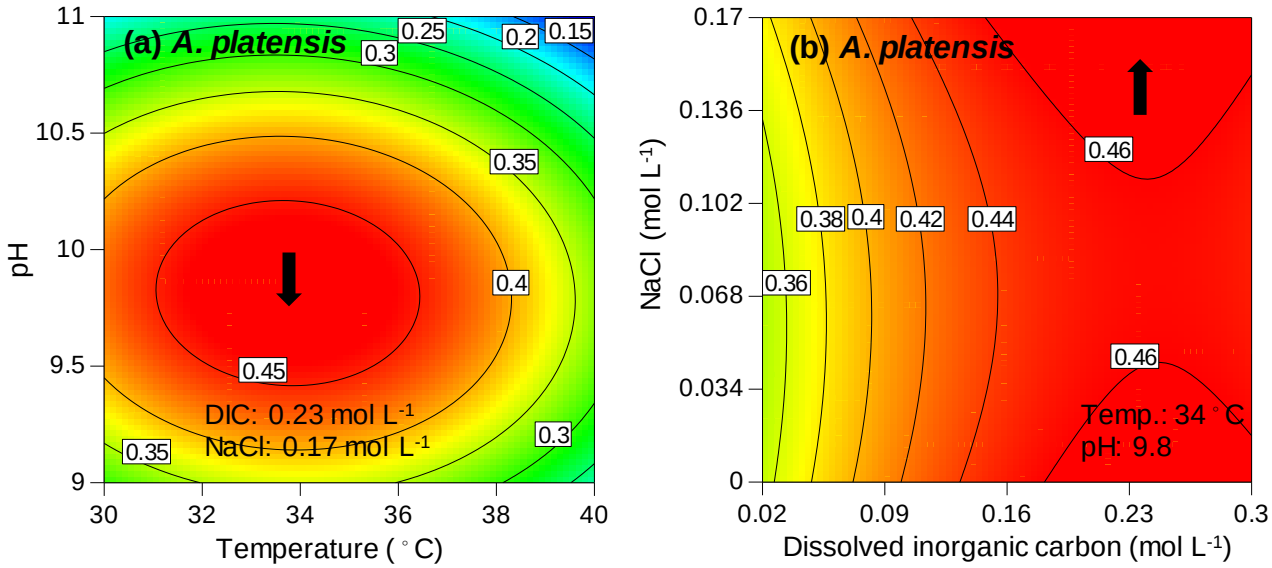

Fig. III-7. Response surfaces of the growth of *Arthrospira platensis* (a) temperature and pH and (b) dissolved inorganic carbon (DIC) and NaCl. The highest predicted points of growth are shown with arrows

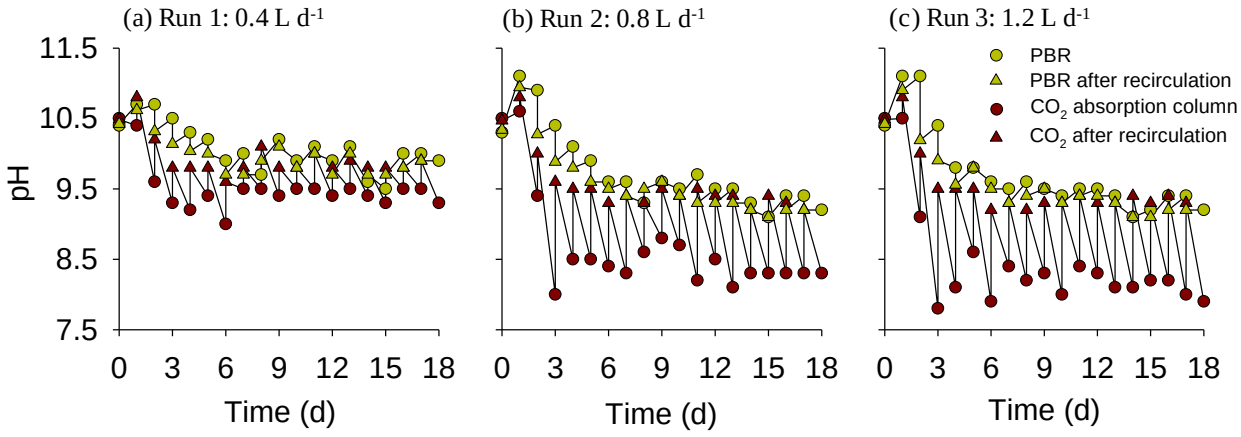

Fig. III-8. Time course of pH of each reactor (photobioreactors: PBR; and CO_2 absorption columns). There are two points in a day, representing pH change due to the circulation of medium between PBR and absorption column.

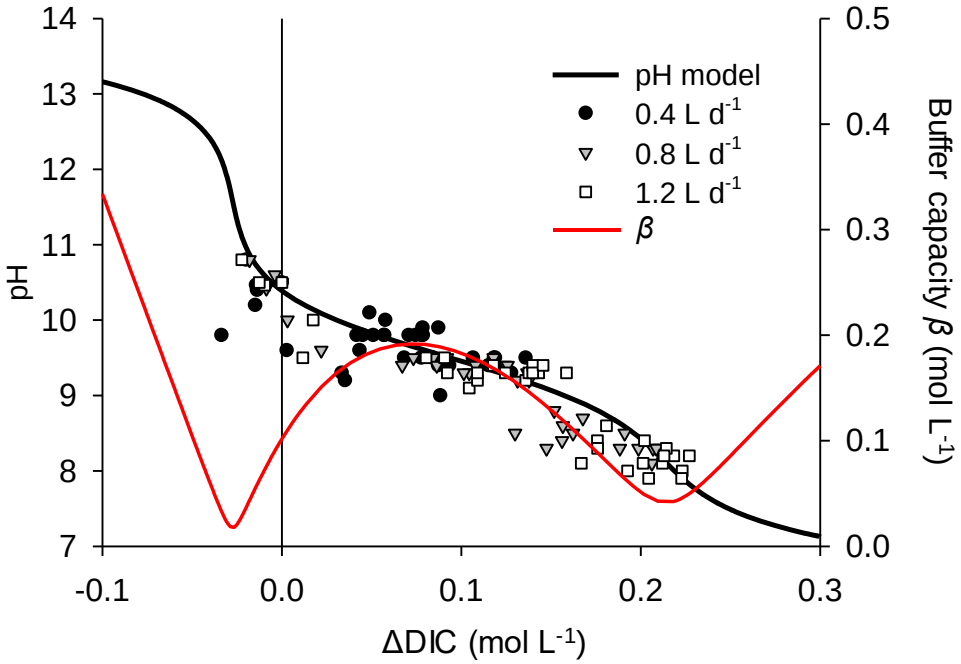

Fig. III-9. Estimation of pH and buffer capacity *β,* from change in dissolved inorganic carbon (ΔDIC). All data points were from absorption columns. ΔDIC was calculated by subtracting the initial DIC (ca. 0.27 mol L^{-1}) from respective DIC on each day.

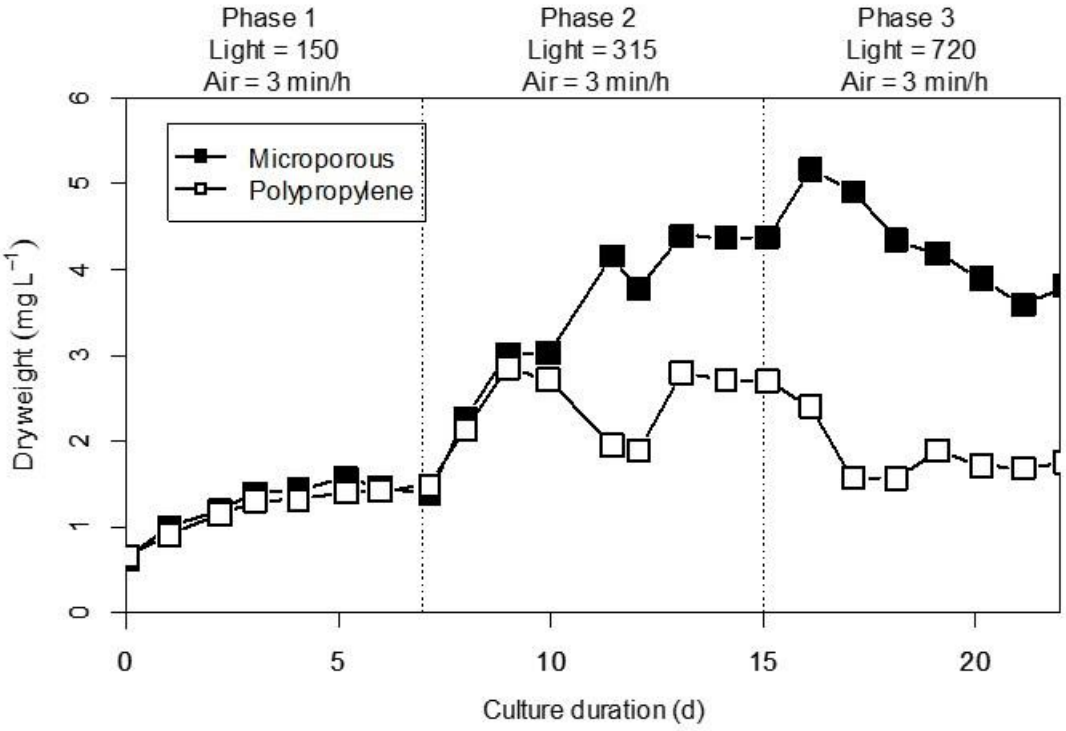

Fig. III-10. Algal dry weight at different culture condition in microporous film and polypropylene film bag reactors.

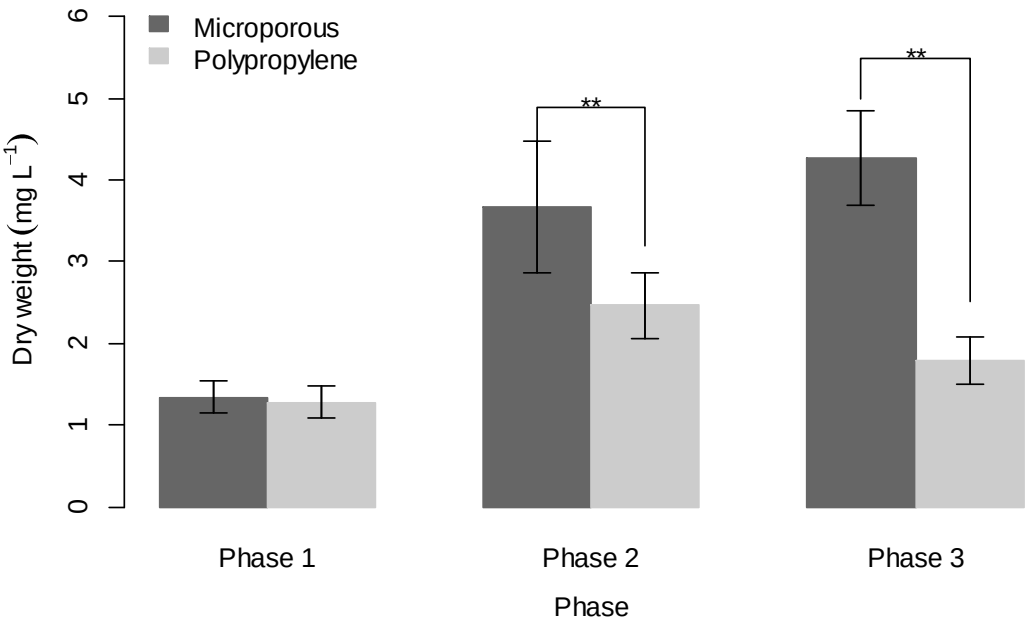

Fig. III-11. The average algal dry weight at each phase in microporous film and polypropylene film bag reactors. ** indicates $P < 0.01$ with student's t-test.

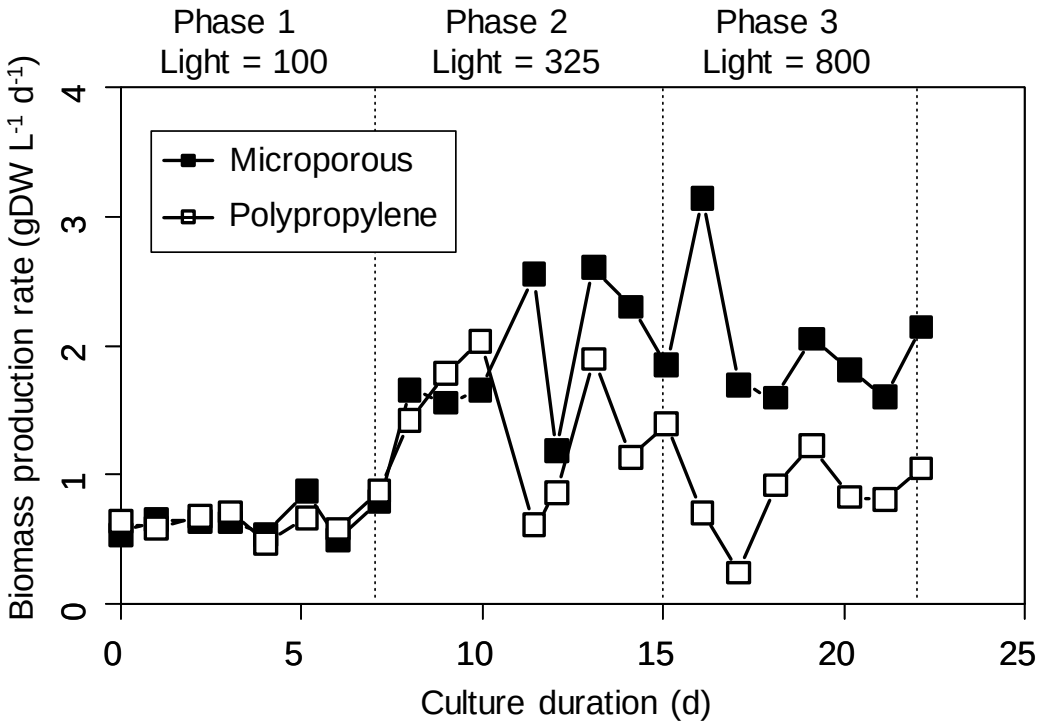

Fig. III-12. Biomass production rate in microporous film and polypropylene film bag reactors.

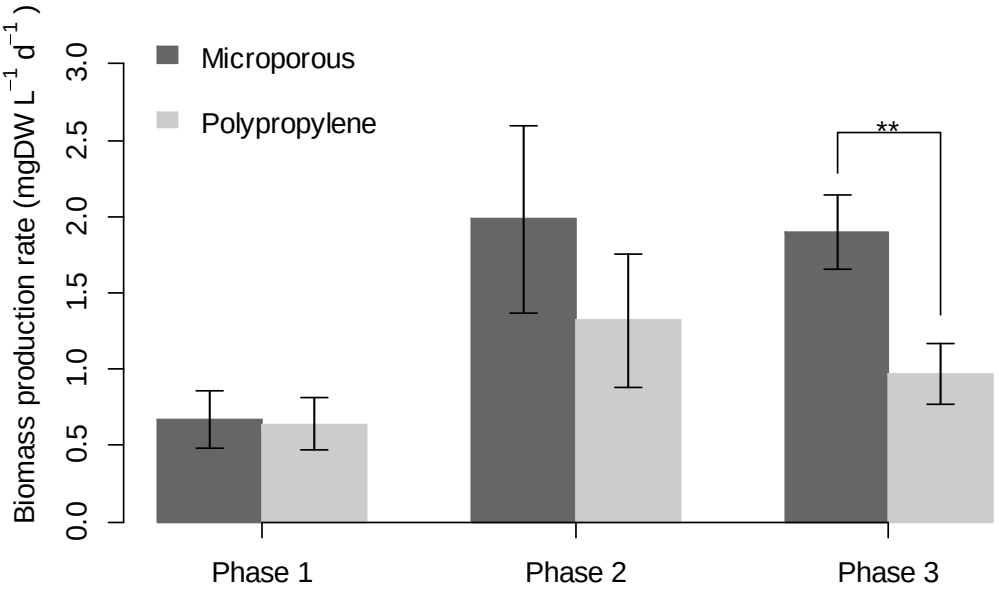

Fig. III-13. Average biomass production rates in each phase for microporous film and polypropylene film bag reactors. ** indicates $P < 0.01$ with student's t-test.

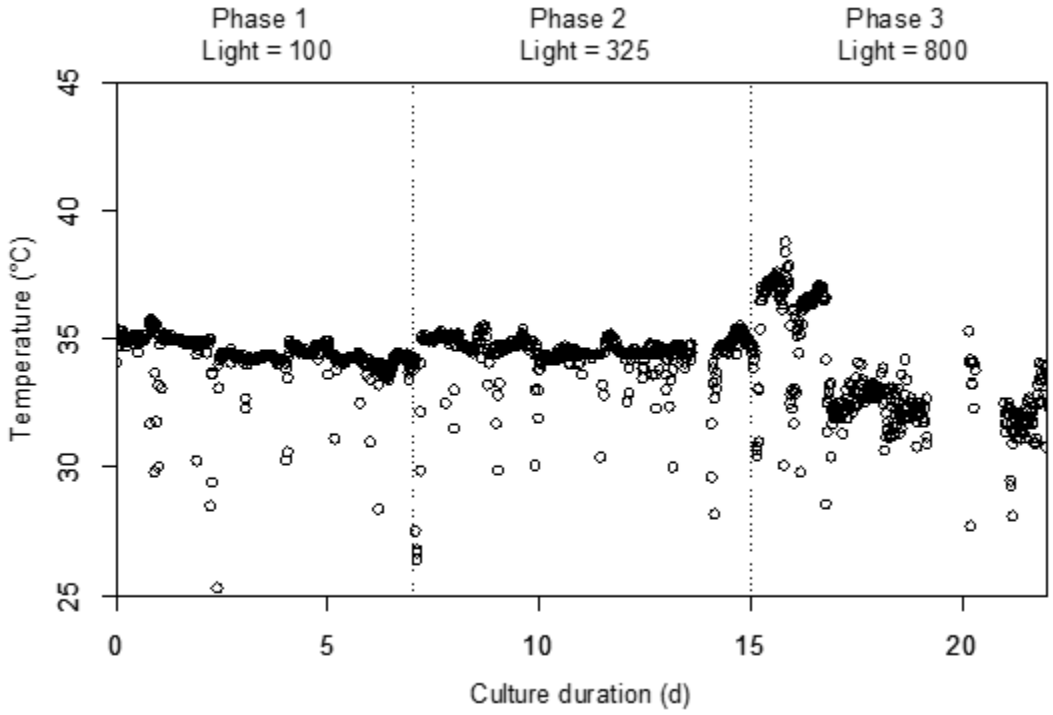

Fig. III-14. Temperature of the microporous film bag reactor.

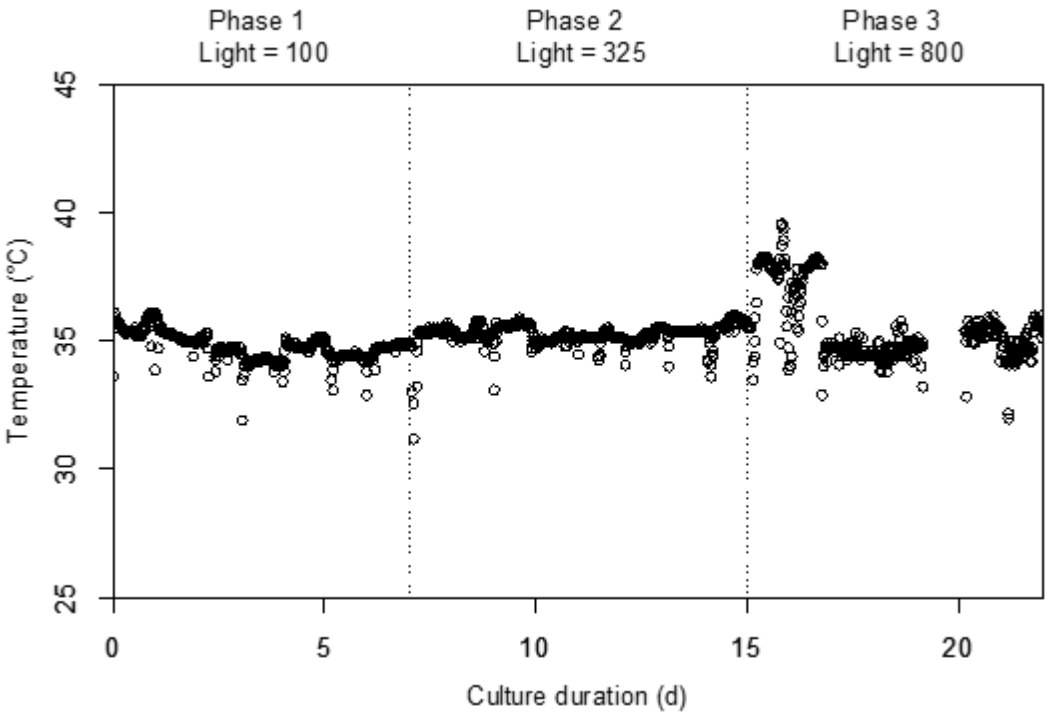

Fig. III-15. Temperature of the polypropylene film bag reactor.

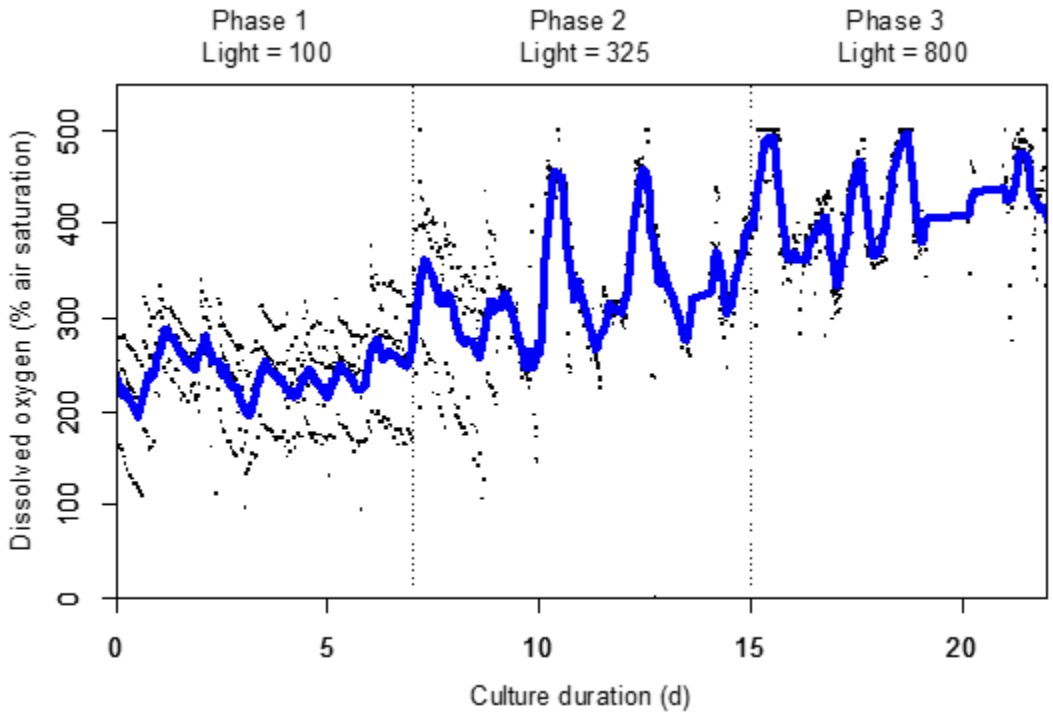

Fig. III-16. Dissolved oxygen concentrations of the microporous film bag reactor. Dotted plots are the raw values, and blue lines are the moving averages for 21 points (approximately 7 hours).

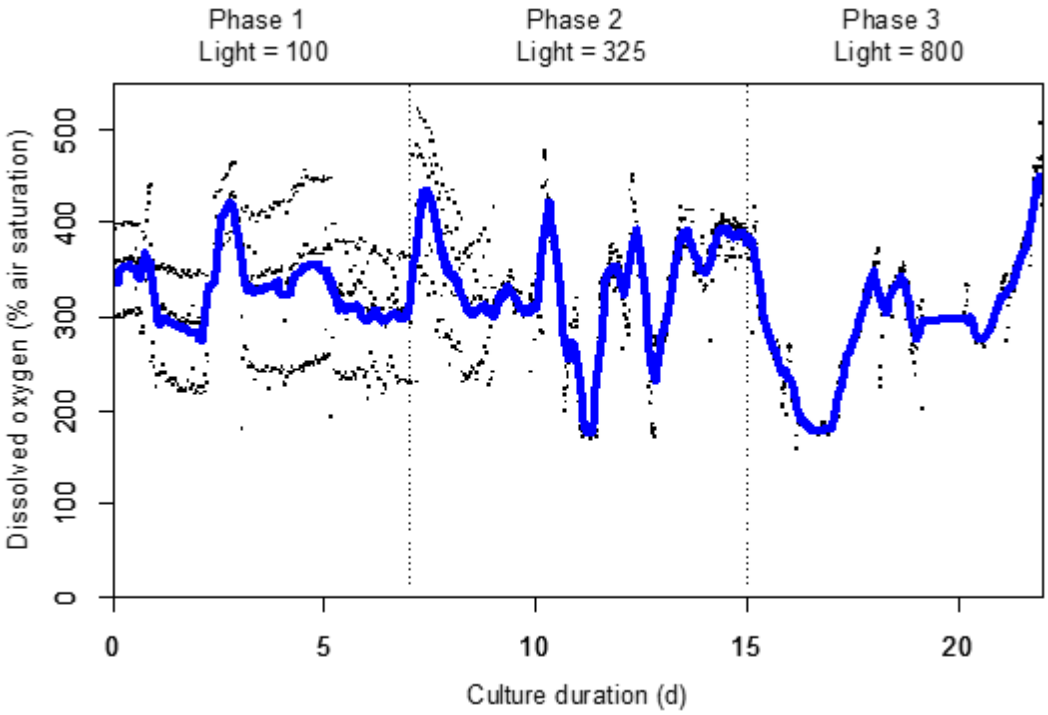

Fig. III-17. Dissolved oxygen concentrations of the polypropylene film bag reactor. Dotted plots are the raw values, and blue lines are the moving averages for 21 points (approximately 7 hours).

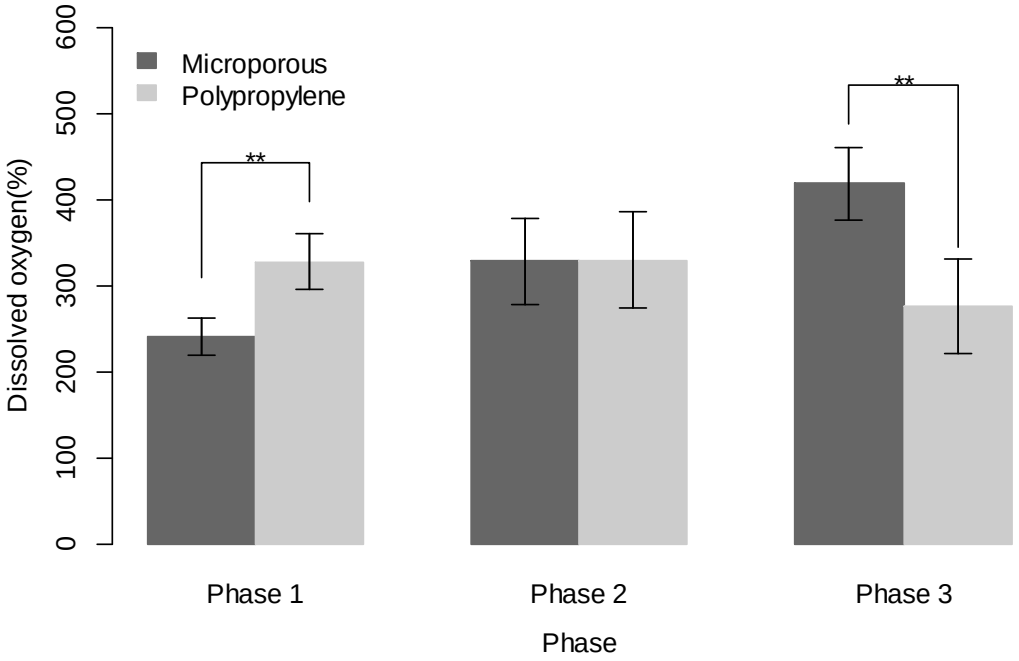

Fig. III-18. Average dissolved oxygen concentrations of microporous film and polypropylene film bag reactors in each phase. ** indicates $P < 0.01$ with student's t-test.

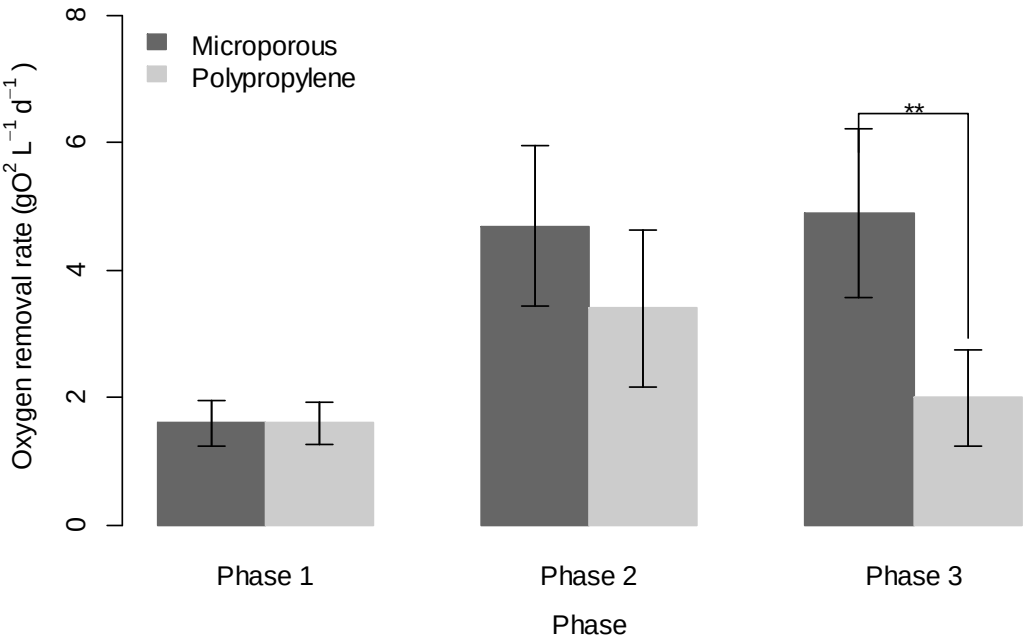

Fig. III-19. Average dissolved oxygen removal rates of microporous film and polypropylene film bag reactors in each phase. ** indicates $P < 0.01$ with student's t-test.

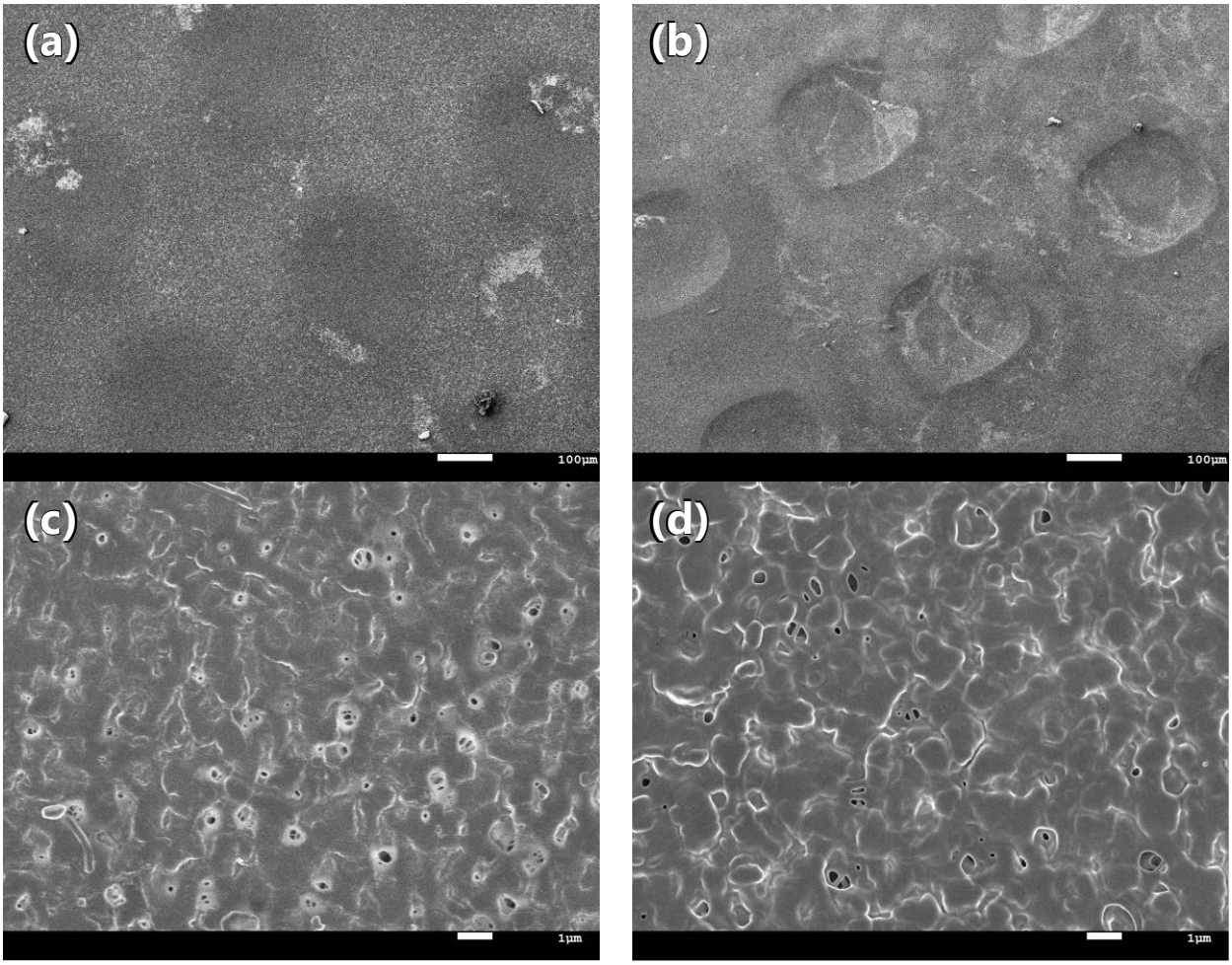

Fig. III-20. Scanning electron microscopic images of (a)(c) before and (b)(d) after 91 days of continuous *A. platensis* cultivation.

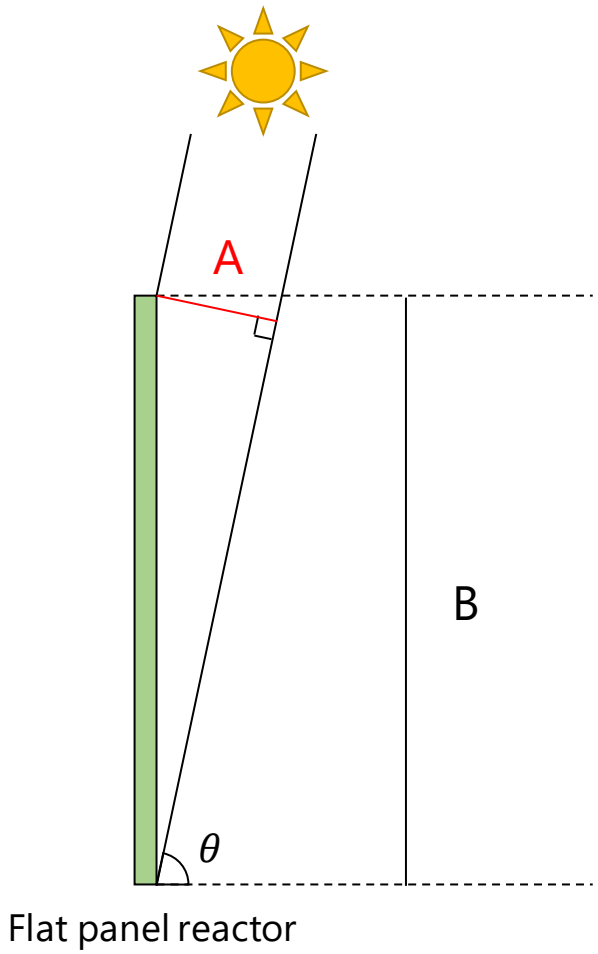

Fig. III-21. A schematic diagram of the effect of spatial light dilution. The areal difference between A and B becomes the diluted light intensity onto the reactor surface.

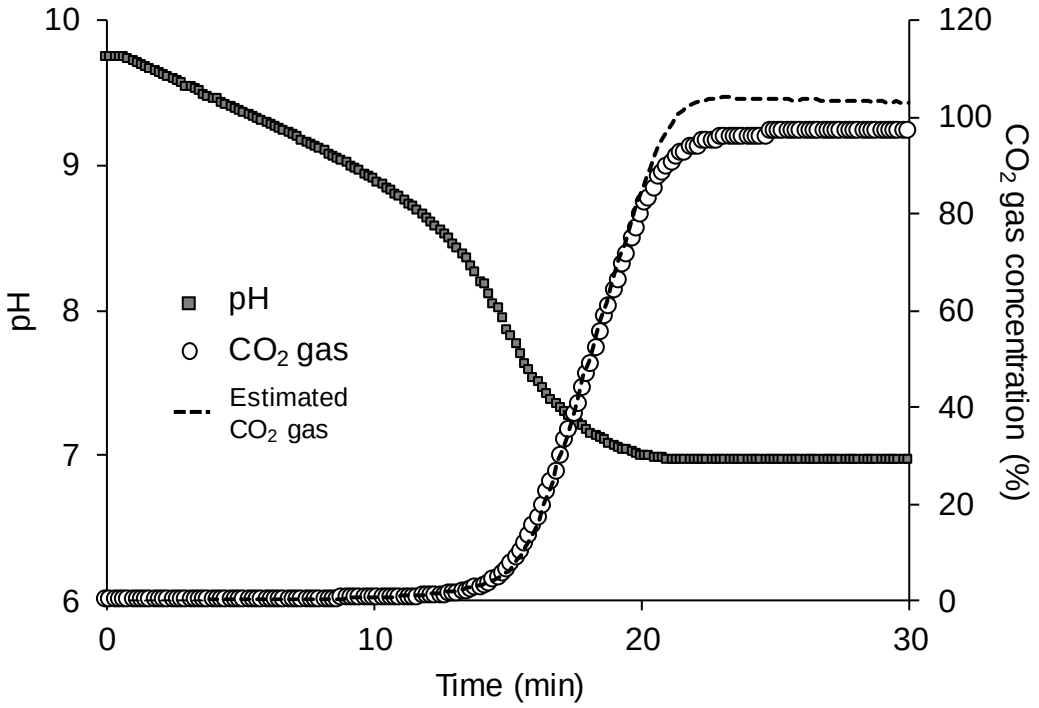

Fig. III-22. A typical time series of pH and headspace CO_2 concentration with 100% CO_2 bubbling into the absorption column.

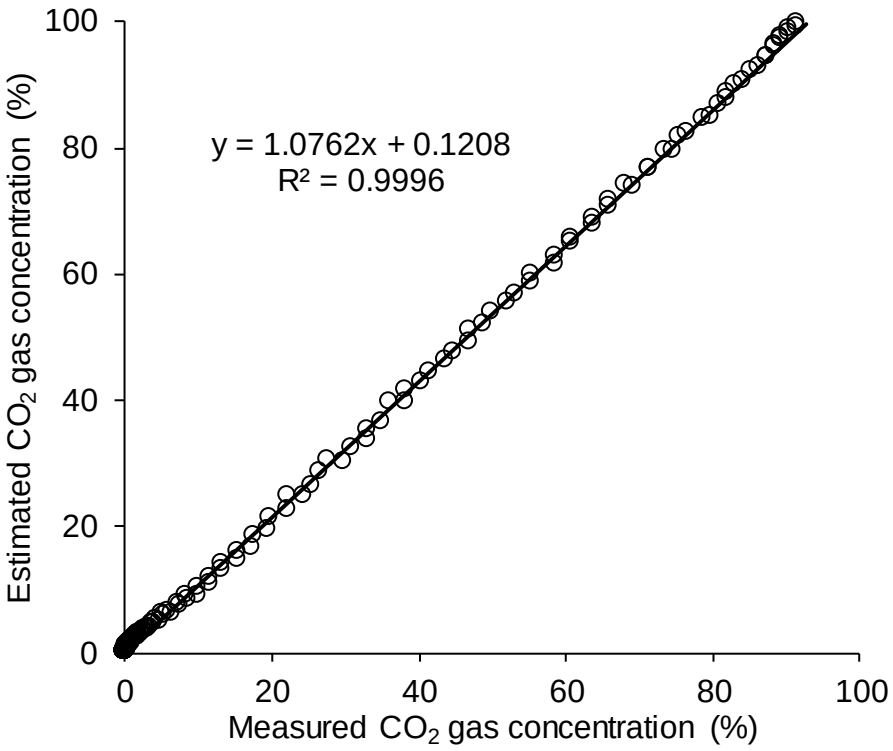

Fig. III-23. Correlation between measured and estimated CO_2 gas concentration in the headspace. The CO_2 gas concentration was calculated from pH of the medium. Data are mixture of duplicated experiments.

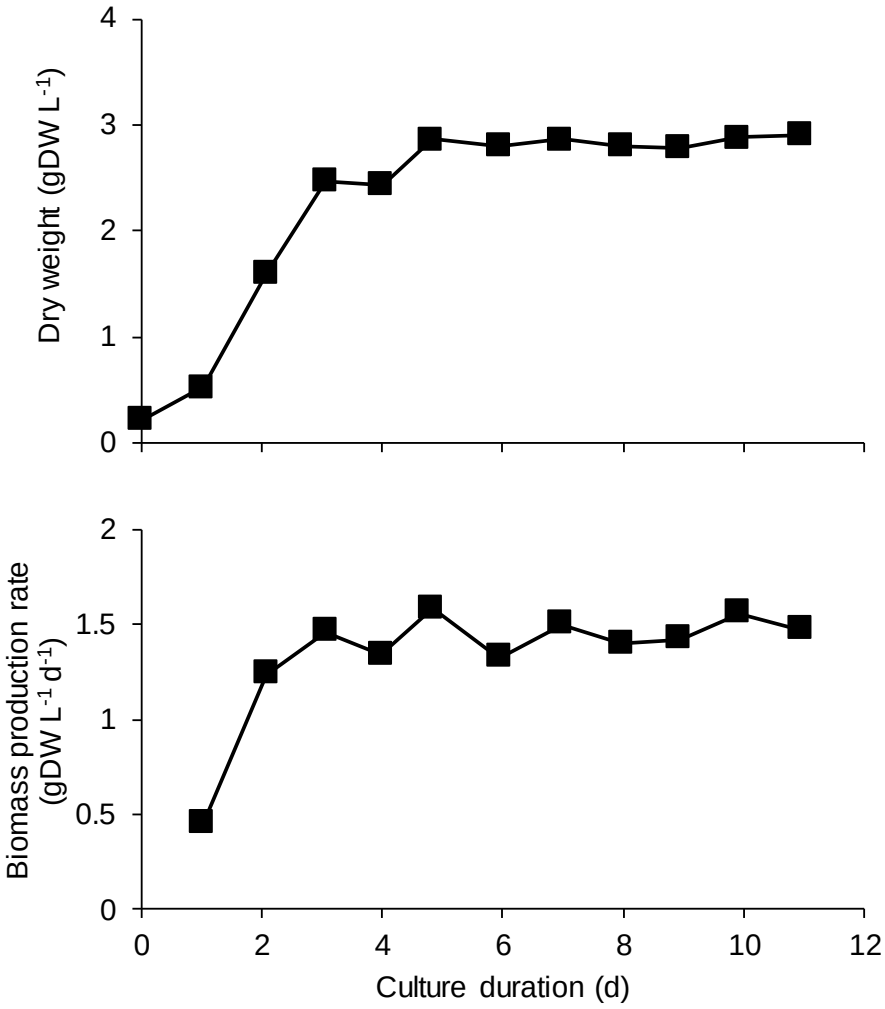

Fig. III-24. Dry weight and biomass production rate of *Arthrospira platensis* in the gas-permeating photobioreactor incorporated with two-phase CO_2 supply.

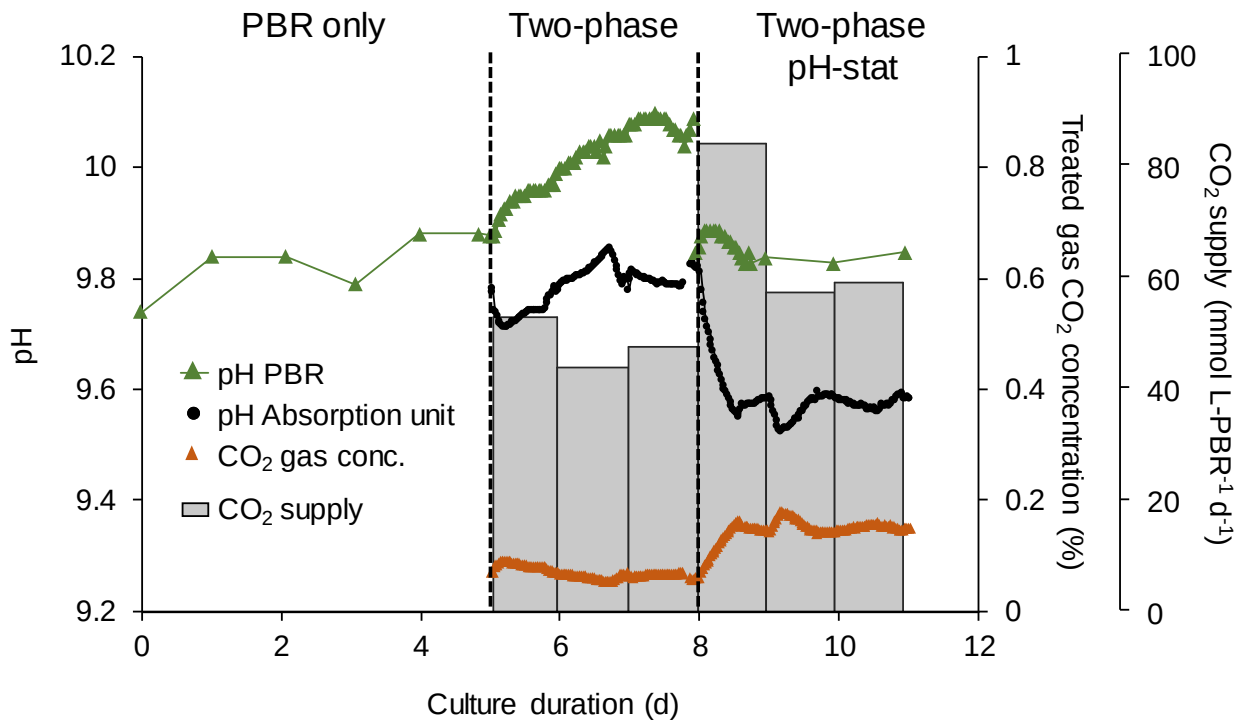

Fig. III-25. Time series of photobioreactor pH, absorption column pH, headspace CO_2 gas concentration, and total supplied CO_2 in a day.

CHAPTER IV

General discussion

The newly developed gas-permeating photobioreactor exhibited nearly one third of oxygen mass transfer coefficient of aeration with nearly one twentieth of energy consumption, and was found to be more energy-efficient and/or applicable than aeration and algal co-culture system for dissolved oxygen removal (Chapter II). By configuring bicarbonate-based two-phase CO_2 supply system, aeration requirements and CO_2 loss can be greatly reduced (Chapter III) indicating potential further improvements in energy and cost consumption of algal mass culture. To confirm the feasibility of the gas-permeating reactor and the processes regarding the usage of it, the economic and energy balance should be concerned. In this chapter, the economic feasibility of gas-permeating photobioreactor for mass cultivation of *A. platensis* was discussed. Furthermore, the discussion includes the effect of different microporous film properties on oxygen permeability, and future studies for improving algal mass-cultivation.

4.1. Comparative evaluation of economic balance of gas-permeating photobioreactor

The gas-permeating photobioreactor developed in the present study was shown to reduce the need of aeration. However, the effect can be more visible in a large-scale implementation of the reactor, since oxygen permeation is more powerful during long incubation in a large-scale system. The reduction of energy cost due to minimized aeration should contribute to the decrease of total culture cost. On the other hand, the cost of relatively more expensive film materials than plastic sheet may become an issue. Therefore, in this section, the economic balance assessment, i.e. the initial and maintenance cost, of the developed gas-permeating photobioreactor was conducted, based on the economic comparison of different algae reactors by Norsker et al. (2011).

4.1.1. Scenarios and assumptions

4.1.1.1. Reactors and land area

In order to compare different types of photobioreactors under the same condition, the total culture area of 100 ha was assumed. The cost was calculated per hectare basis here. According to the previous economic comparison of open pond, tubular reactor, and flat panel reactor, it was discovered that tubular reactor was the most economical option (Norsker et al., 2011). Based on this calculation, the electricity and cost-effectiveness of (1) the newly developed gas-permeating bag photobioreactor was evaluated comparatively with the (2) tubular and (3) flat panel reactors in the previous study.

All the three reactors are simulated to be composed of plastic films, except for one side of the gas-permeating reactor. Tubular reactor (Fig. IV-1-a) is composed of 50-m-long plastic tubes with the inner diameter of 0.057 m. The tube intermittently goes through degassing unit for oxygen removal and CO_2 supply. The circulation time between degassers is 3.3 mins. Vertical flat panel reactor (Fig. IV-1-b) consists of 0.03-m depth plastic bags assisted with steel frames. Each reactor is 0.75 m apart, making it a half of the reactor height 1.5 m. Flat panel reactor is continuously aerated at 1 L L^{-1} min^{-1} for the mixing and gas exchange. Gas-permeating reactor (Fig. IV-1-c) followed the basic configuration of the flat panel reactor, with the same volume, height, depth, steel frame and positioning. Mixing of the culture medium, however, was made similar to the tubular reactor, as the middle of the plastic bag is sealed to formulate 15 pieces of 0.1-m-height tubes (see the right side of Fig. IV-1-c). The reactor shape was assumed to be similar to the current study (Fig. II-3) in which culture medium flows horizontally while flowing down from the top to bottom. In this cost and energy analysis, the reactor width is assumed to be longer (50 m) than the current study (0.35 m; Fig. II-3). Therefore, the total length for the culture medium to travel within the reactor is 1,500 m. This length of the reactor was determined based on the oxygen buildups inside the reactor, which is explained later.

The cost of microporous film was considered as variable, since the cost changes with the material, production system, production volume, and so on. Since the cost of polyethylene films in the current cost analysis was set at a low value (0.03 EUR m^{-1}, equivalent to 0.17 EUR m^{-2}), the effect of film price was evaluated by varying ratio of microporous to polyethylene film price. The base case was set as 25 times polyethylene film, because the consumer price of the microporous film (3M) is approximately 3.7 EUR m^{-2} bag reactor, which is about 22 times higher than estimated polyethylene film.

4.1.1.2. Biomass productivities and oxygen/CO_2 dynamics in gas-permeating reactor

The photosynthetic efficiencies of tubular and flat panel reactors were estimated to be 3% and 5% of solar irradiation based on the review of previous outdoor algal cultivations (Norsker et al., 2011). The photosynthetic efficiencies of gas-permeating reactor was assumed to be the same as the continuous culture with PPFD 325 μmol m^{-2} s^{-1} (Chapter III); photosynthetic efficiencies from photosynthetically available radiation was 9.1%, which is equivalent to approximately 3.9% solar radiation. The areal output rate was estimated from the photosynthetic efficiency and the annual solar irradiance in Netherland (Table IV-1) to compare the productivities with the previous study (Norsker et al., 2011).

The oxygen production was estimated based on the specific oxygen production of 1.97 gO_2 gDW^{-1} for *A. platensis* (Torzillo et al., 1998). The oxygen concentration in the reactor was calculated using the oxygen production rate and the removal through gas-permeating reactor using the K_L obtained in Chapter III (Fig. IV-2-a). The reactor length that makes DO concentration over 300% was set as the maximum, in order to compare with the previous study (Norsker et al., 2011) under the same condition, and degasser unit was set at the end of each maximum length. The aeration unit was assumed to reduce the DO down to 133% (Norsker et al., 2011). According to the estimation, the time to reach DO concentration over 300% were calculated to be 46 mins for gas-permeating reactor. Based on the duration of maximum culture time, the distance between aeration

unit and another need to be less than 1,380 m for gas-permeating reactor, based on a linear flow rate of 0.5 m s^{-1}. While degasser in tubular reactor was installed every 3.3 min, which corresponds to 100-m length, gas-permeating reactor was estimated to reduce the frequency of reactor by nearly 14 times.

The DIC and pH changes inside reactor were estimated from the biomass productivity (Fig. IV-2-b). The DIC assimilation was estimated from the carbon to biomass ratio of 0.4 obtained in Chapter III. The pH of the reactor was also estimated from the DIC concentration using the equation developed in Chapter III (Eq. 18). Assuming 5 unit of reactor module in 1 ha, the time between each CO_2-enriched medium injection is approximately 1,300 mins. The pH at the injection point was estimated to rise only to 9.801 owing to the strong pH buffer capacity of SOT medium. Since pH only slightly increases, a single CO_2 absorption column can supply CO_2-enriched medium to a large number of reactors.

4.1.2. Cost and electricity analysis

The total cost of biomass using gas-permeating bag reactor at the base case (25-times polyethylene film) was 742 cents $kgDW^{-1}$, which was higher than flat panel (596 cents $kgDW^{-1}$) and tubular (480 cents $kgDW^{-1}$) reactors (Fig. IV-3). At the base case, the cost of reactor occupies over 40% of the total cost estimate. However, with decreasing price of the microporous film, the biomass production cost by gas-permeating reactor reduces. The production cost with gas-permeating reactor becomes the cheapest when the cost of microporous film becomes lower than 4-times polyethylene film (Fig. IV-3).

The breakdown of the total cost indicate that the highest cost resides in different categories for each reactor (Table IV-2): capital cost for tubular, energy cost for flat panel, and both capital and reactor costs for gas-permeating reactors. Capital cost becomes high for tubular and gas-permeating reactor owing to the culture circulation pump and degasser. The capital cost of the gas-permeating reactor is cheaper because of the reduced number of degasser by less than one tenth.

The high energy cost in flat panel reactor originates from the aeration cost, although the aeration rate (1 L L^{-1} min^{-1}) is 4 times less than the reported optimum value for high density culture (4.2 L L^{-1} min^{-1}; Qiang and Richmond, 1996). The energy cost was the cheapest with gas-permeating photobioreactor amongst the three photobioreactors, owing to the minimum aeration at degasser.

The energy cost could be further lowered by intermittent operation of the circulation pump. As demonstrated in Chapter III, in which circulation was only implemented for 12 secs every 120 secs, a high photosynthesis efficiency of 9.1% PAR was obtained. Therefore, the biomass production rate may remain at the high value with intermittent circulation. In the case of reduced circulation, however, the energy consumption by degasser may increase due to the longer retention time compared to the current scenario, reaching up to the same level as the tubular reactor (5~6 cents $kgDW^{-1}$). Even still, if the circulation energy can be simply reduced by 10-fold by intermittent circulation, the total energy consumption can be reduced to 14.2 cents $kgDW^{-1}$, which is 4 and 3.5 times lower than the tubular reactor scenario and gas-permeating reactor scenario, respectively (Table IV-2). Nevertheless, since the cost of degasser units compensates the energy cost reduction under the current scenario, the reactor configuration needs to be carefully reviewed to reduce the number of degasser units.

The cost and energy analysis revealed the potential of gas-permeating reactor for algal mass-cultivation. Energy reduction is an apparent direct merit of the gas-permeating reactor. The total cost of biomass production may reach cheaper than other bag reactors once the cost of gas-permeating film is less than 4-times value of polyethylene films. Modification in circulation frequency and reactor configuration could further improve the cost-effectiveness of the gas-permeable reactor.

4.2. Effect of microporous film properties on the oxygen-permeability, strength, and optical properties

While the selected microporous film in this study exhibited practical oxygen-permeability, it is necessary to evaluate different microporous films on their oxygen-permeability, physical strength and optical properties. Five commercial microporous films, with various thickness, pore sizes, and porosities were obtained (in total 10 film types). One of the films, Breathron, is comprised of PE microporous film and unwoven cloth to enhance the physical strength. The oxygen permeability was tested with the method described in section 2.3.1.1, both air-to-air and water-to-air oxygen permeability with an experimental apparatus depicted in Fig. IV-4. The water bearable pressure reported by each company was used for analysis.

The air-to-air oxygen mass transfer coefficient represents mass transfer coefficient through the membrane (k_M) because gas boundary layers are very small and gas transfer coefficient k_G is negligible (Carvalho and Malcata, 2001). The k_M values negatively correlated with film thickness (Fig. IV-5). However, the relative contribution of the membrane oxygen transfer resistance was found to be much smaller than that of liquid layer (Fig. IV-6). Therefore, it was suggested that, although membrane thickness exhibited negative impact on oxygen transfer coefficients through membrane, the effect was found to be nearly 100 times smaller than the change in the coefficients through the liquid layer. The mass transfer coefficient through liquid boundary layer correlated with contact angle, which represents hydrophobicity (Fig. IV-6).

The film physical strength increased with attaching unwoven cloth (Breathron) compared to microporous film only (Fig. IV-7). The water bearable pressure increased also with hydrophobicity of the film (Fig. IV-8). The optical characteristics analysis revealed that most of microporous film had similar properties as the microporous film tested in section 2.2.1.1, and over 80% of exposed light was reflected. The reflectance increased with thickness of the membrane film (Fig. IV-9). These results suggested that by improving membrane characteristics, not only the

strength of the reactor, but also the oxygen permeability would increase. Most suitable microporous film was suggested to be (1) highly hydrophobic, (2) moderately thick, and (3) laminated with strong unwoven cloth, in order to achieve high oxygen permeability and strength.

4.3. Further studies

4.3.1. Applicability of the gas-permeating reactor to other algal species

The present study revealed the improvement in biomass productivity with gas-permeating reactor for *A. platensis* culture (section 3.3.3.1). It also revealed the long-term durability of the oxygen-permeability (section 3.3.3.2). It is necessary, however, to evaluate if these characteristics of the developed gas-permeating reactor are universal across different microalgal and cyanobacterial species.

Firstly, the intensity of biofouling may differ depending on the extracellular polymeric substances (EPS) that microorganisms create. *Arthrospira platensis* is known to excrete highly viscous exopolysaccharides (Shiraishi, 2015). The fact that the membrane gas-permeability remained for long period with *A. platensis* suggest the applicability of gas-permeating reactor to other EPS-excreting microorganisms. However, consideration towards types of EPS might be necessary in critically discussion the practical feasibility. Most of the *A. platensis*-derived polysaccharides are known to be water-soluble (Olguín et al., 2001; Kurd and Samavati, 2015), indicating the hydrophilic properties of the polysaccharides. Since the microporous film adopted in this experiment is hydrophobic, these polysaccharides may have not easily been adhesive to the reactor surface. It was observed during the experiment that, even after certain accumulation of *A. platensis* biomass on the wall due to the gravity, liquid turbulence removed most of the biomass. However, if microorganisms excrete hydrophobic EPS, greater accumulation of biofouling may occur. The differential effects of EPS on adhesiveness can be observed in algal bioflocculation experiments (Oh et al., 2001; Gutzeit et al., 2005; Lee et al., 2009; Li et al., 2013; Wan et al., 2014), where certain bacterial or microalgal species exhibit higher flocculating characteristics than others.

It is therefore necessary to (1) test various algal/cyanobacterial species and (2) maintain bacteria-free unialgal culture to avoid undesirable biofouling development.

Secondly, while intermittent mixing was adopted in this study because it was found that intermittent mixing was enough for moderately high oxygen permeability and high photosynthetic efficiency (9-10%) with *A. platensis*. It is however necessary to demonstrate how different for other microalgal/cyanobacterial species. For example, some fast-growing and physically strong species, such as *Chlorella sorokiniana* (specific growth rate of up to 6 d^{-1}), may produce more biomass when culture is mixed continuously. On the other hand, the current method would be suitable with turbulence-fragile species such as *Haematococcus pluvialis* (Lemoine and Schoefs, 2010) may prefer the current moderate mixing. It is therefore necessary to find the most energy-efficient level of mixing, at which the highest biomass productivity per energy can be achieved, for each species and reactor setting, if highest efficiency is demanded.

4.3.2. Durability of the bag reactor material

While the cost analysis assumed 1-year durability of the gas-permeating reactor, it needs to be tested before practical operation. As described in section 4.2, the physical strength of microporous films can be enhanced by attaching appropriate unwoven cloth. This enhancement of strength needs to be critically evaluated for its cost-effectiveness.

For the long-term durability of the reactor, ultraviolet (UV) radiation compatibility needs to be evaluated. It was found in this study that approximately 40% of UV radiation was absorbed by the microporous film, indicating chemical reaction occurs with UV exposure, which may break the polymeric bridges of the plastic resins. The reactor structure (Fig. II-3) allows most UV radiation absorbed by (1) transparent plastic film, (2) culture suspension, and potentially (3) unwoven clothes from backside, and therefor greatly reducing UV effect on the microporous film. However, an outdoor long-term evaluation is necessary to test whether this assumption is correct.

4.3.3. Applications of the two-phase CO_2 recovery process

The two-phase CO_2 recovery process can be applied to gas purification techniques such as biogas purification. Anaerobic digestion biogas mainly contains methane, but also usually contain up to 40% of CO_2. In order for the biogas to be used as an alternative to natural gas, methane concentration needs to be elevated over 98% by removing CO_2 (Posadas et al., 2015). The two-phase CO_2 recovery process can simultaneously recover CO_2 from biogas for algal DIC supply, while purifying the methane gas.

One of the potential issues of the application of the developed process into biogas upgrading is intrusion of photosynthetic oxygen into biogas. Since the developed combined process of the two-phase CO_2 recovery process and the gas-permeating bag reactor does not aim for the complete removal of oxygen in the photobioreactor, recirculated medium in the CO_2 absorption column may contain up to 40 $mgO_2\ L^{-1}$. In order to reduce the excess oxygen intrusion into purified biogas, a small aeration apparatus could be configured to reduce DO concentration to near 100%-air saturation. The setting of such apparatus does not contradict with the design concept of the combined process that aimed to reduce aeration, because the aeration volume and intensity can be greatly reduced if it is limited to a small volume immediately before the absorption column. Compared to the conventional direct supply of CO_2-containing gas in to algal culture (Meier et al., 2015), the two-phase CO_2 supply system could achieve high methane purification with such apparatus.

Tables

Table IV-1. Estimated productivities of the three types of photobioreactors.

	Photosynthetic efficiency		Areal productivity	Areal daily productivity
	(%PAR)	(%solar)	(ton-DW ha^{-1} yr^{-1})	(gDW m^2 d^{-1})
Tubular reactor	7.1	3	41	11.2
Flat panel reactor	11.8	5	64	17.5
Gas-permeating reactor	9.1	3.9	50	13.8

*Values of tubular and flat panel reactors were derived from Norsker et al. (2011). Those of gas-permeating reactor were estimated based on the other values.

Table IV-2.Unit biomass production cost (in eurocents) calculated from capital and operating costs for tubular, flat panel, and gas-permeating photobioreactors based on the method by Norsker et al. (2011). The cost of microporous film was assumed to be 4-times higher than polyethylene film.

	Tubulars	Flat panels	Gas-permeating
	cents $kgDW^{-1}$	cents $kgDW^{-1}$	cents $kgDW^{-1}$
Major equipment + power			
Centrifuge	9.5	7.2	9.2
Power	4.0	3.0	3.8
Medium preparation	9.3	7.0	8.9
Power	0.8	0.6	0.8
Harvest buffer tank	3.9	2.9	3.7
Culture circulation pump	73.3	-	59.7
Power	47.1	-	44.5
Steel framework	-	11.7	14.9
Degasser*[1]	64.9	-	4.7
Blower/paddle wheel	1.0	69.3	0.1
Power	5.8	240.7	0.4
Other capital			
Installation costs	29.1	29.5	37.4
Instrumentation costs	9.7	9.8	6.0
Piping	29.1	29.5	37.4
Buildings	29.1	29.5	37.4
Variable costs			
Polyethylene tubing/sheet*[2]	12.8	9.8	49.6
Culture medium	44.0	44.0	44.0
Carbon dioxide	33.7	33.7	33.7
Medium filters	18.4	13.9	17.6
Labor	6.3	4.1	5.2
Salary overhead	1.6	1.0	1.3
Maintenance	29.9	30.2	38.4
General plant overheads	17.1	18.9	24.0
Total sum	480	596	483
Sum of capital cost	259	196	219
Sum of energy cost	57.6	244.3	49.4
Sum of variable cost	164	156	214

*1. Degasser was not included in the original text (Norsker et al., 2011) but added in this study. One unit was assumed to cost 150 EUR and last for 10 years.
*2. Sum of polyethylene and microporous film.

Table IV-3. Various commercial microporous films tested in this study.

Product name	Company	Material	Nonwoven fabric	Model number	Thickness (μm)	Pore size (μm)	Porosity (%)
Microporous film							
miraim	TEIJIN	PE[1]		(1) 01-20 (2) 02-35 (3) 05-75	25 30 75	0.1 0.2 0.5	80 80 80
BREATHRON	Nitto	PE	PET[2]	(1) BRN3000E1	250	N.D.	N.D.
			Nylon	(2) BRN-1860	350	N.D.	N.D.
Microporous Film	3M	PP[3]			38	0.3	21
POREFLON	SUMITOMO	PTFE[4]		(1) HP-020-30 (2) FP-022-60 (3) WP-020-80	30 60 80	0.2 0.22 0.2	N.D. N.D. N.D.
SILFINE	TOYOBO	Nylon		EL1044PWR3	40	N.D.	N.D.
Non-microporous film							
Silicone Rubber Sheet	TOGAWA RUBBER CO.	Silicone			500	—	—
PYLEN	TOYOBO	PP		P8128	50	—	—

1) PE: Polyethylene
2) PET: Polyethylene terephthalate
3) PP: Polypropylene
4) PTFE: Polytetrafluoroethylene

N.D. No data
— Not applicable

Figures

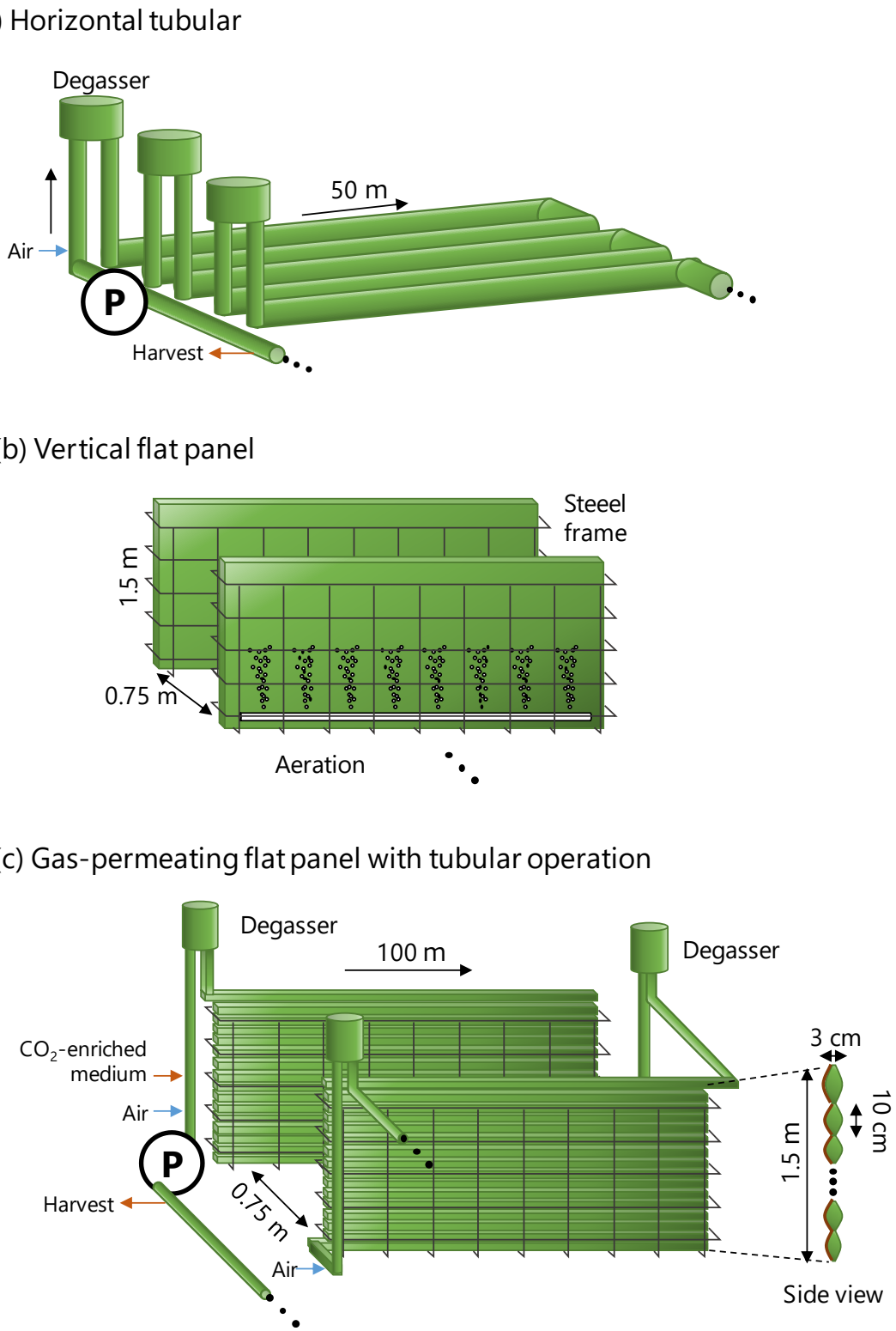

Fig. IV-1. Cost analysis scenarios (a) horizontal tubular, (b) vertical flat panel, and (c) gas-permeating flat panel developed in this study. Gas-permeating reactor was operated in tubular type to reduce aeration.

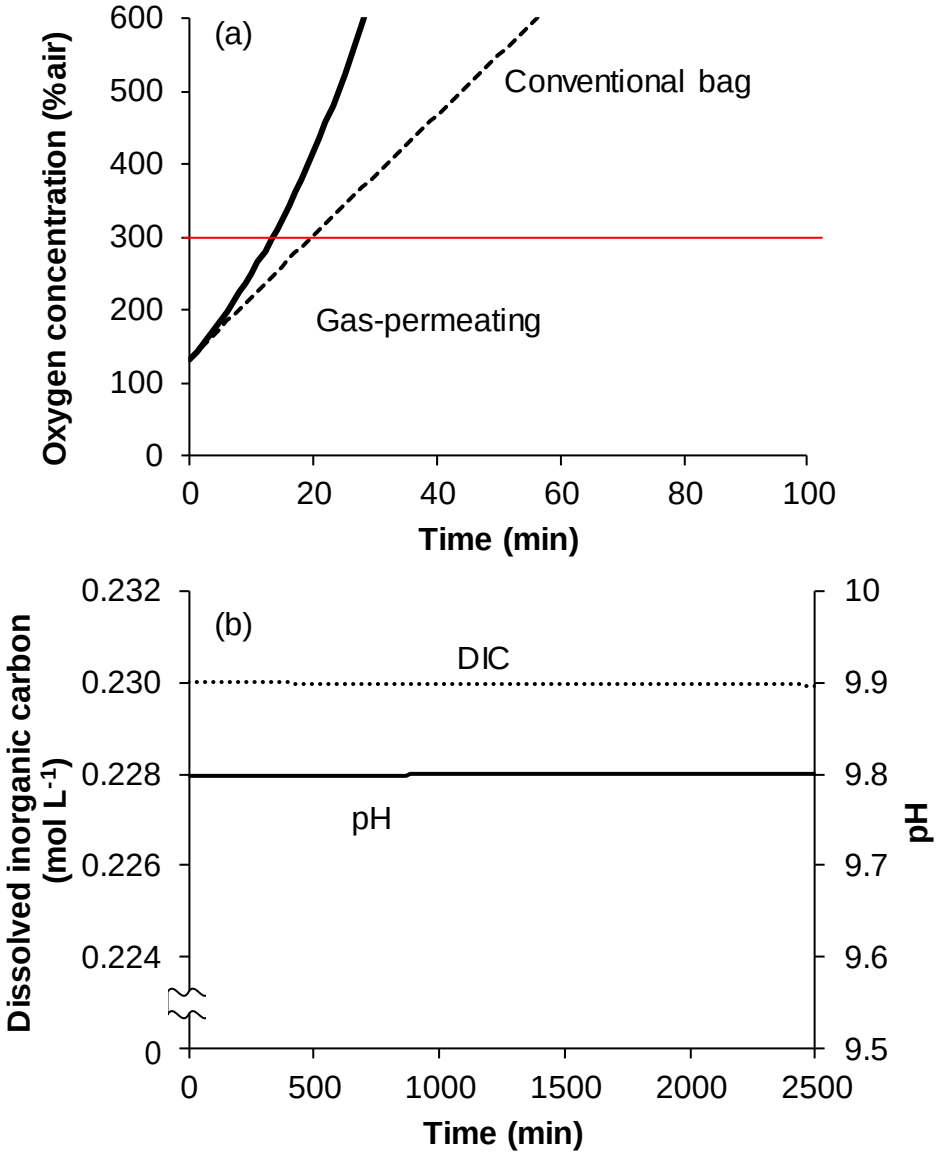

Fig. IV-2. Estimation of oxygen and carbon dynamics; (a) dissolved oxygen concentrations in gas-permeating reactor (solid) and conventional bag reactor (dashed); and (b) dissolved inorganic carbon (DIC) concentration and pH. Red solid line indicate the targeted oxygen concentration 300% as the tubular reactor design criteria (Camacho Rubio et al., 1999; Acién Fernández et al., 2001).

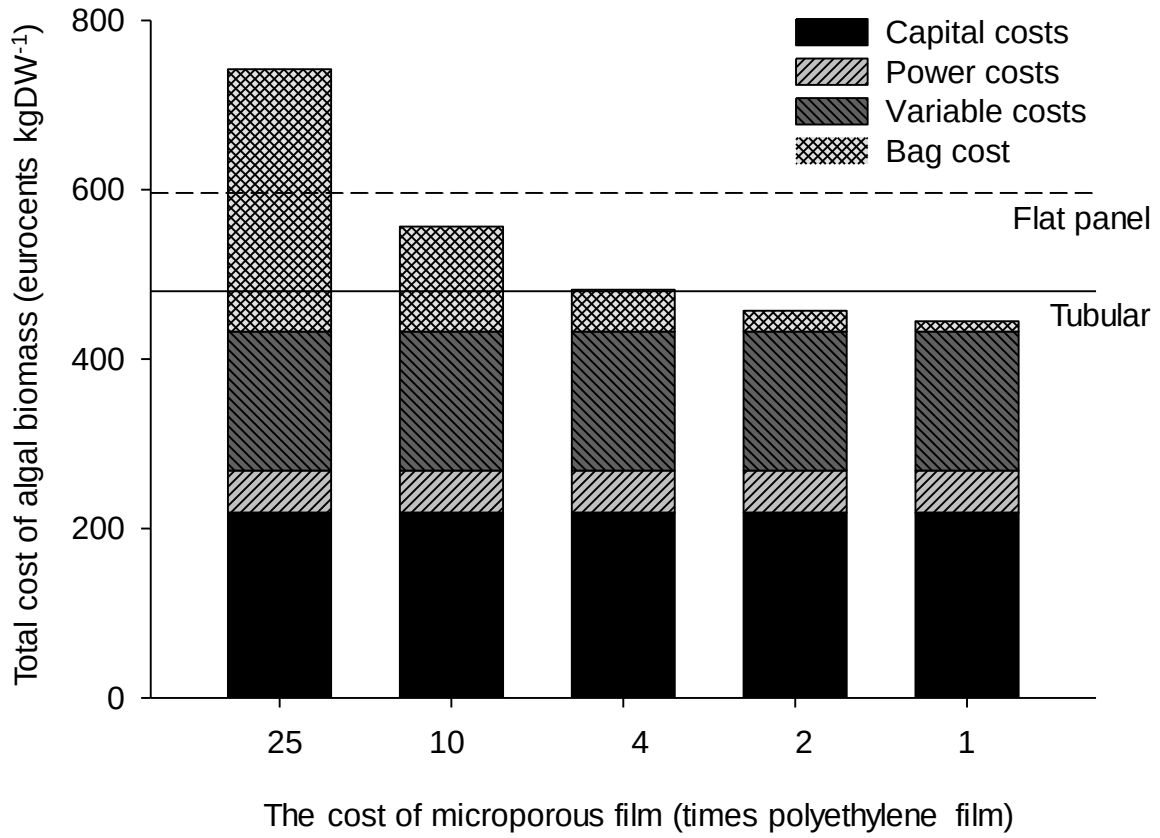

Fig. IV-3. Cost estimation of varying cost for microporous case. Base case is 25 times higher than polyethylene film (0.17 EUR m^{-2}). Dashed and solid lines are total cost of algal biomass production by flat panel and tubular reactors, respectively.

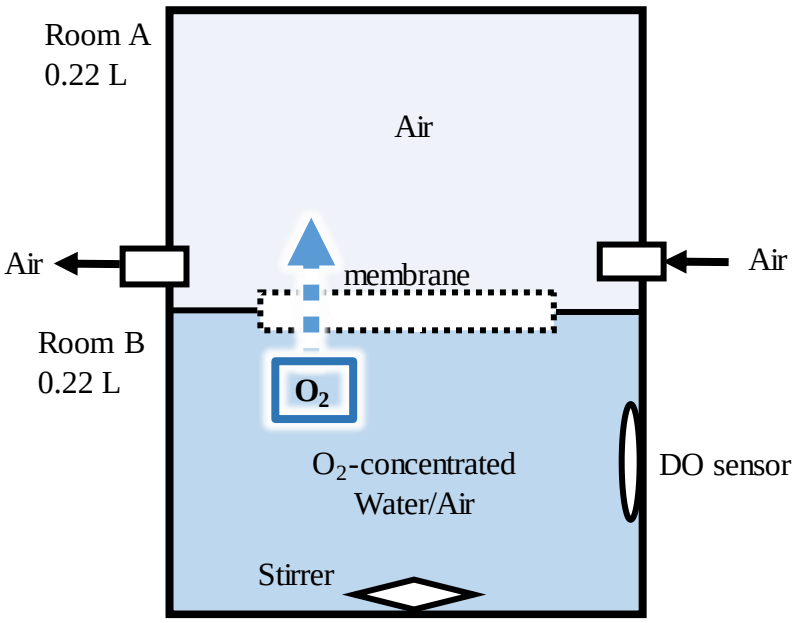

Fig. IV-4. Schematic diagram of dissolved oxygen (DO) removal measurement apparatus.

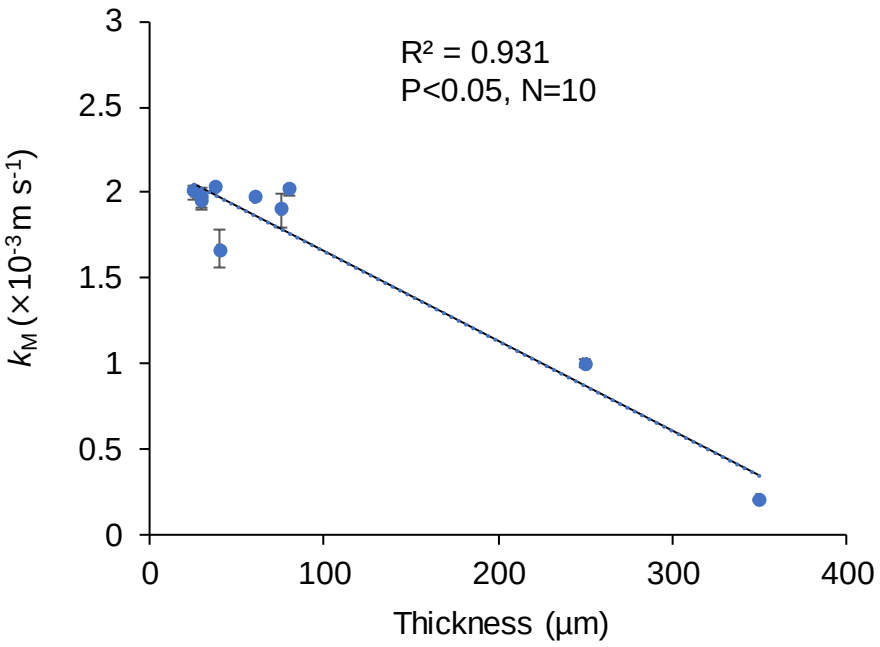

Fig. IV-5. The relationship between transfer coefficient of oxygen at membrane (k_M) and membrane thickness in the air to air condition. N=3 for all the 10 microporous membranes measured in this study.

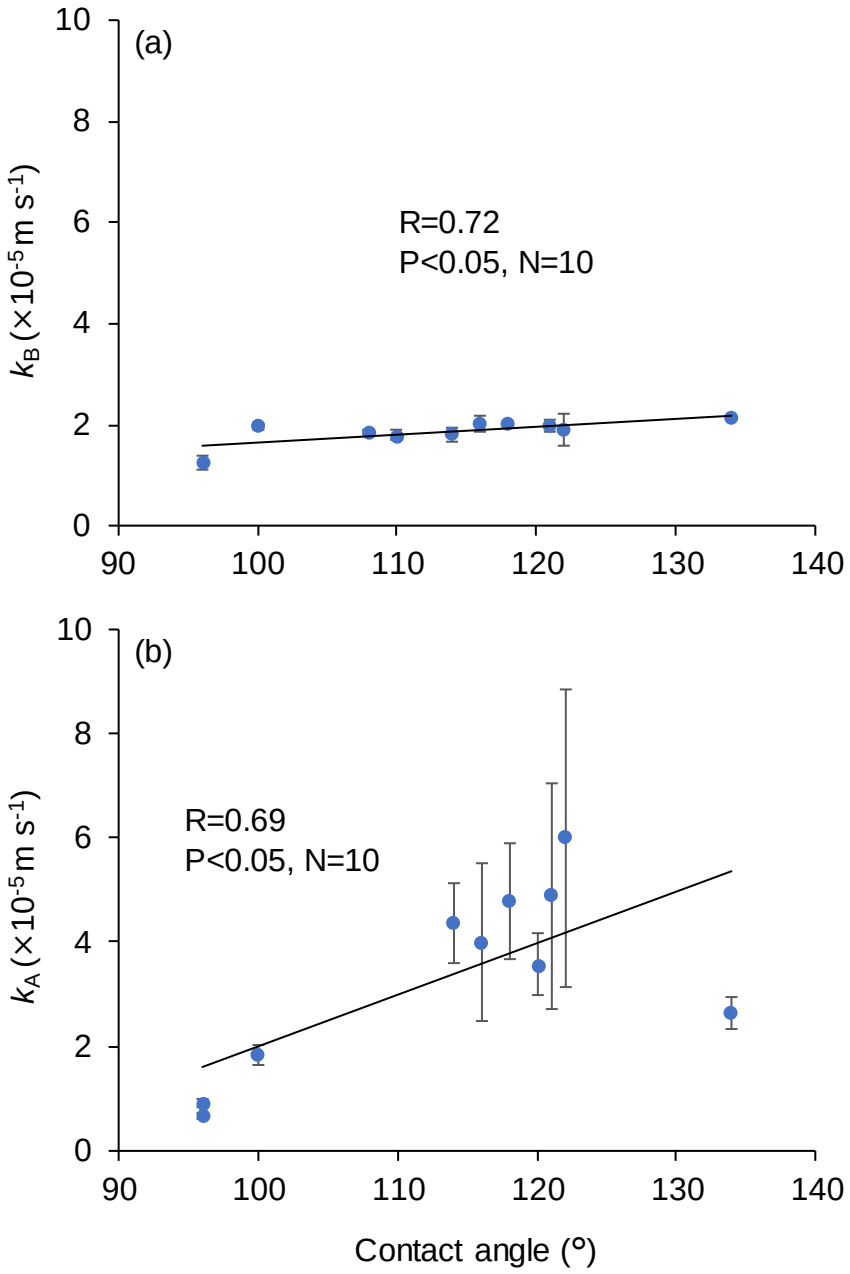

Fig. IV-6. The relationship between transfer coefficient of oxygen at liquid film in (a) Room B (k_B) and membrane thickness, and (b) Room A (k_A) and membrane thickness, with the water-to-air condition. N=3 for all the 10 microporous membranes measured in this study.

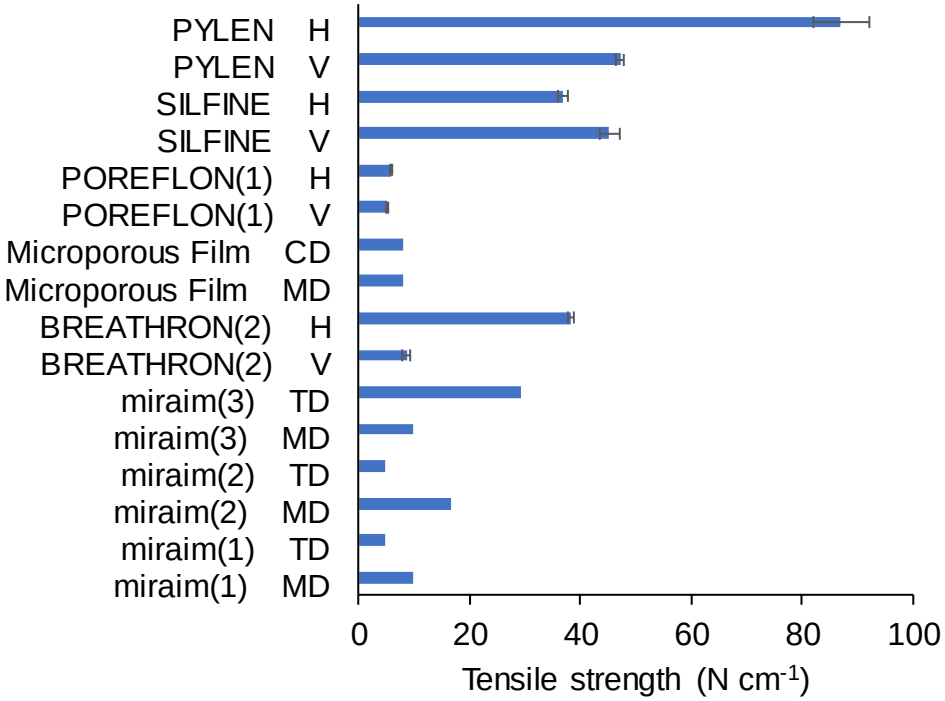

Fig. IV-7. Tensile strength of the membranes. The data is the value measured in this study for BREATHRON(2), POREFLON(1), SILFINE, and PYLEN. H is horizontal direction and V is vertical direction. The error bar shows the standard deviation. N=3 for all the four membranes. The data is the official value on the website of the company for miraim(1), (2), (3) and Microporous Film. MD is machine direction and TD is transverse direction.

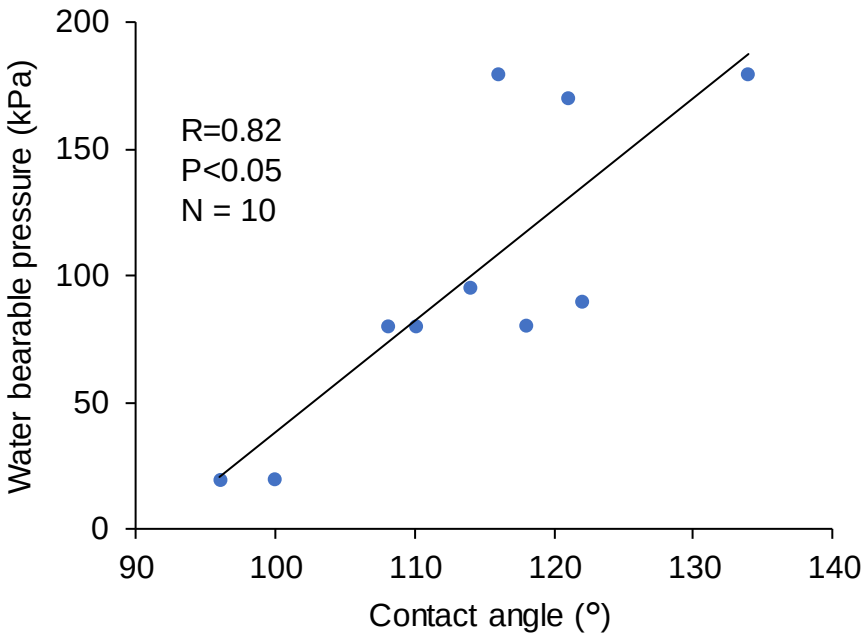

Fig. IV-8. The relationship between water bearable pressure and contact angle of membrane. N=1 for all the 10 microporous membranes measured in this study.

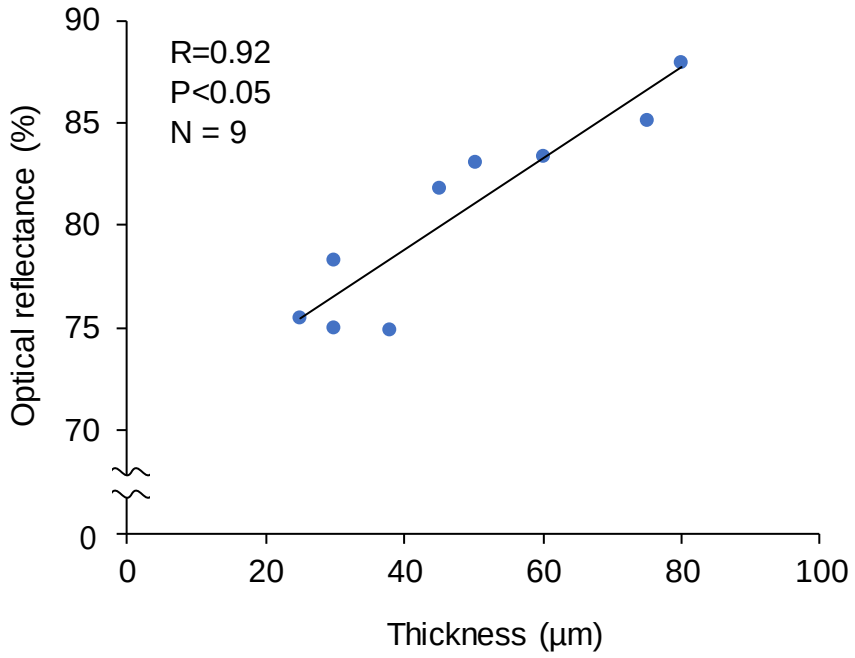

Fig. IV-9. The relationship between optical reflectance and membrane thickness. The thickness of Breathron was that of the microporous membrane section.

References

Acién Fernández F.G., J.M. Fernández Sevilla, J.A. Sánchez Pérez, E. Molina Grima and Y. Chisti (2001). Airlift-driven external-loop tubular photobioreactors for outdoor production of microalgae: Assessment of design and performance. *Chemical Engineering Science*. 56(8): 2721–2732.

Bafana A. (2013). Characterization and optimization of production of exopolysaccharide from Chlamydomonas reinhardtii. *Carbohydrate Polymers*. 95(2): 746–752.

Bahr M., I. Diaz, A. Dominguez, A. Gonzalez Sanchez and R. Munoz (2014). Microalgal-biotechnology as a platform for an integral biogas upgrading and nutrient removal from anaerobic effluents. *Environmental science & technology*. 48(1): 573–581.

Balgobin R. (2012). *Bubble-free oxygen and carbon dioxide mass transfer in bioreactors using microporous membranes*. Unpublished master's thesis. Western University. pp. 127.

Bao Y., M. Liu, X. Wu, W. Cong and Z. Ning (2012). In situ carbon supplementation in large-scale cultivations of *Spirulina platensis* in open raceway pond. *Biotechnology and Bioprocess Engineering*. 17(1): 93–99.

Barker R.W. (2000). *Membrane technology and applications*. West Sussex: John Wiley and Sons Ltd. pp. 592.

Batsanov S.S. (2001). Van der Waals Radii of Elements. *Inorganic Materials*. 37(9): 871–885.

Becker E.W. (1994). *Microalgae: biotechnology and microbiology*. Cambridge University Press. pp. 293.

Belay A. (2013). Biology and industrial production of *Arthrospira* (Spirulina). In Richmond A and Hu Q (eds) *Handbook of Microalgal Culture: Applied Phycology and Biotechnology*. Oxford, UK: John Wiley & Sons, Ltd, 339–358.

Belkin S. and S. Boussiba (1991). Resistance of Spirulina platensis to ammonia at high pH values. *Plant and Cell Physiology*. 32(7): 953–958.

Bell W.H. (1980). Bacterial utilization of algal extracellular products. 1. The kinetic approach. *Limnology and Oceanography*. 25(6): 1007–1020.

Ben-Amotz A., J.E.W. Polle and D. V. Subba Rao eds. (2009). *The alga Dunaliella: biodiversity, physiology, genomics and biotechnology*. Enfield, NH: Science Publishers. pp. 555.

Borde X., B. Guieysse, O. Delgado, R. Muñoz, R. Hatti-Kaul, C. Nugier-Chauvin, H. Patin and B. Mattiasson (2003). Synergistic relationships in algal-bacterial microcosms for the treatment of aromatic pollutants. *Bioresource technology*. 86(3): 293–300.

Borowitzka M.A. (1992). Algal biotechnology products and processes — matching science and economics. *Journal of Applied Phycology*. 4(3): 267–279.

Borowitzka M.A. (1999). Commercial production of microalgae: ponds, tanks, tubes and fermenters. *Journal of Biotechnology*. 70(1–3): 313–321.

Burlew J.S. (1953). Current status of the large-scale culture of algae. In Burlew JS (ed.) *Algal Culture, From Laboratory to Pilot Plant*. Washington, DC: Carnegie Institution of Washington Publication 600, 3–23.

Camacho Rubio F., F.G. Acién Fernández, J. a. Sánchez Pérez, F. García Camacho and E. Molina Grima (1999). Prediction of dissolved oxygen and carbon dioxide concentration profiles in tubular photobioreactors for microalgal culture. *Biotechnology and Bioengineering*. 62(1): 71–86.

Canon-Rubio K.A., C.E. Sharp, J. Bergerson, M. Strous and H. De la Hoz Siegler (2016). Use of highly alkaline conditions to improve cost-effectiveness of algal biotechnology. *Applied Microbiology and Biotechnology*. 100(4): 1611–1622.

Carvalho A.P. and F.X. Malcata (2001). Transfer on carbon dioxide within cultures of micro algae: Plain bubbling versus hollow-fibre modules. *Biotechnology Progress*. 17(2): 265–272.

Carvalho A.P. and L.A. Meireles (2006). Microalgae reactors: A review of enclosed systems and performances. *Biotechnology progress*. 3(1): 1490–1506.

Carvalho A.P., L.A. Meireles and F.X. Malcata (2006). *Microalgal reactors: A review of enclosed system designs and performances*. *Biotechnol. Prog.* 22p.: 1490–1506.

Chen C.-Y., K.-L. Yeh, R. Aisyah, D. Lee and J. Chang (2011). Cultivation, photobioreactor design and harvesting of microalgae for biodiesel production: A critical review. *Bioresource Technology*. 102(1): 71–81.

Chi Z., J. V O'Fallon and S. Chen (2011). Bicarbonate produced from carbon capture for algae culture. *Trends in biotechnology*. 29(11): 537–541.

Chi Z., Y. Xie, F. Elloy, Y. Zheng, Y. Hu and S. Chen (2013). Bicarbonate-based Integrated Carbon Capture and Algae Production System with alkalihalophilic cyanobacterium. *Bioresource technology*. 133: 513–521.

Chiu S.-Y., C.-Y. Kao, T.-Y. Chen, Y.-B. Chang, C.-M. Kuo and C.-S. Lin (2015). Cultivation of microalgal *Chlorella* for biomass and lipid production using wastewater as nutrient resource. *Bioresource Technology*. 184: 179–189.

Christenson L. and R. Sims (2011). Production and harvesting of microalgae for wastewater treatment, biofuels, and bioproducts. *Biotechnology advances*. 29(6): 686–702.

Clausen J. and W. Junge (2005). Search for intermediates of photosynthetic water oxidation. *Photosynthesis Research*. 84(1–3): 339–345.

Clerck O. De, M.D. Guiry, F. Leliaert, Y. Samyn and H. Verbruggen (2013). Algal taxonomy: A road to nowhere? *Journal of Phycology*. 49(2): 215–225.

Côté P., J.L. Bersillon and A. Huyard (1989). Bubble-free aeration using membranes: mass transfer analysis. *Journal of Membrane Science*. 47(1–2): 91–106.

Delattre C., G. Pierre, C. Laroche and P. Michaud (2016). Production, extraction and characterization of microalgal and cyanobacterial exopolysaccharides. *Biotechnology Advances*. 34(7): 1159–1179.

Devgoswami C., M. Kalita, J. Talukdar, R. Bora and P. Sharma (2011). Studies on the growth behavior of *Chlorella*, *Haematococcus* and *Scenedesmus* sp. in culture media with different concentrations of sodium bicarbonate and carbon dioxide gas. *African Journal of Biotechnology*. 10(61): 13128–13138.

Duan C., M. Luo, C. Yang, H. Jiang and X. Xing (2010). Effects of different hollow fiber membrane modules on bubbleless aeration of methane and oxygen. *The Chinese Journal of Process Engineering*. 10(2): 395–399.

Dubinsky Z. (1992). The functional and optical absorption cross-sections of phytoplankton photosynthesis. In Falkowski PG Woodhead AD and Vivirito K (eds) *Primary Productivity and Biogeochemical Cycles in the Sea*. Boston, MA: Springer US, 31–45.

Dye D.J. and R. Sims (2010). *Spatial Light Dilution as a Technique for Conversion of Solar Energy to Algal Biomass*. Unpublished doctor's dissertation. Utah State University. pp. 142.

Ferreira L.S., M.S. Rodrigues, A. Converti, S. Sato and J.C.M. Carvalho (2012). *Arthrospira* (Spirulina) *platensis* cultivation in tubular photobioreactor: Use of no-cost CO_2 from ethanol fermentation. *Applied Energy*. 92: 379–385.

Fuentes J., I. Garbayo, M. Cuaresma, Z. Montero, M. González-del-Valle and C. Vílchez (2016). Impact of microalgae-bacteria interactions on the production of algal biomass and associated compounds. *Marine Drugs*. 14(5): 100.

García-González M., J. Moreno, J.C. Manzano, F.J. Florencio and M.G. Guerrero (2005). Production of *Dunaliella salina* biomass rich in 9-cis-beta-carotene and lutein in a closed tubular photobioreactor. *Journal of biotechnology*. 115(1): 81–90.

González-Fernández C., B. Molinuevo-Salces and M.C. García-González (2011). Nitrogen transformations under different conditions in open ponds by means of microalgae-bacteria consortium treating pig slurry. *Bioresource technology*. 102(2): 960–966.

González-López C.V., F.G. Acién Fernández, J.M. Fernández-Sevilla, J.F. Sánchez Fernández and E. Molina Grima (2012). Development of a process for efficient use of CO_2 from flue gases in the production of photosynthetic microorganisms. *Biotechnology and Bioengineering*. 109(7): 1637–1650.

González C., J. Marciniak, S. Villaverde, P. a García-Encina and R. Muñoz (2008). Microalgae-based processes for the biodegradation of pretreated piggery wastewaters. *Applied microbiology and biotechnology*. 80(5): 891–898.

Gordillo F.J.L., C. Jiménez, F.L. Figueroa and F.X. Niell (1998). Effects of increased atmospheric CO_2 and N supply on photosynthesis, growth and cell composition of the cyanobacterium *Spirulina platensis (Arthrospira)*. *Journal of Applied Phycology*. 10(5): 461–469.

Grobbelaar J.U., L. Nedbal and V. Tichý (1996). Influence of high frequency light/dark fluctuations on photosynthetic characteristics of microalgae photoacclimated to different light intensities and implications for mass algal cultivation. *Journal of Applied Phycology*. 8(4–5): 335–343.

Guiry M.D. (2012). How many species of algae are there? *Journal of Phycology*. 48(5): 1057–1063.

Gutzeit G., D. Lorch, A. Weber, M. Engels and U. Neis (2005). Bioflocculent algalbacterial biomass improves low-cost wastewater treatment. *Water Science & Technology*. 52(12): 9–18.

Hall D.O., F.G. Acién Fernández, E.C. Guerrero, K.K. Rao and E.M. Grima (2003). Outdoor helical tubular photobioreactors for microalgal production: Modeling of fluid-dynamics and

mass transfer and assessment of biomass productivity. *Biotechnology and Bioengineering*. 82(1): 62–73.

Hu J., D. Nagarajan, Q. Zhang, J.S. Chang and D.J. Lee (2017). Heterotrophic cultivation of microalgae for pigment production: A review. *Biotechnology Advances*.(June): 0–1.

Hu Q., H. Guterman and A. Richmond (1996). A flat inclined modular photobioreactor for outdoor mass cultivation of photoautotrophs. *Biotechnology and Bioengineering*. 51(1): 51–60.

Hu Q., N. Kurano, M. Kawachi, I. Iwasaki and S. Miyachi (1998). (a). Ultrahigh-cell-density culture of a marine green alga *Chlorococcum littorale* in a flat-plate photobioreactor. *Applied Microbiology and Biotechnology*. 49(6): 655–662.

Hu Q., Y. Zarmi and A. Richmond (1998). (b). Combined effects of light intensity, light-path and culture density on output rate of *Spirulina platensis* (Cyanobacteria). *European Journal of Phycology*. 33(2): 165–171.

Imaizumi Y., N. Nagao, F.M. Yusoff, N. Kurosawa, N. Kawasaki and T. Toda (2016). Lumostatic operation controlled by the optimum light intensity per dry weight for the effective production of *Chlorella zofingiensis* in the high cell density continuous culture. *Algal Research*. 20: 110–117.

Imaizumi Y., N. Nagao, F.M. Yusoff, S. Taguchi and T. Toda (2014). Estimation of optimum specific light intensity per cell on a high-cell-density continuous culture of *Chlorella zofingiensis* not limited by nutrients or CO_2. *Bioresource technology*. 162: 53–59.

Imase M., K. Watanabe, H. Aoyagi and H. Tanaka (2008). Construction of an artificial symbiotic community using a *Chlorella*-symbiont association as a model. *FEMS microbiology ecology*. 63(3): 273–282.

Ip P.-F. and F. Chen (2005). Employment of reactive oxygen species to enhance astaxanthin formation in Chlorella zofingiensis in heterotrophic culture. *Process Biochemistry*. 40(11): 3491–3496.

Ito A., K. Yamagiwa, M. Tamura and M. Furusawa (1998). Removal of dissolved oxygen using non-porous hollow-fiber membranes. *Journal of Membrane Science*. 145(1): 111–117.

Jacob-Lopes E., L.M. Cacia Ferreira Lacerda and T.T. Franco (2008). Biomass production and carbon dioxide fixation by Aphanothece microscopica N??geli in a bubble column photobioreactor. *Biochemical Engineering Journal*. 40(1): 27–34.

Janssen M., J. Tramper, L.R. Mur and R.H. Wijffels (2003). Enclosed outdoor photobioreactors: Light regime, photosynthetic efficiency, scale-up, and future prospects. *Biotechnology and Bioengineering*. 81(2): 193–210.

Kang C.D., J.S. Lee, T.H. Park and S.J. Sim (2005). Comparison of heterotrophic and photoautotrophic induction on astaxanthin production by *Haematococcus pluvialis*. *Applied Microbiology and Biotechnology*. 68(2): 237–241.

Kao C.-Y., S.-Y. Chiu, T.-T. Huang, L. Dai, L.-K. Hsu and C.-S. Lin (2012). Ability of a mutant strain of the microalga Chlorella sp. to capture carbon dioxide for biogas upgrading. *Applied Energy*. 93: 176–183.

Karapinar M. and Ş.A. Gönül (1992). Effects of sodium bicarbonate, vinegar, acetic and citric acids on growth and survival of *Yersinia enterocolitica*. *International Journal of Food Microbiology*. 16(4): 343–347.

Kazamia E., H. Czesnick, T.T. Van Nguyen, M.T. Croft, E. Sherwood, S. Sasso, S.J. Hodson, M.J. Warren and A.G. Smith (2012). Mutualistic interactions between vitamin B12 - dependent algae and heterotrophic bacteria exhibit regulation. *Environmental microbiology*. 14(6): 1466–1476.

Kishi M., M. Kawai and T. Toda (2015). Heterotrophic utilization of ethylene glycol and propylene glycol by *Chlorella protothecoides*. *Algal Research*. 11: 428–434.

Kishi M., M. Kawai, K. Tsuchiya, M. Koyama, N. Nagao and T. Toda in press. Enhancement of microalgal production through bacterial mineralization of ethylene glycol. *Journal of Environmental Biology*.

Kishi M., H. Takee, M. Kawai, N. Nagao and T. Toda in press. Sequential high rate algal ponds operation for enhanced treatment of organic wastewater. *Journal of Environmental Biology*.

Kishi M. and T. Toda (2017). Carbon fixation properties of three alkalihalophilic microalgal strains under high alkalinity. *Journal of Applied Phycology*. Online: 1–10.

Klanchui A., S. Cheevadhanarak, P. Prommeenate and A. Meechai (2017). Exploring Components of the CO2-Concentrating Mechanism in Alkaliphilic Cyanobacteria Through Genome-Based Analysis. *Computational and Structural Biotechnology Journal*. 15: 340–350.

Kujawski W. (2000). Application of Pervaporation and Vapor Permeation in Environmental Protection. *Polish Journal of Environmental Studies*. 9(1): 13–26.

Kumar A., S. Ergas, X. Yuan, A. Sahu, Q. Zhang, J. Dewulf, F.X. Malcata and H. van Langenhove (2010). (a). Enhanced CO_2 fixation and biofuel production via microalgae: recent developments and future directions. *Trends in biotechnology*. 28(7): 371–380.

Kumar A., X. Yuan, A.K. Sahu, J. Dewulf, S.J. Ergas and H. Van Langenhove (2010). (b). A hollow fiber membrane photo-bioreactor for CO_2 sequestration from combustion gas coupled with wastewater treatment: a process engineering approach. *Journal of Chemical Technology & Biotechnology*. 85(3): 387–394.

Kurd F. and V. Samavati (2015). International Journal of Biological Macromolecules Water soluble polysaccharides from Spirulina platensis : Extraction and in vitro anti-cancer activity. *International Journal of Biological Macromolecules*. 74: 498–506.

Lee A.K., D.M. Lewis and P.J. Ashman (2009). Microbial flocculation, a potentially low-cost harvesting technique for marine microalgae for the production of biodiesel. *Journal of Applied Phycology*. 21(5): 559–567.

Lee Y.-H., Y.-L. Yeh, K.-H. Lin and Y.-C. Hsu (2013). Using fluorochemical as oxygen carrier to enhance the growth of marine microalga *Nannochloropsis oculata*. *Bioprocess and Biosystems Engineering*. 36(8): 1071–1078.

Lemoine Y. and B. Schoefs (2010). Secondary ketocarotenoid astaxanthin biosynthesis in algae: a multifunctional response to stress. *Photosynthesis research*. 106(1–2): 155–177.

Li O., C. Lu, A. Liu, L. Zhu, P.-M. Wang, C.-D. Qian, X.-H. Jiang and X.-C. Wu (2013). Optimization and characterization of polysaccharide-based bioflocculant produced by Paenibacillus elgii B69 and its application in wastewater treatment. *Bioresource technology*. 134: 87–93.

Liu J., Z. Sun, H. Gerken, Z. Liu, Y. Jiang and F. Chen (2014). *Chlorella zofingiensis* as an alternative microalgal producer of astaxanthin: biology and industrial potential. *Marine Drugs*. 12(6): 3487–3515.

Lorenz R.T. and G.R. Cysewski (2000). Commercial potential for *Haematococcus* microalgae as a natural source of astaxanthin. *Trends in Biotechnology*. 18(4): 160–167.

Marquez F.J., K. Sasaki, N. Nishio and S. Nagai (1995). Inhibitory effect of oxygen accumulation on the growth of *Spirulina platensis*. *Biotechnology Letters*. 17(2): 225–228.

Meier L., R. Pérez, L. Azócar, M. Rivas and D. Jeison (2015). Photosynthetic CO_2 uptake by microalgae: An attractive tool for biogas upgrading. *Biomass and Bioenergy*. 73: 102–109.

Miyasaki K.T., R.J. Genco and M.E. Wilson (1986). Antimicrobial properties of hydrogen peroxide and sodium bicarbonate individually and in combination against selected oral, gram-negative, facultative bacteria. *Journal of Dental Research*. 65(9): 1142–1148.

Molina E., J. Fernández, F.G. Acién and Y. Chisti (2001). Tubular photobioreactor design for algal cultures. *Journal of Biotechnology*. 92(2): 113–131.

Montemezzani V., I.C. Duggan, I.D. Hogg and R.J. Craggs (2015). A review of potential methods for zooplankton control in wastewater treatment High Rate Algal Ponds and algal production raceways. *Algal Research*. 11: 211–226.

Mortezaeikia V., R. Yegani, M.A. Hejazi and S. Chegini (2016). CO_2 biofixation by *Dunaliella salina* in batch and semi-continuous cultivations, using hydrophobic and hydrophilic poly ethylene (PE) hollow fiber membrane photobioreactors. *Iranian Journal of Chemical Engineering*. 13(1): 47–59.

Muñoz R., M.T. Alvarez, A. Muñoz, E. Terrazas, B. Guieysse and B. Mattiasson (2006). Sequential removal of heavy metals ions and organic pollutants using an algal-bacterial consortium. *Chemosphere*. 63(6): 903–911.

Muñoz R. and B. Guieysse (2006). Algal-bacterial processes for the treatment of hazardous contaminants: a review. *Water research*. 40(15): 2799–2815.

Muñoz R., B. Guieysse and B. Mattiasson (2003). Phenanthrene biodegradation by an algal-bacterial consortium in two-phase partitioning bioreactors. *Applied microbiology and biotechnology*. 61(3): 261–267.

Muñoz R., C. Köllner, B. Guieysse and B. Mattiasson (2004). Photosynthetically oxygenated salicylate biodegradation in a continuous stirred tank photobioreactor. *Biotechnology and bioengineering*. 87(6): 797–803.

Natori N., M. Kuwata, T. Suzuki and T. Toda (2017). A novel fracturing device to observe the gut contents of copepod nauplii using a scanning electron microscope. *Limnology and Oceanography: Methods*. 15(6): 567–571.

Norsker N.H., M.J. Barbosa, M.H. Vermuë and R.H. Wijffels (2011). Microalgal production - A close look at the economics. *Biotechnology Advances*. 29(1): 24–27.

Ogawa T. and G. Terui (1970). Studies on the growth of *Spirulina platensis*: (I) On the pure culture of *Spirulina platensis*. *Journal of Fermentation Technology*. 48(6): 361–367.

Oh H.-M., S. Lee, M.-H. Park, H.-S. Kim, H.-C. Kim, J.-H. Yoon, G.-S. Kwon and B.-D. Yoon (2001). Harvesting of Chlorella vulgaris using a bioflocculant from Paenibacillus sp. AM49. *Biotechnology Letters*. 23(15): 1229–1234.

Olaizola M. (2003). Commercial development of microalgal biotechnology: From the test tube to the marketplace. *Biomolecular Engineering*. 20(4–6): 459–466.

Olguín E.J., S. Galicia, O. Angulo-Guerrero and E. Hernández (2001). The effect of low light flux and nitrogen deficiency on the chemical composition of Spirulina sp. (Arthrospira) grown on digested pig waste. *Bioresource technology*. 77(1): 19–24.

Orosa M., J.F.F. Valero, C. Herrero and J. Abalde (2001). Comparison of the accumulation of astaxanthin in *Haematococcus pluvialis* and other green microalgae under N-starvation and high light conditions. *Biotechnology Letters*. 23(13): 1079–1085.

Oswald W.J. (1977). *Method of waste treatment and algae recovery*. Patent US4005546 A.

Oswald W.J., H.B. Gotaas, H.F. Ludwig and V. Lynch (1953). Algae symbiosis in oxidation ponds - III. Photosynthetic oxygenation. *Sewage and Industrial Wastes*. 25(6): 692–705.

Park J.B.K., R.J. Craggs and a N. Shilton (2011). Wastewater treatment high rate algal ponds for biofuel production. *Bioresource technology*. 102(1): 35–42.

Peng L., C.Q. Lan and Z. Zhang (2013). Evolution, detrimental effects, and removal of oxygen in microalga cultures: A review. *Environmental Progress & Sustainable Energy*. 32(4): 982–988.

Pittman J.K., A.P. Dean and O. Osundeko (2011). The potential of sustainable algal biofuel production using wastewater resources. *Bioresource technology*. 102(1): 17–25.

Posadas E., M.L. Serejo, S. Blanco, R. Pérez, P. a. García-Encina and R. Muñoz (2015). Minimization of biomethane oxygen concentration during biogas upgrading in algal–bacterial photobioreactors. *Algal Research*. 12: 221–229.

Posten C. (2009). Design principles of photo-bioreactors for cultivation of microalgae. *Engineering in Life Sciences*. 9(3): 165–177.

Pulz O. (2001). Photobioreactors: Production systems for phototrophic microorganisms. *Applied Microbiology and Biotechnology*. 57(3): 287–293.

Pyle D. (2008). *Use of biodiesel-derived crude glycerol for the production of omega-3 polyunsaturated fatty acids by the microalga Schizochytrium limacinum*. Unpublished master's thesis. Virginia Polytechnic Institute and State University. pp. 72.

Qiang H. and A. Richmond (1996). Productivity and photosynthetic efficiency of *Spirulina platensis* as affected by light intensity, algal density and rate of mixing in a flat plate photobioreactor. *Journal of Applied Phycology*. 8(2): 139–145.

Qiang H.U., D. Faiman and A. Richmond (1998). Optimal tilt angles of enclosed reactors for growing photoautotrophic microorganisms outdoors. *Journal of Fermentation and Bioengineering*. 85(2): 230–236.

Ramanan R., K. Kannan, A. Deshkar, R. Yadav and T. Chakrabarti (2010). Enhanced algal CO_2 sequestration through calcite deposition by Chlorella sp. and Spirulina platensis in a mini-raceway pond. *Bioresource technology*. 101(8): 2616–2622.

Rawat I., R. Ranjith Kumar, T. Mutanda and F. Bux (2011). Dual role of microalgae: Phycoremediation of domestic wastewater and biomass production for sustainable biofuels production. *Applied Energy*. 88(10): 3411–3424.

Richardson J.W., M.D. Johnson and J.L. Outlaw (2012). Economic comparison of open pond raceways to photo bio-reactors for profitable production of algae for transportation fuels in the Southwest. *Algal Research*. 1(1): 93–100.

Richardson J.W., M.D. Johnson, X. Zhang, P. Zemke, W. Chen and Q. Hu (2014). A financial assessment of two alternative cultivation systems and their contributions to algae biofuel economic viability. *Algal Research*. 4(1): 96–104.

Richmond A. (2013). Biological principles of mass cultivation of photoautotrophic microalgae. In *Handbook of Microalgal Culture: Applied Phycology and Biotechnology*. 169–204.

Shelp B.J. and D.T. Canvin (1980). Photorespiration and oxygen inhibition of photosynthesis in *Chlorella pyrenoidosa*. *Plant Physiology*. 65(5): 780–784.

Shiraishi H. (2015). Association of heterotrophic bacteria with aggregated Arthrospira platensis exopolysaccharides: Implications in the induction of axenic cultures. *Bioscience, Biotechnology and Biochemistry*. 79(2): 231–241.

Solak E.K. and O. Şanlı (2008). Separation characteristics of dimethylformamide/water mixtures using sodium alginate-g-N-vinyl-2-pyrrolidone membranes by pervaporation method. *Chemical Engineering and Processing: Process Intensification*. 47(4): 633–641.

Spolaore P., C. Joannis-Cassan, E. Duran and A. Isambert (2006). Commercial applications of microalgae. *Journal of Bioscience and Bioengineering*. 101(2): 87–96.

Stumm W. and J.J. Morgan (1993). *Aquatic Chemistry: Chemical Equilibria and Rates in Natural Waters*. 3rd ed. New York: Wiley-Interscience. pp. 1022.

Takizawa E. (1993). *Cultivation methods and reactor design for photosynthetic microorganism (Japanese)*. Patent 5–64577.

Toledo-Cervantes A., M.L. Serejo, S. Blanco, R. Pérez, R. Lebrero and R. Muñoz (2016). Photosynthetic biogas upgrading to bio-methane: Boosting nutrient recovery via biomass productivity control. *Algal Research*. 17: 46–52.

Torzillo G., P. Bernardini, J. Masojidek and J. Masojídek (1998). On-line monitoring of chlorophyll fluorescence to assess the extent of photoinhibition of photosynthesis induced

by high oxygen concentration and low temperature and its effect on the productivity of outdoor cultures of *Spirulina platensis* (cyanoba. *Journal of Phycology*. 34(3): 504–510.

Tredici M. and G.C. Zittelli (1997). Cultivation of *Spirulina* (Arthrospira) *platensis* in flat plate reactors. In Vonshak A (ed.) *Spirulina Platensis Arthrospira: Physiology, Cell-Biology And Biotechnology*. CRC Press, 117–130.

Tredici M.R. and G.C. Zittelli (1998). Efficiency of sunlight utilization: Tubular versus flat photobioreactors. *Biotechnology and Bioengineering*. 57(2): 187–197.

Uragami T. and K. Takigawa (1990). Permeation and separation characteristics of ethanol-water mixtures through chitosan derivative membranes by pervaporation and evapomeation. *Polymer*. 31(4): 668–672.

Vonshak A. (1997). Spirulina platensis Arthrospira*: Physiology, Cell-Biology and Biotechnology*. Vonshak A (ed.) CRC Press. pp. 233.

Vonshak A., G. Torzillo, P. Accolla and L. Tomaselli (1996). Light and oxygen stress in *Spirulina platensis* (cyanobacteria) grown outdoors in tubular reactors. *Physiologia Plantarum*. 97(1): 175–179.

Wan C., M.A. Alam, X.-Q. Zhao, X.-Y. Zhang, S.-L. Guo, S.-H. Ho, J.-S. Chang and F.-W. Bai (2014). Current progress and future prospect of microalgal biomass harvest using various flocculation technologies. *Bioresource Technology*.

Wang L., Y. Li, P. Chen, M. Min, Y. Chen, J. Zhu and R.R. Ruan (2010). Anaerobic digested dairy manure as a nutrient supplement for cultivation of oil-rich green microalgae *Chlorella* sp. *Bioresource technology*. 101(8): 2623–2628.

Wang Y. and T. Chen (2008). The biosynthetic pathway of carotenoids in the astaxanthin-producing green alga *Chlorella zofingiensis*. *World Journal of Microbiology and Biotechnology*. 24(12): 2927–2932.

Wen Z.-Y. and F. Chen (2003). Heterotrophic production of eicosapentaenoic acid by microalgae. *Biotechnology Advances*. 21(4): 273–294.

Willson B.D., C.W. Turner, G.R. Babbitt, P.A. Letvin and S.R. Wickrmaskinghe (2009). *Permeable membranes in film photobioreactors*. Patent US 20090305389A1.

Yeh K.L., J.S. Chang and W.M. Chen (2010). Effect of light supply and carbon source on cell growth and cellular composition of a newly isolated microalga *Chlorella vulgaris* ESP-31. *Engineering in Life Sciences*. 10(3): 201–208.

Zeebe R. and D. Wolf-Gladrow (2001). *CO_2 in Seawater-Equilibrium, Kinetics, Isotopes*. 1st ed. Halpern D (ed.) Amsterdam: Elsevier Science B.V. pp. 100.

Zengling M., G. Kunshan and W. Teruo (2006). Effects of dissolved organic matter on the growth and pigments synthesis of *Spirulina platensis* (Arthospira). *Progress in Natural Science*. 16(1): 50–54.